Open access • Journal Article • DOI:10.1088/0951-7715/11/3/015

Towards global models near homoclinic tangencies of dissipative diffeomorphisms

Henk Broer, Carles Simó, Joan Carles Tatjer

Institutions: University of Groningen, University of Barcelona

Published on: 01 May 1998 - Nonlinearity (IOP PUBLISHING LTD)

Topics: Homoclinic bifurcation, Homoclinic orbit, Attractor, Numerical continuation and Quasiperiodicity

Towards global models near homoclinic tangencies of dissipative diffeomorphisms

Broer, H; Simo, C; Tatjer, JC

Published in:
Nonlinearity

Publication date:
1998

Nonlinearity **11** (1998) 667–770. Printed in the UK PII: S0951-7715(98)81276-0

Towards global models near homoclinic tangencies of dissipative diffeomorphisms

Henk Broer†, Carles Simó‡ and Joan Carles Tatjer‡

† Afdeling Wiskunde en Informatica, Rijksuniversiteit Groningen, Postbus 800, 9700 AV Groningen, The Netherlands

‡ Departament de Matemàtica Aplicada i Anàlisi, Universitat de Barcelona, Gran Via 585, 08007 Barcelona, Spain

Received 21 January 1997, in final form 29 December 1997
Recommended by R S MacKay

Abstract. A representative model of a return map near homoclinic bifurcation is studied. This model is the so-called fattened Arnold map, a diffeomorphism of the annulus. The dynamics is extremely rich, involving periodicity, quasiperiodicity and chaos.

The method of study is a mixture of analytic perturbation theory, numerical continuation, iteration to an attractor and experiments, in which the guesses are inspired by the theory. In turn the results lead to fine-tuning of the theory. This approach is a natural paradigm for the study of complicated dynamical systems.

By following generic bifurcations, both local and homoclinic, various routes to chaos and strange attractors are detected. Here, particularly, the 'large' strange attractors which wind around the annulus are of interest. Furthermore, a global phenomenon regarding Arnold tongues is important. This concerns the accumulation of tongues on lines of homoclinic bifurcation. This phenomenon sheds some new light on the occurrence of infinitely many sinks in certain cases, as predicted by the theory.

AMS classification scheme numbers: 58F08, 58F14

Contents

0951-7715/98/030667+104$19.50

1. Introduction

1.1. Motivation

This paper involves a dissipative family of diffeomorphisms of the annulus, the so-called fattened Arnold family, which can be regarded as a perturbation of the Arnold family of circle maps. It turns out that in a certain setting, the fattened Arnold family can be regarded as a simplified global model for the return map of a dissipative diffeomorphism near homoclinic bifurcation. This implies that its dynamics has a universal character in the world of two-dimensional (2D) maps. This dynamics itself turns out to involve periodicity, quasiperiodicity and chaos, between which there are various transitions (bifurcations). In this respect it can be compared with classical examples such as the Hénon map and the standard map (cf Broer *et al* [54, 10, 11], Roussaine and Simó [48]).

We study the fattened Arnold family in dependence of three parameters, using both analytic perturbation theory and numerical methods. In certain parameter regimes, our family is quite near the Arnold family of circle maps. Perturbation theory here reveals periodicity and quasiperiodicity, parametrically organized by Arnold (resonance) tongues. Outside these parameter regimes the perturbation becomes larger and bifurcations complicate the dynamics, often involving chaos. On the one hand, this concerns local bifurcations, e.g. cascades of flips (period doublings) and of cusp bifurcations. On the other hand, we have to deal with homoclinic bifurcations. Here the dynamical features are further explored by numerical methods, with an emphasis on numerical continuation of the bifurcations such as the boundaries of the Arnold tongues. Also, we often just iterate to a periodic attractor. The numerical search is then guided by the corresponding theory. This approach seems a natural paradigm for the study of complicated systems.

The dynamics of the model expectedly is extremely rich. In several cases we find interesting dynamical objects as predicted by the theory, such as 'large' strange attractors that wind around the entire annulus (cf Díaz *et al* [19] and Viana [60]). Also we discover an interesting global phenomenon in the parameter plane. This concerns the accumulation of the boundaries of certain Arnold tongues on lines of homoclinic bifurcations. This sheds

some new light on the existence of infinitely many periodic attractors (sinks) near such a tangency (cf Newhouse [38] or Palis and Takens [45]).

1.2. Object of study

To fix thoughts, we first introduce the fattened Arnold family of annulus diffeomorphisms by

$$\begin{array}{rccl} \bar{F}_{\alpha,\omega,\beta}: & \mathbb{S}^1\times\mathbb{R} & \to & \mathbb{S}^1\times\mathbb{R} \\ & (x,y) & \mapsto & (x+\omega+\alpha(y+\sin x)(\mathrm{mod}\,2\pi),\,\beta(y+\sin x)), \end{array} \tag{1}$$

where $\omega \in \mathbb{S}^1 = \mathbb{R}/2\pi\mathbb{Z}$, $\alpha \in \mathbb{R}$ and $\beta \in \mathbb{R}$ are parameters. The map $\bar{F}_{\alpha,\omega,\beta}$ has constant Jacobian $\mathrm{Jac}\bar{F}_{\alpha,\omega,\beta} \equiv \beta$. Moreover, if $\beta \neq 0$, by using the change of coordinates $x \leftrightarrow -x+\omega+\alpha\beta^{-1}y$, $y \leftrightarrow \beta^{-1}y$ we obtain $\tilde{F}^{-1}_{\alpha,\omega,\beta} = \bar{F}_{\alpha\beta^{-1},\omega,\beta^{-1}}$, where $\tilde{F}_{\alpha,\omega,\beta}$ is the family (1) in the new coordinates. Hence, without loss of generality we can assume $|\beta| \leqslant 1$.

Instead of $\bar{F}_{\alpha,\omega,\beta}$ we may consider a lift $F_{\alpha,\omega,\beta}: \mathbb{R}^2 \to \mathbb{R}^2$. The only difference with (1) is that in the x-direction we refrain from counting $\mathrm{mod}\,2\pi$. Also, the parameter ω now varies over $\mathbb{R}$. Notice that in this setting a periodic point (x, y) of rotation number p/q is determined by the equation $F^q_{\alpha,\omega,\beta}(x, y) = (x + 2p\pi, y)$. We recall the simple fact that, for any $k \in \mathbb{Z}$, the map $F_{\alpha,\omega+2k\pi,\beta}$ is also a lift of $\bar{F}_{\alpha,\omega,\beta}$.

Note that for $\beta = 0$ the circle $y = 0$ is invariant. Inside this circle we have $\bar{F}_{\alpha,\omega,0}(x, 0) = (\bar{f}_{\alpha,\omega}(x), 0)$, where $\bar{f}_{\alpha,\omega}(x) = x + \omega + \alpha\sin x \ (\mathrm{mod}\,2\pi)$ is the classical Arnold family of circle maps, see Arnold [1], which explains the name of this object of study. We recall that the Arnold map $\bar{f}_{\alpha,\omega}$ is a diffeomorphism for $|\alpha| < 1$, only a homeomorphism for $|\alpha| = 1$ and an endomorphism for $|\alpha| > 1$. For $|\alpha| > 1$ it is, for example, known that there are at most two attracting periodic orbits (see Boyland [8]).

This paper deals mainly with the dissipative case $|\beta| < 1$. Some facts about the (near) conservative cases are further elaborated in section 5.3.4 and appendices C and D. In most of the sections, we shall fix β and study the bifurcation set in the (α, ω)-plane. However, sometimes we also vary the parameter β, in order to see transitions between several of these two-parameter scenarios. For $|\beta| < 1$, the set

$$T := S^1 \times \left[-\frac{|\beta|}{1-|\beta|}, \frac{|\beta|}{1-|\beta|}\right]$$

satisfies $\bar{F}_{\alpha,\omega,\beta}(T) \subset T$. Therefore there exists a global (or universal) attractor $\Omega = \bigcap_{n\in\mathbb{N}} \bar{F}^n_{\alpha,\omega,\beta}(T)$, of zero Lebesgue measure. One of our interests is to understand the structure of this set Ω. For many values of the parameters α and β the attractor Ω is just an invariant circle, displaying either periodic or quasiperiodic dynamics. The question then becomes: How is this 'simple' structure destroyed when changing the parameters?

Remarks.

(i) Note that $\bar{F}_{\alpha,\omega,\beta}$ for $\beta = 1$ coincides with the standard map. For general $0 < \beta < 1$ we have a shifted dissipative standard map. For $-1 < \beta < 0$ the map is similar, but orientation reversing. This property has important qualitative implications for the dynamics. Some other interesting families of maps are also particular cases or limit cases of (1), such as the Hénon and logistic maps, the so-called 'twist map'. An extension introduced in appendix A (given by (6)) also contains the whisker map as a particular case.

(ii) We observe that the transformations $(x, y, \alpha, \omega, \beta) \leftrightarrow (-x, -y, \alpha, -\omega, \beta)$ and $(x, y, \alpha, \omega, \beta) \leftrightarrow (x + \pi, -y, -\alpha, \omega, \beta)$ again give the initial family. Therefore, we can restrict ourselves to the case $\omega \in [0, \pi]$, $\alpha \geqslant 0$.

1.3. Outline, sketch of some results

The analytic study of the dynamical behaviour of the family F, given by (1), in general is not easy. However, there are two regions in the parameter space, given by $|\beta| \ll 1$ and $|\alpha| \ll 1$ respectively, in which some information can be obtained using perturbation theory. Here the main conclusion is that the attractor Ω is an invariant circle.

In fact, as said before, for $|\beta| \ll 1$ our family (1) is a perturbation of the one-dimensional (1D) Arnold family. A similar relationship exists between the Hénon map, given by $H_{a,b}(x, y) = (1 + y - ax^2, bx)$ and the 1D logistic map. In the latter case a perturbation analysis allows us to obtain many details about the dynamics of $H_{a,b}(x, y)$ for $|b| \ll 1$ (see Holmes and Whitley [30], Benedicks and Carleson [5], Mora and Viana [36], Tatjer [57, 56]). It is our aim to use similar techniques in the present Arnold case. In section 2 we shall see, that here indeed Ω is a globally attracting invariant circle. In the case where $|\alpha| \ll 1$, our family (1) cannot always be viewed as a perturbation of a 1D map. Here, however, using normal hyperbolicity directly, we still obtain the same conclusion regarding Ω. Another conclusion of section 2 will be that this invariant circle is quasiperiodic and hence of class C^∞, or even C^ω, for a subset of the (α, ω)-plane of large Lebesgue measure.

We also have to consider periodic attractors, which for small values of $|\alpha|$ lie inside the invariant circle Ω. In the (α, ω)-plane periodic attractors are organized by Arnold tongues, the properties of which will be treated systematically. Near $\alpha = 0$ a normal-form approach gives all the information needed, as will also be seen in section 2. Relevant generic conditions have been checked with suitable computer programs, both symbolically and numerically. Some new material concerning the resonant normal form can be found in appendix B.

The perturbation theory also gives an important contribution to the theory of homoclinic bifurcation (again cf [30, 56]). It turns out to be useful to explicitly regard the unperturbed Arnold family of circle maps as the 'trivial' annulus map:

$$F_{\alpha,\omega}(x, y) = (x + \omega + \alpha \sin x, 0).$$

In this way a good perturbation theory for small $|\beta|$ is particularly possible, so we can keep track of the winding of the unstable manifold around the annulus and a good description of homoclinic tangencies can be given, also with respect to the strong stable foliation. Since we are dealing with more than one parameter, combinations of homoclinic and fold (saddle-node) bifurcations also have to be considered. Furthermore, we briefly touch upon primary homo- and heteroclinic tangencies in this 'trivial' case.

Section 2 gives the starting point for the numerical exploration of section 5. What is new in it is the *application* of the theory (generally known, however see appendix B) to our fattened Arnold model.

In section 3 we briefly discuss the present knowledge of the possible transitions to complicated and chaotic dynamics as the parameters move. One element concerns the loss of smoothness of the invariant circle as well as its destruction. The second element is the birth and death of chaos. Here we just briefly introduce the elements of local and homoclinic bifurcation involved. It is to be noted that all scenarios sketched in this section indeed seem to occur in the fattened Arnold example.

Section 4 contains an extensive theoretical review of generic possibilities concerning bifurcations of periodic points and homoclinic bifurcations. This material is of basic importance for the numerical continuation starting from the perturbative situation in section 2, in search of the scenarios of section 3. Notably, all the possibilities mentioned seem to appear in our fattened Arnold family.

We will restrict ourselves mainly to bifurcations of codimension 2. However, in the semiglobal organisation of these phenomena also codimension 3 phenomena necessarily come into play, since our example depends on three parameters. As mentioned earlier, also infinite cascades of some bifurcations (flips and cusps) are relevant. Another part of this survey concerns codimension 1 and 2 homoclinic bifurcations, so related to both saddle and fold points.

This section is closed with some remarks regarding the role of heteroclinic intersections and the differences between the orientation-preserving and reversing cases. A further question is how to deal with genericity. Indeed, our numerical search in section 5 is theory guided, but often genericity can only be checked partially. Our solution to this predicament is simply to assume genericity and to interpret the numerical output from this, until absurdities arise.

Section 5 then, contains the numerical exploration of the fattened Arnold model, starting from the results of section 2. As earlier stated, all the scenarios and bifurcations sketched so far are relevant for the model. Detailed graphics and other data can be found below, including tests for the generic differentiability of circle attractors. Instead of summing up many details, let us here restrict ourselves to sketching a few of the objectives.

In figure 1 the (ω, α)-plane is depicted, for β fixed at $\beta = 0.1$. Each point (pixel) in the plane is given a grey tone, encoding the existence of a periodic attractor, different periods giving rise to different grey tones. A black parameter point indicates an invariant circle (close to the bottom of the figure) or a strange attractor (further upward). The organization of the parameter points with periodic attractors in overlapping Arnold tongues is immanent from the picture. Often, several attractors can coexist for the same value of the parameters.

Figure 1 certainly indicates that the model displays a great richness, which we attempt to understand better in this paper. Let us single out two aspects. One of these concerns the accumulation of Arnold tongues. To indicate what we mean by this we refer to figures 2 and 3, where the latter is a magnification of the former. These figures show that the Arnold tongues accumulate on lines of homoclinic tangency, indicated by $T_0^{2,0.3}$ and $S_1^{0.3}$. This is an experimental fact with a partial theoretical explanation. One thing it helps to understand is the occurrence of infinitely many periodic attractors (sinks) in this situation (see again Newhouse [38], Palis and Takens [45]).

Remark. Accumulation or 'trend' of resonance tongues is sometimes met in applications (cf van der Heijden [28]). Also see Broer, Roussarie and Simó [10, 54] regarding the Bogdanov–Takens bifurcation for diffeomorphisms.

Another aspect is the occurrence of 'large' strange attractors, for examples see figures 4 and 5. Such attractors occur near homoclinic tangency, as theoretically predicted by Díaz *et al* [19] and Viana [60]. Compare with the 'small' attractors as predicted by Newhouse [38], Palis and Takens [45], Benedicks and Carleson [5], Mora and Viana [36] and Tatjer [57, 56], and which show up also abundantly in our model. This remark is of special importance when viewing the fattened Arnold family as modelling the return map near homoclinic tangency. This is used to try to capture the full dynamics on a fundamental domain (for details also see appendix A).

Furthermore, in section 5.3.4 some open problems are mentioned, while in section 5.5 we invite the reader to join us in a computer experiment. This verbal 'movie' concludes the paper, illustrating the claim that 2D maps should no longer have any secrets.

An essential tool for the numerical computations is continuation. It has been used for most of the bifurcation diagrams, to trace curves of: folds, flips, constant trace, double

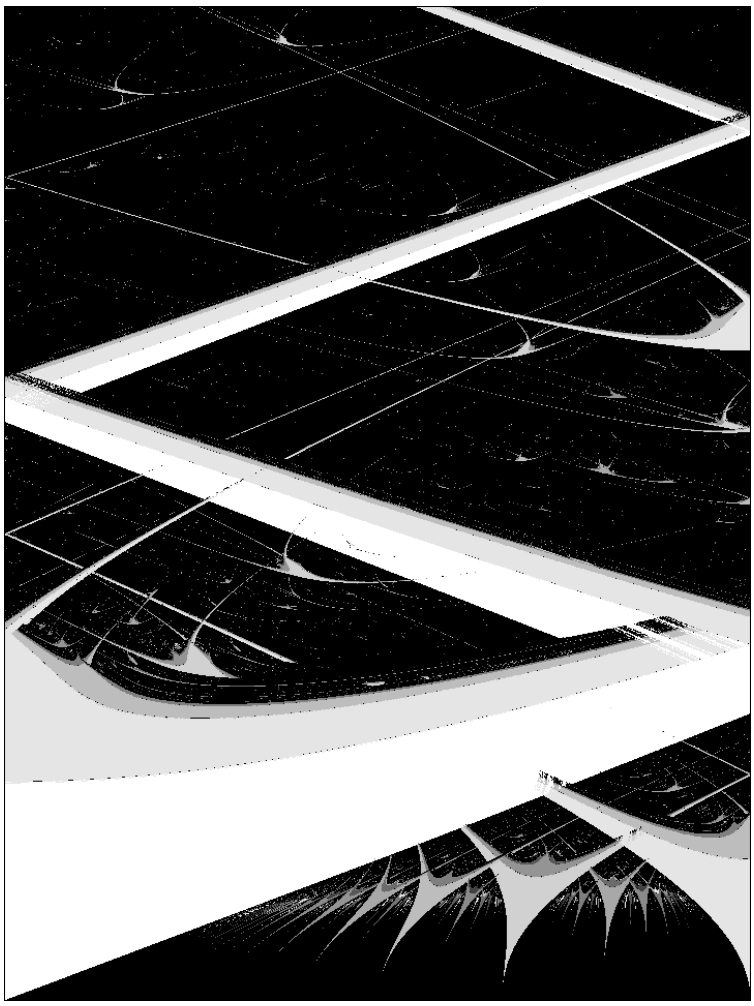

Figure 1. Arnold tongues: $\beta = 0.1$, $\omega \in [0, \pi]$ and $\alpha \in [0, 10]$.

eigenvalues, homoclinic and heteroclinic tangencies (both to saddles and folds) and cubic tangencies to strong stable foliations. When required, several symbolic computations have been carried out to high order, for example to obtain good starting approximations of invariant manifolds or to have local approximations of tongues. Typically, truncated power series in one or several variables, with numerical coefficients, have been used. For details we refer to [51].

2. Perturbation properties of the fattened Arnold family

We consider the fattened Arnold family $\bar{F}_{\alpha,\omega,\beta}$ given by (1). The properties presented here are mainly based on a perturbation analysis of 1D maps. Our results concern the existence and differentiability of the invariant circle Ω, using normal hyperbolicity. The dynamics inside this circle can then be either periodic or quasiperiodic. The (α, ω)-plane is organized by Arnold tongues, which will also be defined here. Moreover, we discuss homoclinic

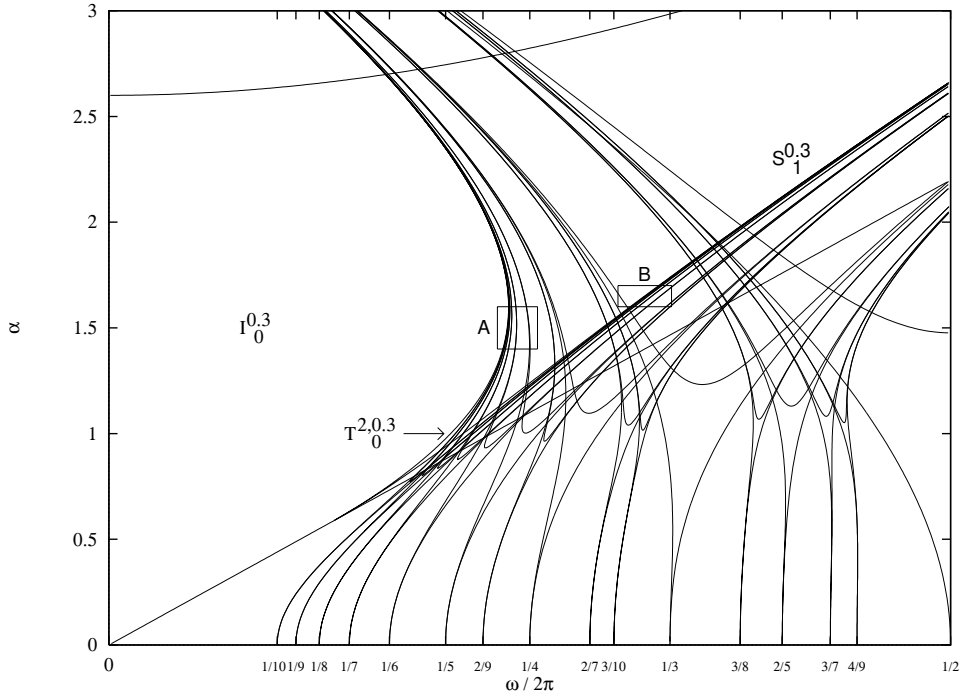

Figure 2. Arnold tongues for $\beta = 0.3$ up to period 10. We include two homoclinic bifurcation curves at which the tongues accumulate.

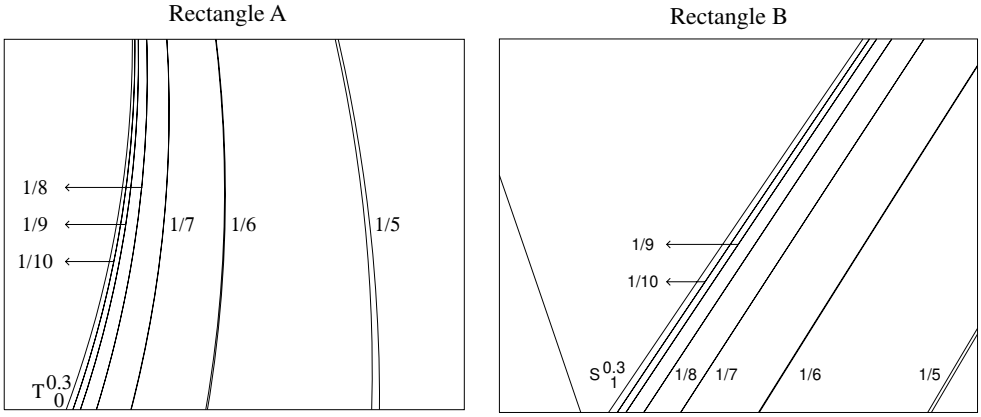

Figure 3. Magnifications of the rectangles in the previous figure. The number indicates the rotation number associated to each invariant circle. Windows: $[1.45, 1.6] \times [1.4, 1.6]$ (left) and $[1.9, 2.1] \times [1.4, 1.6]$ (right).

bifurcations from the perturbative point of view.

First, however, we briefly review some generalities about circle maps and about the perturbation relation between 1D and certain 2D maps.

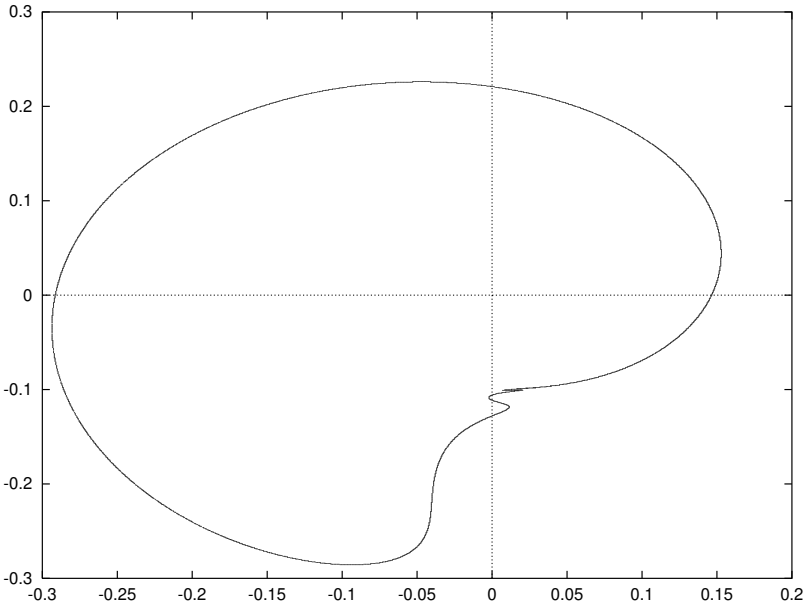

Figure 4. 'Large' strange attractor for $\alpha = 1.1$, $\beta = 0.1$ and $\omega = 1.3$, outside (but near) the tongue I_0^β, considering x as the angle and $r = y + \beta/(1-\beta) + 0.1$ as the radius in polar coordinates, and displaying it in Cartesian coordinates.

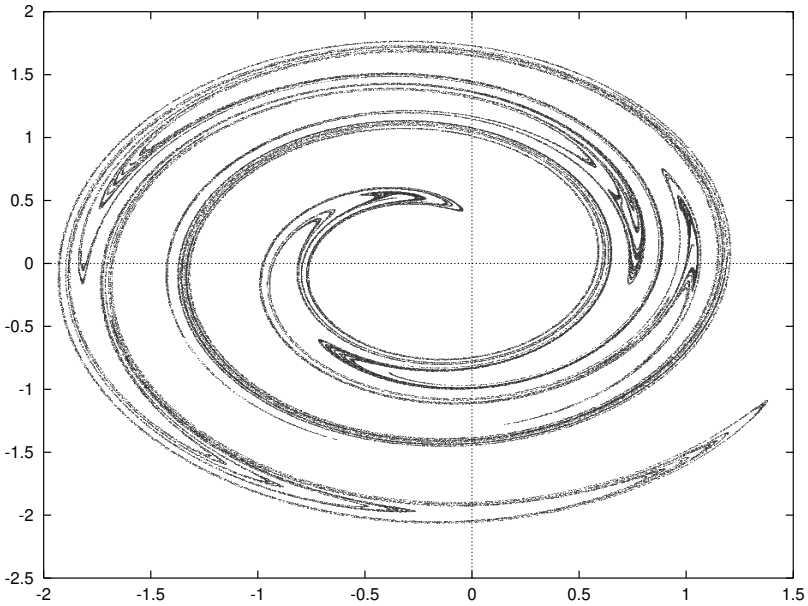

Figure 5. 'Large' strange attractor for $\alpha = 4.5$, $\beta = 0.55$ and $\omega = 10$ (on the boundary of the tongue I_0^β). The polar coordinates are the same as in figure 4.

2.1. Circle maps

We commence by recalling some general facts about circle maps. Every orientation-preserving homeomorphism of $\mathbb{S}^1 = \mathbb{R}/2\pi\mathbb{R}$ can be lifted to a homeomorphism f of

$\mathbb{R}$ where $f(x+2\pi) = f(x) + 2\pi$. This is equivalent to saying that $f = Id + \varphi$, where φ is a 2π-periodic map. Let us introduce the following notation. For $r = 0$, $r \geqslant 1$, $r = \infty$ or $r = \omega$ by $D^r(\mathbb{S}^1)$ we denote the set of C^r diffeomorphisms ($r > 0$) or homeomorphisms ($r = 0$) f on $\mathbb{R}$, with $f = Id + \varphi$ and φ a 2π-periodic C^r map.

The rotation number of any map $f \in D^0(\mathbb{S}^1)$ is defined by

$$\rho(f) := \lim_{n\to\infty} \frac{f^n(x) - x}{2n\pi}.$$

This limit exists independent of x. Also it is independent of the lift, if defined modulo $\mathbb{Z}$. Note that in the case of the rigid rotation, $R_\omega(x) = x + 2\pi\omega$, one has $\rho(R_\omega) = \omega$.

We list some well known properties of ρ (see, e.g. Nitecki [41]). Let $f \in D^0(\mathbb{S}^1)$. Then there exists $x \in \mathbb{R}$ such that $f^q(x) = x + 2\pi p$ if and only if $\rho(f) = p/q \in \mathbb{Q}$. The rotation number depends continuously on f in the C^0-topology. Conjugate homeomorphisms have the same rotation number. In general the converse is not true. However, if f is of class C^1, with $\rho(f) \in \mathbb{R} \setminus \mathbb{Q}$ and $\log f'$ of bounded variation then f is C^0-conjugate to $R_{\rho(f)}$; this it the content of the Denjoy theorem. For such diffeomorphisms every orbit is dense. In such a case one says that the dynamics of the map is quasiperiodic. Finally, an orientation-preserving diffeomorphism of the circle is structurally stable if and only if the rotation number is rational and all its periodic points are hyperbolic. Moreover, the set of structurally stable diffeomorphisms is open and dense in the space $D^1(\mathbb{S}^1)$.

In the following propositions, we quote some other properties related to the maps under consideration. Proofs of these results can be found in Herman [27] and Yoccoz [61]. First, however, we need the following definition.

Definition 2.1. Let $\{f_t\}_{t\in\mathbb{R}}$ be a family of maps in $D^0(\mathbb{S}^1)$.

(1) We say that $\{f_t\}_{t\in\mathbb{R}}$ is *positive* if: (a) $f_{t+1} = 2\pi + f_t$, for all $t \in \mathbb{R}$ and (b) If $t_1 < t_2$ then $f_{t_1}(x) < f_{t_2}(x)$, for all $x \in \mathbb{R}$;

(2) We say that the family $\{f_t\}_{t\in\mathbb{R}}$ satisfies property $\mathcal{A}$ if $f_t^q \neq R_p$ for all $t \in \mathbb{R}$, $p \in \mathbb{Z}$ and $q \in \mathbb{Z} \setminus \{0\}$.

We observe that if $f_t = R_t \circ f$, then $\{f_t\}_{t\in\mathbb{R}}$ is a positive family. If, moreover, f is a non-affine entire function, then $\{f_t\}_{t\in\mathbb{R}}$ satisfies property $\mathcal{A}$, see [47]. In particular the Arnold family is both positive and satisfies property $\mathcal{A}$, if we take $t = \omega/2\pi$ and $0 < |\alpha| < 1$. Finally we note that $\mathcal{A}$ is a generic property.

The two results we wish to consider are now formulated as propositions.

Proposition 2.2. *If $f_t = R_t \circ f$ and $\rho(t) = \rho(f_t)$ then:*

(1) $\rho(t+1) = \rho(t)$;

(2) ρ is a continuous increasing map. It is strictly increasing at t_0 if $\rho(t_0) \in \mathbb{R} \setminus \mathbb{Q}$;

(3) if $\{f_t\}_{t\in\mathbb{R}}$ satisfies the hypothesis $\mathcal{A}$, then for all $p/q \in \mathbb{Q}$, the set $\rho^{-1}(p/q)$ is an interval with non-empty interior. Moreover $\mathbb{R} \setminus int\,(\rho^{-1}(\mathbb{Q}))$ is a Cantor set.

Proposition 2.3. *For $r \geqslant 2$, let $f \in D^r(\mathbb{S}^1)$ and $\rho(f) = \rho_0$. Then there exists a set $A \subset [0,1] \setminus \mathbb{Q}$ of Lebesge measure 1, such that if $\rho_0 \in A$ then f is C^{r-2} conjugate to R_{ρ_0}. (Here $\infty - 2 = \infty$ and $\omega - 2 = \omega$.)*

2.2. Normally hyperbolic invariant circles

We show that both for small $|\alpha|$ and also for small $|\beta|$, the attractor Ω is a normally hyperbolic invariant circle. A definition of normal hyperbolicity can be found in Hirsh *et al* [29] or in Palis and Takens [45]. Indeed, for a smooth diffeomorphism $\varphi : M \to M$, where M is a compact manifold, consider an invariant submanifold $V \subset M$. One says

that V is normally hyperbolic if for each $x \in V$ there is a continuous, invariant splitting $T_x(M) = T_x(V) \oplus N_x^s \oplus N_x^u$ with the following properties. There exist constants $C > 0$, $\sigma > 1$, $r \geqslant 1$, such for every triple of unit vectors $v \in T_x(V)$, $n^s \in N_x^s$, and $n^u \in N_x^u$ and for any $k \in \mathbb{N}$

$$\frac{\|(d\varphi^k)n^u\|}{\|(d\varphi^k)v\|^r} \geqslant C\sigma^k \qquad \text{and} \qquad \frac{\|(d\varphi^k)n^s\|}{\|(d\varphi^k)v\|^r} \leqslant C^{-1}\sigma^{-k},$$

where the norms are taken with respect to some Riemannian metric. In this case one calls V r-normally hyperbolic.

It is known [29, theorem 4.1], that r-normal hyperbolicity of V implies that V is of class C^r. If we apply this to the fattened Arnold family $F_{\alpha,\omega,\beta}$, with $|\alpha| \ll 1$, we obtain the following.

Proposition 2.4. *Let us fix $0 < |\beta| < 1$ and $r \geqslant 1$. Then, there exists $\alpha_r > 0$ such that for $|\alpha| < \alpha_r$:*

(1) for all $\omega \in \mathbb{R}$ there exists an r-normally hyperbolic F-invariant circle $C_{\alpha,\omega,\beta}$ and, hence, it is of class C^r;

(2) $C_{\alpha,\omega,\beta} = \Omega$ is a global attractor.

For fixed β and r let $\bar{\alpha}_r$ be the supremum of the values of $|\alpha|$ such that $C_{\alpha,\omega,\beta}$ is r-normally hyperbolic for all $\omega \in \mathbb{R}$. If we allow r or β to vary, one has:

(3) $\bar{\alpha}_r \to 0$ as $r \to \infty$, for fixed β, while for fixed r one has $\bar{\alpha}_r \to 0$ as $|\beta| \to 1$.

Proof. We perturb from the case $\alpha = 0$. It is easy to see that $F_{0,\omega,\beta}$ has a globally attracting, hyperbolic invariant circle $C_{0,\omega,\beta}$ given by the equation $y = y_{\omega,\beta}(x)$, where

$$y_{\omega,\beta}(x) = \frac{\beta \sin(x-\omega) - \beta^2 \sin x}{1 - 2\beta\cos\omega + \beta^2}.$$

Moreover, this circle is r-normally hyperbolic for any $r \geqslant 1$. Therefore, the items (1) and (2) follow from [29, theorem 4.1].

In order to prove (3), consider a value of ω for which $F_{\alpha,\omega,\beta}$ has a fixed point with eigenvalues λ_1, λ_2, such that $|\lambda_1| < |\lambda_2|$. That this is possible follows from a direct study of $\bar{F}_{\alpha,\omega,\beta}$ (see below). If there exists a r-normally hyperbolic invariant circle, then $|\lambda_1|/|\lambda_2|^r < 1$. An easy calculation now shows that $\bar{\alpha}_r \leqslant N_r(\beta) = \min_{\omega\in\mathbb{R}} N_{r,\omega}(\beta)$, where

$$N_r(\beta) := (1 - |\beta|^{1/(r+1)})(1 - \text{sign}(\beta)|\beta|^{r/(r+1)}),$$

and $N_{r,\omega}(\beta) = (\omega^2(1-\beta)^2 + N_r(\beta)^2)^{1/2}$. This proves (3). □

Remarks.

(i) For $|\beta| < 1$ and $|\alpha| \ll 1$ the invariant circle $C_{\alpha,\omega,\beta}$ is the graph of a 2π-periodic C^r-map $g_{\alpha,\omega,\beta}$. Moreover, by the unicity of $C_{\alpha,\omega,\beta}$, one has $g_{\alpha,\omega+2\pi,\beta} = g_{\alpha,\omega,\beta}$.

(ii) One may ask whether $C_{\alpha,\omega,\beta}$ is of class C^r even if it is not r-normally hyperbolic. If $\rho(C_{\alpha,\omega,\beta}) \in \mathbb{Q}$ then it is an open property that $C_{\alpha,\omega,\beta}$ contains two periodic orbits, one consisting of sinks, the other of saddles. The invariant curve itself then consists of branches of the unstable manifolds of the saddles which meet at the sinks. Within this setting, generically the matching of the branches at the sinks is not better than C^r, where $r := \log\lambda_1^s / \log\lambda_2^s$, $1 > \lambda_2^s > \lambda_1^s > 0$ being the eigenvalues at the sinks if $r \notin \mathbb{N}$. This differentiability is not higher than $C^{r-\epsilon}$ for any $\epsilon > 0$ if $r \in \mathbb{N}$. Numerical evidence that our family (1) has these generic properties will be given in section 5.3.1.

For $\beta = 0$ the map F degenerates to an endomorphism with a critically attracting invariant circle. We want to perturb from $\beta = 0$, investigating the persistence of this circle.

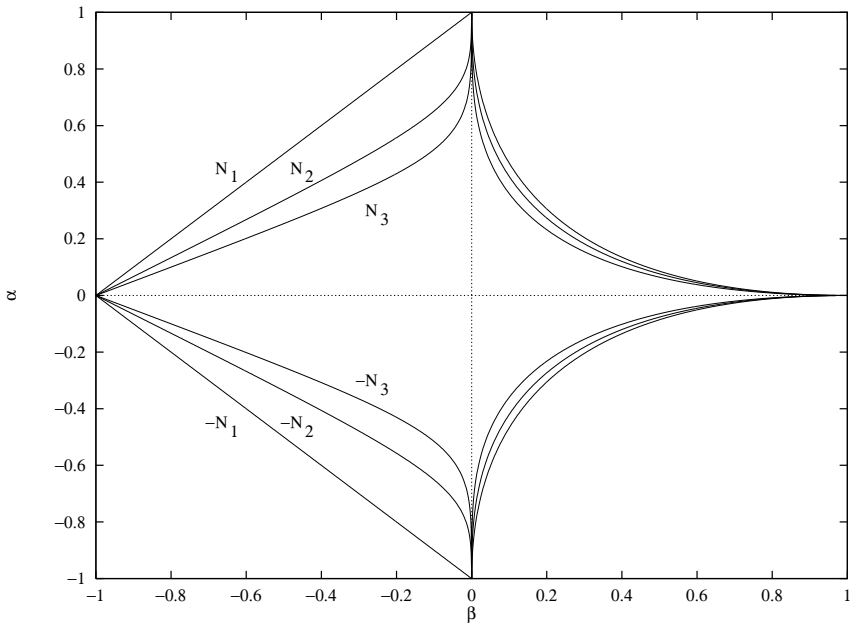

Figure 6. The curves $\alpha = \pm N_r(\beta)$, for $r = 1, 2, 3$.

Proposition 2.5. *Let $r \geqslant 1$ be given. Then for any $|\alpha| < 1$ and $|\beta|$ sufficiently small (the smallness depending on $|\alpha|$) and for all ω, there exists an invariant circle $C_{\alpha,\omega,\beta}$ of class C^r. Moreover, $C_{\alpha,\omega,\beta}$ is r-normally hyperbolic.*

Proof. We use a graph transform as in the proof of the stable manifold theorem (cf Shub [49]), only explaining the Lipschitz case. Indeed, let $\mathcal{L}_K$ be the set of 2π-periodic maps in $\mathbb{R}$ with a Lipschitz constant less than or equal to K. Then define the map $\mathcal{F} : \mathcal{L}_K \to \mathcal{L}_K$ by $\mathcal{F}(g)(x) = \beta(g(G^{-1}(x)) + \sin(G^{-1}(x)))$, where $G(x) = x + \omega + \alpha(g(x) + \sin x))$. Let $K > 0$ be such that $(K+1)|\alpha| < 1$ and $|\beta| \leqslant \frac{K}{K+1}(1 - |\alpha|(K+1))$. One can show that $\mathcal{F}$ has a unique fixed point g. By definition, the graph of g is an invariant circle. In the case $r \geqslant 1$, we have to take smaller values of $|\alpha|$ and $|\beta|$. The normal hyperbolicity is due to the persistence of the invariant circle if the map is perturbed. The final statement follows applying Mañé [33]. □

Remark. Let M_r be the subset of the (α, β)-plane bounded by N_r and $-N_r$ and containing $(0, 0)$ (cf the proof of proposition 2.4 and figure 6). By proposition 2.4, if $(\alpha, \beta) \notin M_r$, there exists a value of ω for which $F_{\alpha,\omega,\beta}$ does not have an r-normally hyperbolic invariant circle. Generically one expects that the curves $\pm N_r$ are the boundary of the set $\bar{M}_r$ of (α, β)-values, for which $F_{\alpha,\omega,\beta}$ has r-normally hyperbolic invariant circles for all ω-values. Also it seems that $\alpha = \pm N_{r,\omega}(\beta)$ form the boundary, for any given value of ω, of the α values for which there exists a r-normally hyperbolic invariant circle. As we shall see below, these expectations can be frustrated by different mechanisms. Note that the two previous propositions only ensure that $\bar{M}_r$ contains a neighbourhood of the union of the α and β axes. Moreover, from the proof of proposition 2.5, it follows that, for a fixed value

of $|\alpha|$, the optimal choice of K is $K = |\alpha|^{-1/2} - 1$ and then the bound on $|\beta|$ is given by $|\alpha|^{-1/2} + |\beta|^{-1/2} \leqslant 1$. This bound coincides with $N_1^{-1}(|\alpha|)$ for positive values of β.

We complete these general considerations by deriving a normal form for the map $F_{\alpha,\omega,\beta}$, restricted to the invariant circle $C_{\alpha,\omega,\beta}$.

Proposition 2.6. *Fixing $|\beta| < 1$ and $r \geqslant 1$, let $\bar{\alpha}_r > 0$ be as in proposition 2.4. Then, for $|\alpha|$ sufficiently small and, in any case, less than $\bar{\alpha}_r$, the restriction $F_{\alpha,\omega,\beta|C_{\alpha,\omega,\beta}}$ is smoothly conjugate to a normal form*

$$h_{\bar{\alpha},\omega,\beta}(\bar{x}) = \bar{x} + \omega + \bar{\alpha}\sin\bar{x} + \mathrm{O}(\bar{\alpha}^2),$$

where $\bar{\alpha} = \alpha H(\omega)$, $\bar{x} = x + G(\omega)$, for some function $H(\omega) \neq 0$ for all $\omega \in \mathbb{R}$, H and G being 2π-periodic functions. Moreover, $h_{\bar{\alpha},\omega,\beta}$ is a positive family with respect to ω.

Proof. First, we parametrize $C_{\alpha,\omega,\beta}$ by the x variable. It follows directly that

$$h_{\alpha,\omega,\beta}(x) = x + \omega + \alpha\left(-\frac{\beta\sin\omega}{1 - 2\beta\cos\omega + \beta^2}\cos x + \frac{1 - \beta\cos\omega}{1 - 2\beta\cos\omega + \beta^2}\sin x\right) + \mathrm{O}(\alpha^2).$$

Let $G(\omega) = \arctan(-\beta\sin\omega/(1 - \beta\cos\omega))$ (in the suitable quadrant) and $H(\omega) = (1 - 2\beta\cos\omega + \beta^2)^{-1/2}$. Then

$$h_{\alpha,\omega,\beta}(x) = x + \omega + \alpha H(\omega)\sin(x + G(\omega)) + \mathrm{O}(\alpha^2).$$

Using the maps G and H we obtain the normal form for h as desired. The second part of the proposition is a consequence of the remark following proposition 2.4 and the fact that G is 2π-periodic. □

2.3. Quasiperiodicity, smooth invariant circles

In this section we consider the case in which $|\alpha|$ is sufficiently small to ensure, by normal hyperbolicity, the existence of a smooth invariant circle. Let $h_{\alpha,\omega,\beta}$ denote the map $F_{\alpha,\omega,\beta}$ restricted to the circle $C_{\alpha,\omega,\beta}$. First, we present a result concerning to the measure of the values of the parameter ω for which the map $h_{\alpha,\omega,\beta}$ is smoothly conjugate to a rigid rotation. As we shall see, this is a way of obtaining values of the parameters (α, ω) for which the invariant circle is of class C^∞.

Proposition 2.7. *Fix $|\beta| < 1$ and $r \geqslant 2$, while $\alpha_r > 0$ is as in proposition 2.6. Also fix $|\alpha|$ sufficiently small (less than $\bar{\alpha}_r$). Then:*

(1) there exists a set $M \subset [0, 2\pi]$, of non-zero Lebesgue measure, such that for $\omega \in M$ the restriction $h_{\alpha,\omega,\beta}$ is smoothly conjugate to an irrational rigid rotation;

(2) for all $\omega \in M$, the invariant circle $C_{\alpha,\omega,\beta}$ is of class C^∞;

(3) for $\alpha \to 0$, the measure of M tends to 2π.

Proof. The starting point here is the normal form $h_{\alpha,\omega,\beta}$, obtained in proposition 2.6. Here we take $|\alpha| < \bar{\alpha}_r$, for r sufficiently large, say $r = 12$. For simplicity we omit all bars.

The first step of this proof is to obtain a further normal form for h, assuming that $\omega/2\pi$ is a diophantine number. This means that for some τ, $\gamma > 0$, for all p/q one has

$$\left|\frac{\omega}{2\pi} - \frac{p}{q}\right| \geqslant \gamma q^{-\tau}.$$

Indeed, provided this condition on ω, by successive changes of variables one obtains

$$h_{\alpha,\omega,\beta}(x) = x + \omega + f(\alpha, \beta, \omega) + \mathrm{O}(\alpha^{r+1}).$$

The idea is to expand into powers of α and to average away the x-dependence in an inductive process. Compare with Broer *et al* [9], or Broer and Takens [12].

The second step applies a finite differentiable version of the KAM theorem for families of diffeomorphisms, see e.g. [9, section 8d]. Therefore we fix $\tau = 3$ and $\gamma > 0$ in the above diophantine condition. The corresponding set of ω then contains a Cantor set of positive measure. The conclusion is that the family $h_{\alpha,\omega,\beta}$, with α fixed sufficiently small, is conjugate to a family of irrational rotations. Here the conjugacy has lost some smoothness, but is still of class C^6. In the ω-direction this smoothness is understood in the sense of Whitney.

Since the perturbation term in the above normal form is of order α^{r+1} it now follows that we can take $\gamma = \alpha^r$. The set M obtained in this way is larger than the one obtained so far with a fixed value of γ. Indeed, locally the measure of its complement in $[0, 2\pi]$ is of order α^r as $\alpha \to 0$. This proves the items (1) and (3) of our proposition.

In order to show the second item, we prove that $C_{\alpha,\omega,\beta}$ is l-normally hyperbolic for any l. Indeed, just apply the definition of normal hyperbolicity to $V = C_{\alpha,\omega,\beta}$, $\varphi = F_{\alpha,\omega,\beta}$, $N^u_x = 0$. One then has to prove that

$$\frac{\|(d\varphi^k)n^s\|}{\|(d\varphi^k)v\|^l} \leqslant C^{-1}\sigma^{-k}.$$

However, this is trivial, since $h_{\alpha,\omega,\beta}$ is at least C^1-conjugate to a rigid rotation, whence $\|(d\varphi^k)v\| \geqslant D > 0$, for some D that does not depend on k. Another application of [29, theorem 4.1] gives that the unique circle $C_{\alpha,\omega,\beta}$ must be of class C^∞. □

Remark. Our example is real analytic and one may ask whether some of the above quasiperiodic circles are also analytic. It turns out that, for small $|\alpha|$ these correspond to a similar set $\tilde{M}$, the measure of which again tends to full measure for $\alpha \to 0$. Indeed, for $\alpha = 0$ the invariant circle $C_{0,\omega,\beta}$ is real analytic, while here we have $h_{0,\omega,\beta}(x) = x + \omega$ for the restriction. Moreover, if we write $y = y_{\omega,\beta} + z$, at $C_{0,\omega,\beta}$ we obtain the normal linear form $F_{0,\omega,\beta}(x, z) = (x + \omega, \beta z)$. We now proceed similarly to in the above proof, applying the analogue of [9, theorem 4.1] for diffeomorphisms. Up to diophantine conditions with $\tau = 3$ and $\gamma > 0$, this yields a conjugacy with the family $F_{\alpha,\omega,\beta}$, again with α fixed sufficiently small. This conjugacy is of class (Whitney-) C^∞ and even analytic in x, z, β and α. Finally, by taking $\gamma = 2\alpha$, one obtains a set $\tilde{M}$ as desired, such that measure of $[0, 2\pi] \setminus \tilde{M}$ is of order α.

2.4. Periodicity, Arnold tongues

In this section we consider the periodic points of our family $F_{\alpha,\omega,\beta}$, in particular studying the corresponding organization of the (α, ω)-parameter plane. Recall that $|\beta| < 1$ was fixed. Given $p/q \in \mathbb{Q}$, we now define the Arnold tongue $I^\beta_{p/q} \subset \mathbb{R}^2$ as follows

$$(\omega, \alpha) \in I^\beta_{p/q} :\Longleftrightarrow F^q_{\alpha,\omega,\beta}(x, y) = (x + 2\pi p, y), \qquad \text{for some } (x, y) \in \mathbb{R}^2.$$

As stated earlier, this condition means that (x, y) corresponds to a periodic point of rotation number p/q. Note that this definition does not need the existence of an invariant circle. Our

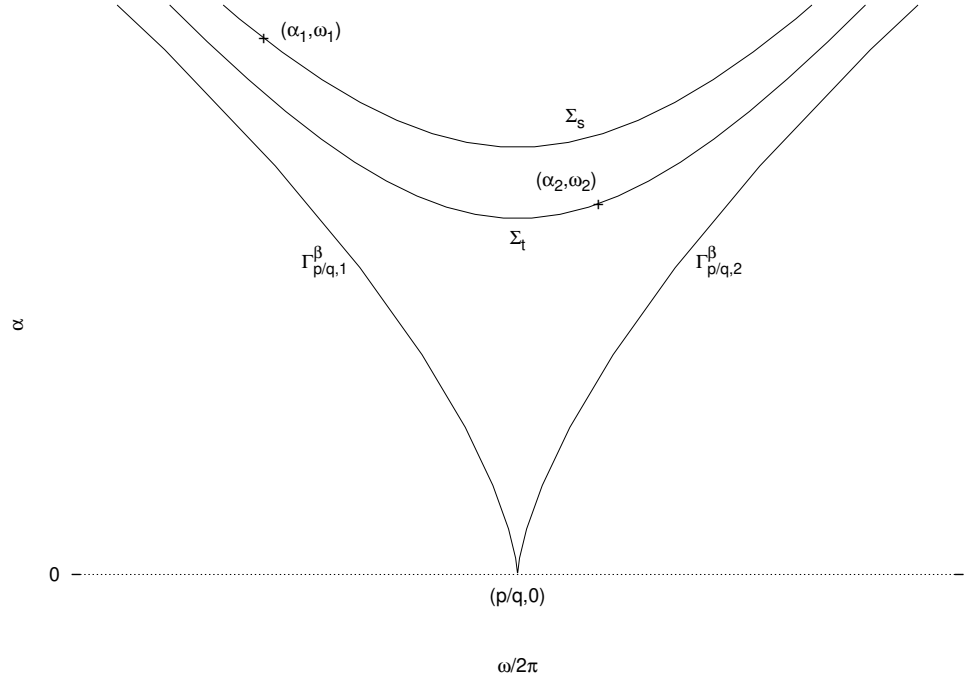

Figure 7. The structure of $I^{\beta}_{p/q}$: $C_{\alpha_1,\omega_1,\beta}$ is less differentiable than $C_{\alpha_2,\omega_2,\beta}$.

first concern is with the geometry of the tongue $I^{\beta}_{p/q}$, related to some dynamical properties. The situation is illustrated in figure 7.

We first need more detailed information about $h_{\alpha,\omega,\beta}$ than given in propositions 2.6 and 2.7. To this end we formally expand $h_{\alpha,\omega,\beta}$ and the invariant circle $y = g(x)$ to powers of α. Indeed, let

$$h_{\alpha,\omega,\beta}(x) = x + \omega + \sum_{j\geqslant 1} \alpha^j h_j(x), \qquad g(x) = \sum_{m\geqslant 0} \alpha^m g_m(x),$$

where the coefficient functions h_j and g_m are trigonometrical polynomials also depending on the parameters β and ω.

The invariance requires

$$x + \omega + \sum_{j\geqslant 1} \alpha^j h_j(x) = x + \omega + \alpha\left(\sum_{m\geqslant 0} \alpha^m g_m(x) + \sin x\right),$$

$$\beta\left(\sum_{m\geqslant 0} \alpha^m g_m(x) + \sin x\right) = \sum_{n\geqslant 0} \alpha^n g_n\left(x + \omega + \sum_{j\geqslant 1} \alpha^j h_j(x)\right).$$

From the first relation it follows immediately that $h_1(x) = g_0(x) + \sin x$ and $h_j(x) = g_{j-1}(x)$ $(j > 1)$. Inserting this into the second relation we obtain

$$\beta \sum_{j\geqslant 1} \alpha^{j-1} h_j(x) = -\sin\left(x + \omega + \sum_{j\geqslant 1} \alpha^j h_j(x)\right) + \sum_{k\geqslant 1} \alpha^{k-1} h_k\left(x + \omega + \sum_{j\geqslant 1} \alpha^j h_j(x)\right).$$

Comparing powers of α we recurrently obtain $h_1, h_2, \ldots$ which are all of the form

$$h_j(x) = \sum_{|k|\leqslant j, k-j=\dot{2}} c_{j,k} \mathrm{e}^{\mathrm{i}kx},$$

where h_j take real values whenever x is real and $\dot{2}$ denotes a multiple of 2.

Next we further simplify $h_{\alpha,\omega,\beta}$, reducing it to normal form. Indeed, let

$$h_{\alpha,\omega,\beta}(x) = x + 2\pi p/q + \delta + \sum_{j\geqslant 1} \alpha^j \sum_{|k|\leqslant j, k-j=\dot{2}} c_{j,k} \mathrm{e}^{\mathrm{i}kx},$$

where δ is small. We perform successive changes of variables of the form

$$z = x + \alpha^j \sum_{|k|\leqslant j, k-j=\dot{2}, k\neq 0} d_{j,k} \mathrm{e}^{\mathrm{i}kx} \qquad \text{if } j < q,$$

$$z = x + \alpha^q \sum_{|k|<q, k-q=\dot{2}, k\neq 0} d_{q,k} \mathrm{e}^{\mathrm{i}kx} \qquad \text{if } j = q.$$

Keeping the names h and x for the new function and variable, we obtain a normal form

$$h(x) = x + 2\pi p/q + \delta + c_1(\delta)\alpha^2 + \cdots + c_{[q/2]}(\delta)\alpha^{2[q/2]} + \alpha^q A_{p/q}(\delta)\sin(qx + \varphi_{p/q}) + \mathrm{O}(\alpha^{q+1}),$$

where $c_1, \ldots, c_{[q/2]}$ and $A_{p/q} \geqslant 0$ are analytic in δ around $\delta = 0$. The $\mathrm{O}(\alpha^{q+1})$ terms are also analytic in δ. The angle $\varphi_{p/q}$ is a suitable phase, depending on δ. By shifting the origin of x we can take $\varphi_{p/q} = 0$.

Before stating the next results we make the following conjecture.

Conjecture 2.8. *Given $0 < p/q < 1$, $(p, q) = 1$, $q > 0$, consider $A_{p/q}(\delta = 0)$ as a function of β: $A = A(p, q, \beta)$. Then for all p/q as before and $|\beta| < 1$ we have $A(p, q, \beta) \neq 0$.*

Appendix B gives support for this conjecture.

Proposition 2.9. *Assume $|\beta| < 1$ and $p/q \in \mathbb{Q}$, $q > 1$ $(p, q) = 1$, and that conjecture 2.8 holds true. Then there exists a positive constant α_0 depending on β and p/q, such that there exist two analytic curves $\Gamma^{\beta}_{p/q,i}$, of the form $\omega = \gamma_i(\alpha)$, $i = 1, 2$, with the following properties:*

(1) $\gamma_i(\alpha) = 2\pi\, p/q + \bar{c}_1\alpha^2 + \cdots + \bar{c}_{q-2}\alpha^{q-1} + \mathrm{O}_i(\alpha^q)$, for suitable constants $\bar{c}_1, \ldots, \bar{c}_{q-2}$ and $|\alpha| < \alpha_0$;

(2) for $|\alpha| < \alpha_0$, both $\gamma_1(\alpha) < \gamma_2(\alpha)$ and if $(\alpha, \omega) \in I^{\beta}_{p/q}$, then $\gamma_1(\alpha) \leqslant \omega \leqslant \gamma_2(\alpha)$.

Proof. By demanding that the qth power of h has a double fixed point we obtain

$$\delta + c_1(\delta)\alpha^2 + c_2(\delta)\alpha^4 + \cdots + c_{[q/2]}(\delta)\alpha^{2[q/2]} \pm \alpha^q A_{p/q}(\delta) + \mathrm{O}(\alpha^{q+1}) = 0.$$

From this the proposition follows because $A_{p/q} \neq 0$ by conjecture 2.8. □

Remarks.

(i) Note that from this proposition it follows that the order of contact of the tongue boundaries at the resonance p/q is of q. Even for the familiar case $\beta = 0$ (i.e. the Arnold family of circle maps) we did not find a complete proof anywhere in the literature. See also appendix B where, in particular, conjecture 2.8 is proven for $\beta = 0$.

(ii) If $A_{p/q} = 0$ the normal form must be computed to higher order. Eventually, some coefficient of $\alpha^m \sin(nqx + \varphi_{n,m})$ for $n \geqslant 1$, $m \geqslant nq$, is different from zero. Then a similar formula holds. If all of these are zero then $\gamma_1(\alpha) = \gamma_2(\alpha)$ or the difference is infinitely flat.

(iii) Compare with item (3) of proposition 2.7. The fact that the measure of the quasiperiodic ω-domain M increases to full measure as $\alpha \to 0$, is in accordance with the sharpness of the Arnold tongues.

We are now interested in the smoothness of the invariant circle, in particular how this smoothness decreases as α increases. It turns out that this occurs on curves Σ_t inside the tongues.

Proposition 2.10. *Assume $|\beta| < 1$, $p/q \in \mathbb{Q}$ and that conjecture 2.8 holds true. Then for all $|\alpha| < \alpha_0$, a positive constant depending on β and p/q, we have:*

(1) the curve $\Gamma^{\beta}_{p/q,i}$ is a line of generic fold bifurcations of the corresponding periodic orbit.

Moreover, if $0 \leqslant |\beta| < 1$, let $p_{\alpha,\omega}$ be a p/q-periodic sink with $(\alpha, \omega) \in I^{\beta}_{p/q}$. Given $t \in \mathbb{R}$, let $\Sigma_t \subset I^{\beta}_{p/q}$ be given by the equation $\operatorname{tr} DF^q_{\alpha,\omega}(p_{\alpha,\omega}) = t$. Then:

(2) Σ_t is an analytic curve, defined for t in a punctured left-hand neighbourhood of $1 + \beta^q$, for $t = 1 + \beta^q$ degenerating to $\Gamma^{\beta}_{p/q,1} \cup \Gamma^{\beta}_{p/q,2}$;

(3) these curves Σ_t analytically foliate the interior of the set $I^{\beta}_{p/q} \cap \{|\alpha| \leqslant \alpha_0\}$;

(4) the r-normally hyperbolic invariant circle $C_{\alpha,\omega,\beta}$ exists for all $|\alpha| < \alpha_0$, and r increases to ∞ as $t \uparrow 1 + \beta^q$.

Proof. The genericity of the fold bifurcation is ensured by the fact that at the saddle-nodes (folds) the second derivative of h^q equals $\pm q^3 \alpha^q A_{p/q} + \mathrm{O}(\alpha^{q+1})$.

As $\det DF^q_{\alpha,\omega}(p_{\alpha,\omega}) = \beta^q$, the trace of the sink, t, ranges below $1 + \beta^q$. Let λ_2 be the eigenvalue of the sink along the curve and λ_1 the one transversal to it. For the boundary of the domain of r-normally hyperbolic invariant circles, we must have $|\lambda_1| = |\lambda_2|^r$, $\lambda_1 \lambda_2 = \beta^q$. Hence $\lambda_2 = |\beta|^{q/(r+1)}$. Let $\bar{\delta} = \alpha^{-q}(\delta + c_1(\delta)\alpha^2 + \cdots + c_{[q/2]}(\delta)\alpha^{2[q/2]})$. Let $q\xi \in [\pi/2, 3\pi/2)$ be the approximate location of the sink (up to $\mathrm{O}(\alpha)$). Then we have $q\bar{\delta} + qA_{p/q} \sin q\xi = \mathrm{O}(\alpha)$ and $\lambda_2 = 1 + q^2 A_{p/q} \alpha^q \cos q\xi + \mathrm{O}(\alpha^{q+1}) = |\beta|^{q/(r+1)}$. Hence, we obtain for Σ_{t_r}, with $t_r = |\beta|^{q/(r+1)} + \operatorname{sign}(\beta)|\beta|^{rq/(r+1)}$, the expression

$$\bar{\delta}^2 + \left(\frac{1 - |\beta|^{q/(r+1)}}{q^2 \alpha^q} \right)^2 = A^2_{p/q} + \mathrm{O}(\alpha).$$

This curve is analytic because of the non-degeneracy and because it is obtained as a solution of the analytic system

$$F^q_{\alpha,\omega,\beta}(x, y) = (x, y), \qquad \operatorname{tr} DF^q_{\alpha,\omega,\beta}(x, y) = t.$$

Figure 8 illustrates the behaviour of the Σ_{t_r} curves, in the $(\bar{\delta}, \alpha)$ parameters, when changing r for fixed values of β and q. Along Σ_{t_r} the minimum value of α is given by $\alpha^q_{\min} = (1 - |\beta|^{q/(r+1)})/(q^2 A_{p/q})$ and $\alpha^q_{\min} \downarrow 0$ if $r \uparrow \infty$. This completes the proof of (2)–(4). □

Remarks.

(i) The assumption in proposition 2.10, for small values of α, relies on conjecture 2.8. We shall show that the hypothesis $\mathcal{A}$ also plays a role in this. For the case $\beta = 0$ (the Arnold family) it is generally only known that $I^0_{p/q} = \{(\omega, \alpha) \in \mathbb{R}^2 : \gamma_1(\alpha) \leqslant \omega \leqslant \gamma_2(\alpha)\}$, for continuous functions γ_1 and γ_2 with $\gamma_1(0) = \gamma_2(0) = 2\pi p/q$. However, these functions are analytic for $|\alpha|$ small. See Herman [26] for the case $|\alpha| < 1$ and Boyland [8] for the general non-invertible case. Moreover, by proposition 2.2, since the Arnold family satisfies the hypothesis $\mathcal{A}$, the set $I^0_{p/q}$ has non-empty interior. The hypothesis $\mathcal{A}$, for small values of α, is equivalent to either that $A_{p/q} > 0$ or that some coefficient of $\alpha^m \sin(nq\xi)$, $n \geqslant 1$, $m \geqslant nq$, is non-zero. Hence, conjecture 2.8 implies that the hypothesis $\mathcal{A}$ is true 'at the first opportunity', when just considering the terms in α^q.

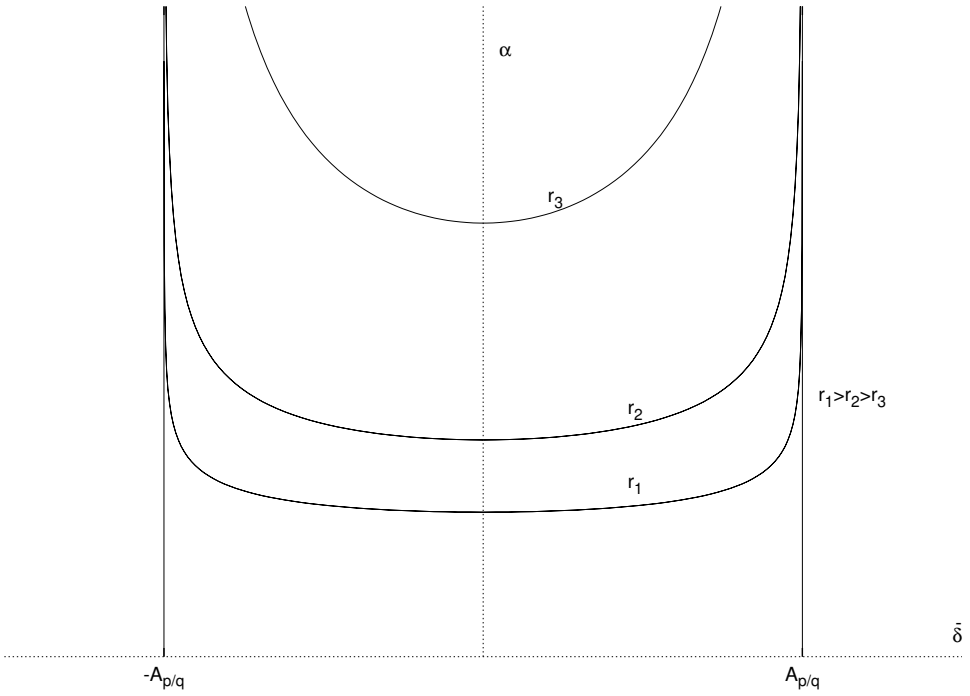

Figure 8. Some curves Σ_r in the coordinates $(\bar{\delta}, \alpha)$.

(ii) In view of the dynamics of the Arnold family $f_{\alpha,\omega}$ inside the tongues, the following is known (again see [8]). For any given value of $p/q \in [0, 1]$, there exist two smooth curves $\sigma_1, \sigma_2 : [1, \infty) \to \mathbb{R}$ such that the following holds. (a) For $\alpha > 1$, $\gamma_1(\alpha) < \sigma_1(\alpha) < \sigma_2(\alpha) < \gamma_2(\alpha)$ while (b) $\gamma_1(1) < \sigma_1(1) = \sigma_2(1) < \gamma_2(1)$, moreover (c) for $\omega \in (\gamma_1(\alpha), \sigma_1(\alpha)) \cup (\sigma_2(\alpha), \gamma_2(\alpha))$, $\alpha > 1$, the Arnold family $f_{\alpha,\omega}$ has an attracting p/q-periodic point.

(iii) Next we consider the case $\beta \neq 0$. First, it is easy to check the assumption made in proposition 2.10 for the first tongue I_0^β. For a general tongue, if β and α satisfy the hypotheses of proposition 2.4 or 2.5, there exists a globally attracting invariant circle $C_{\alpha,\omega,\beta}$. Moreover, by proposition 2.6 it follows that $F_{\alpha,\omega,\beta}$ restricted to $C_{\alpha,\omega,\beta}$ is conjugate to a positive family, which is a perturbation of the Arnold family.

The results of propositions 2.7, 2.9 and 2.10 are a starting point of our numerical continuation programme. As already stated, our main interest is how the structure of the tongues develops as $|\alpha|$ increases and how bifurcations of the periodic points and their invariant manifolds play a role in this.

2.5. On homoclinic bifurcations

The fattened Arnold family fits in a quite general perturbation programme for small values of β, the unperturbed case $\beta = 0$ corresponding to the Arnold family of circle maps. In this section we shall see how homoclinic phenomena for the 1D case translate to the 2D case.

2.5.1. Preliminaries. We explain this in a general setting. Given any one-parameter family of 1D maps f_a, we define the two-parameter family of 2D diffeomorphisms $F_{a,b}$ by

$$F_{a,b}(x, y) := (f_a(x) + y, bg_a(x, y)).$$

It is easily verified that if f_a is the logistic family and $g_a(x, y) = x$, then $F_{a,b}$ is the Hénon family. Presently our interest is in the case where $a = (\alpha, \omega)$ (meaning that a is a parameter-vector with two components) and where f_a is the Arnold family of circle maps given by $f_a(x) = x + \omega + \alpha \sin x$. If we introduce $\tilde{y} = \alpha y$, we set $g_a(x, \tilde{y}) = \tilde{y} + \alpha^{-1} \sin x$ and $b = \beta$, in which case the corresponding family $F_{a,b}$ is exactly our fattened Arnold family.

Thus, here the interest is in small values of $|b|$. In the 'unperturbed' case $b = 0$, the 2D family reads $F_{a,0}(x, y) := (f_a(x) + y, 0)$. For geometric reasons, however, it is often useful not actually to reduce to dimension 1. Compare the approach of Tatjer [57] studying the Hénon map, and of Bosch [7] in a more general case. At the level of periodic points, there is an obvious relationship between f_a, $F_{a,0}$ and $F_{a,b}$, for small $|b|$, but for the moment we shall focus on the homoclinic phenomena.

So suppose that f is a 1D map with a repelling fixed point p. We say that p has a homoclinic tangency if there exists x and n such that $f'(x) = 0$ and $f^n(x) = p$. This situation can be seen as the limiting case of a homoclinic tangency for a one-parameter family of dissipative 2D diffeomorphisms, as the dissipation tends to infinity, i.e. as $b \to 0$ (see e.g. Tatjer [57]).

Under suitable assumptions the following result holds, see Holmes-Whitley [30]. If for $a = a_0$ the map f_a has a homoclinic tangency of some saddle point, then in the (a, b)-plane, originating from the point $(a_0, 0)$, there exists a countable infinite number of homoclinic bifurcation curves γ_n, $n \in \mathbb{N}$. We shall explain this now.

2.5.2. Homoclinic tangencies coming from 1D. We first explore the various effects of tangencies in a 1D map $f = f_a(x)$ on its 'trivial' 2D extension $F_{a,0}(x, y) = (f_a(x) + y, 0)$, that is, when the parameter b is set to zero.

Although the idea of this is quite general, for simplicity we restrict ourselves to the case of the Arnold family $F_{\alpha,\omega,0}(x, y) = (x + \omega + \alpha(y + \sin x), 0)$, to be regarded as a 2D map. In view of the relevance of the fold bifurcation, we restrict the parameters to the right-hand boundary curve $\Gamma^0_{0,2}$, given by the equation $\alpha = \omega$. This leads to the one-parameter family

$$F_{\omega,\omega,0}(x, y) := (x + \omega(1 + y + \sin x), 0).$$

Let $p_\omega = (x_\omega, 0)$ be the fold fixed point of $\bar{F}_{\omega,\omega,0}$, recalling from section 1 that F is a lift of $\bar{F}$. Also write $x_{\omega,k} := x_\omega + 2\pi k$. We study this lift in order to keep track of the winding of the unstable manifold around the annulus (cylinder).

For $\epsilon > 0$, sufficiently small, the interval $[x_\omega, x_\omega + \epsilon]$ is entirely contained in the unstable manifold $W^u(x_\omega)$ of the 'ordinary' Arnold map $f_{\omega,\omega}(x) = x + \omega(1 + \sin x)$. Hereafter, we shall abbreviate $\tilde{f}_\omega := f_{\omega,\omega}$. If t parametrizes this interval, then the iterates $g_{n,\omega}(t) = \tilde{f}^n_\omega(t)$ fill up the whole of this manifold $W^u(x_\omega)$. The graph of the map $g_{n,\omega}$ gives much information on the dynamics of $\tilde{f}_\omega$.

The translation of all this for the 2D map $F_{\omega,\omega,0}$ is immediate. Indeed, for the unstable manifold $W^u(p_\omega)$ we have $W^u(p_\omega) = W^u(x_\omega) \times \{0\}$, with the interval $[x_\omega, x_\omega + \epsilon] \times \{0\}$ contained in it. Moreover, for $G_{n,\omega}(t) = F^n_{\omega,\omega,0}(t, 0)$ we have $G_{n,\omega} = (g_{n,\omega}, 0)$.

We continue by listing the various possibilities for the map $g_{n,\omega}$, thereby following the same scheme as in section 4.3 below, indicating the parameter values in the corresponding

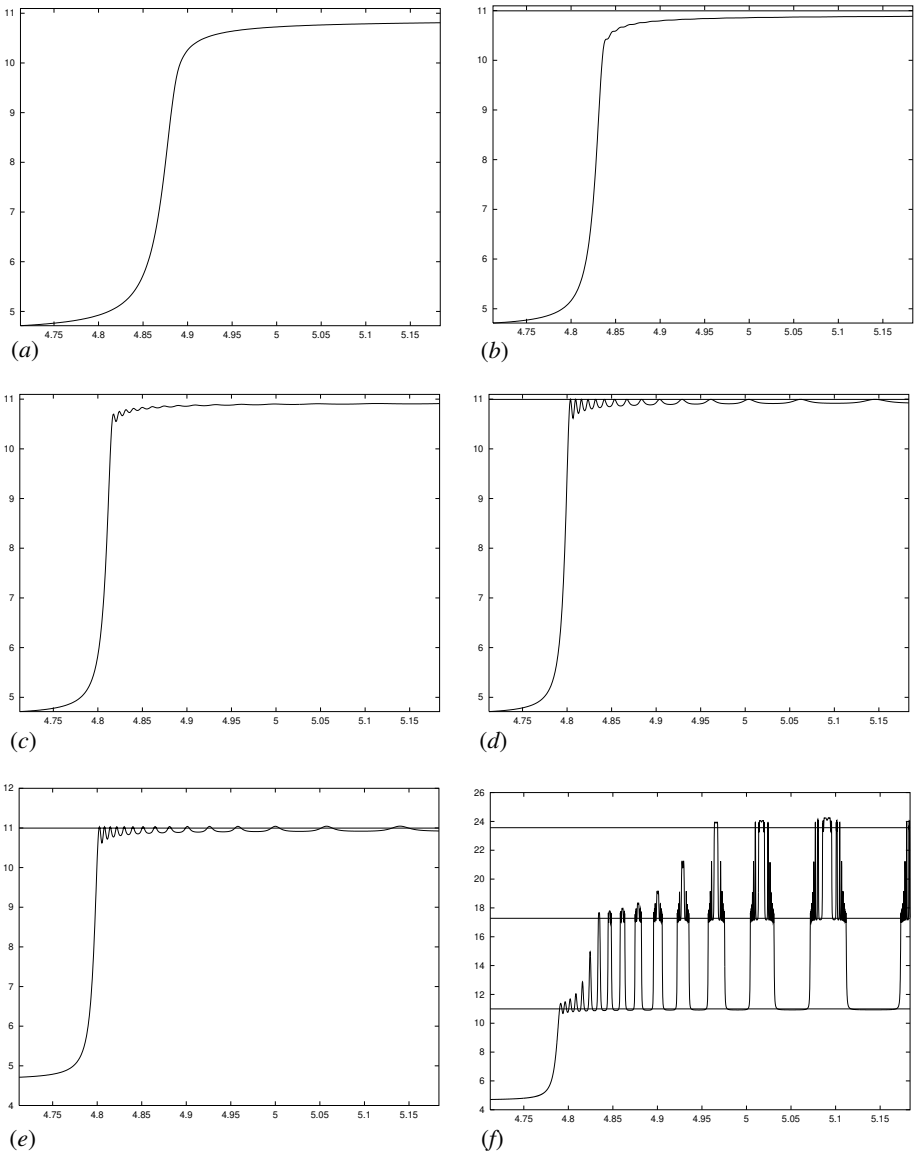

Figure 9. The map $g_{20,\omega}$ for several values of ω. The horizontal lines are given by $x = 3\pi/2+2k\pi$, $k = 1, 2, 3$. (*a*) Fold cycle: $g_{20,0.7}$, (*b*) cubic critical cycle: $g_{20,1}$, (*c*) quadratic critical cycles: $g_{20,1.2}$, (*d*) fold homoclinic tangency: $g_{20,1.380\,050\,14}$, (*e*) quadratic critical cycles: $g_{20,1.4}$ and (*f*) quadratic critical cycles: $g_{20,1.6}$.

plots, as displayed in figure 9. The whole scenario, in the transfer for $0 < |\beta| \ll 1$, certainly promises a complicated geometric structure of the unstable manifold!

(1) *Fold cycle*. By definition, for all the points $t \in (x_\omega, x_\omega + \epsilon]$, one has $g_{n,\omega}(t) \uparrow x_{\omega,1}$ as $n \to \infty$. As a consequence $x_{\omega,0} < g_{n,\omega}(t) < x_{\omega,1}$ for all n and all $t \in (x_\omega, x_\omega + \epsilon]$. Moreover, since the cycle is non-critical, we have $g'_{n,\omega}(t) \neq 0$ for all n and all $t \in (x_\omega, x_\omega + \epsilon]$. In particular this implies that the map $\tilde{f}_\omega$ is invertible, and, thererefore, this situation is only possible for $|\omega| < 1$.

(2) *Quadratic critical cycle*. The strong stable foliation $\mathcal{F}^{ss}(p_\omega)$ intersects the line $y = 0$ transversally. In order to have quadratic tangency of $W^u(p_\omega)$ with $\mathcal{F}^{ss}(p_\omega)$ it is necessary to have some point t_0 and some $n \in \mathbb{N}$ such that $g'_{n,\omega}(t_0) = 0$ and $g''_{n,\omega}(t_0) \neq 0$. Furthermore, we require that $g_{n,\omega}(t_0) \to x_{\omega,k}$, for some k, as $n \to \infty$. Since here we are not in the case of a fold homoclinic bifurcation, see below, we also have $g_{n,\omega}(t_0) \neq x_{\omega,k}$. We call this situation a k-quadratic critical cycle. Its occurrence necessarily requires $|\omega| > 1$.

(3) *Cubic critical cycle*. This case is much like the previous one. Indeed, now $g'_{n,\omega}(t_0) = g''_{n,\omega}(t_0) = 0$, while $g'''_{n,\omega}(t_0) \neq 0$. Observe that this can only occur for $|\omega| = 1$.

(4) *Fold homoclinic bifurcation*. In order to have a quadratic tangency with $W^{ss}(p_\omega)$, a point t_0 is needed and some $k > 0$, satisfying $g_{n,\omega}(t_0) = x_{\omega,k}$, while $g'_{n,\omega}(t_0) = 0$ and $g''_{n,\omega}(t_0) \neq 0$. We call this situation a homoclinic bifurcation of type k.

In figure 9 we show the graph of the map $g_{n,\omega}$ for several, increasing values of ω. Moreover, in each case the corresponding type of homoclinic behaviour is indicated. For the domain of definition of $g_{n,\omega}$ we took a large interval $J = [3\pi/2, 33\pi/20]$, with $x_\omega = 3\pi/2$ as its left endpoint. In figure 9(f) one sees that there are points x_k that, by iteration under $\tilde{f}_\omega$, accumulate at the fixed points $x_{\omega,k} = 3\pi/2 + 2k\pi$ for $k = 1, 2, 3$.

What does this mean for the invariant manifolds of p_ω? As we have seen before, for $0 < \omega < 1$ the map $\tilde{f}_\omega$ has a fold cycle, and for $\omega = 1$ a cubic critical cycle. As is suggested by figure 9(d), there exists a value $\omega_1 \approx 1.380\,050\,14$ such that $\tilde{f}_{\omega_1}$ has a fold homoclinic tangency. Moreover, if $\omega > \omega_1$, then for any $k > 0$ the map $\tilde{f}_\omega$ has a k-quadratic critical cycle.

2.5.3. Primary homo- and heteroclinic tangencies in 1D. For the sake of completeness and for later use we look in greater detail at some other facts concerning homoclinic tangencies for the Arnold family of circle maps. Given the value of the parameters (α, ω), to have a homoclinic tangency a point x_c should exist, such that:

(1) $f'_{\alpha,\omega}(x_c) = 0$;

(2) $f_{\alpha,\omega}(x_c)$ is a fixed point while x_c is not fixed;

(3) $f_{\alpha,\omega}(x_c)$ is a repellor or a fold fixed point.

Using the explicit expression for $f_{\alpha,\omega}$, the first two conditions lead to the following parametric representation of the (α, ω) couple. Let t be a real parameter ranging over $\mathbb{R} \setminus \{2\pi k, k \in \mathbb{Z}\}$. Let $\gamma(t)$ be defined as

$$\gamma(t) := \frac{t - \sin t}{1 - \cos t}. \tag{2}$$

Then one has

$$\alpha(t) = (1 + \gamma^2)^{1/2}, \qquad \omega(t) = t - \gamma(t). \tag{3}$$

Note that the excluded set in the range of t corresponds to unbounded values of the parameters (except for the trivial case $t = 0, \alpha = 1, \omega = 0$). Different t-intervals of the form $(2k\pi, 2(k + 1)\pi)$ correspond to different fixed points. The values of t for which one has a homoclinic tangency to a fold fixed point are obtained by setting $|\omega| = \alpha$. This gives for t the very simple condition $t = 2 \arctan t$.

Figure 10 shows the values of (α, ω) obtained by using (2) and (3). Note that not all of these values satisfy the third condition above. If $k \geqslant 0$ in the range $(2k\pi, 2(k + 1)\pi)$ the value t_k leads to a homoclinic tangency of a fold fixed point. For $t \in (t_k, 2(k + 1)\pi)$ one has a homoclinic tangency of a saddle, while for $t \in (2k\pi, t_k)$ a heteroclinic tangency occurs, since a branch of the unstable manifold of the saddle is tangent to the strong stable manifold of the node. Different values of k produce unstable manifolds which perform a different number of windings before tangency. It is similarly true for negative values of k.

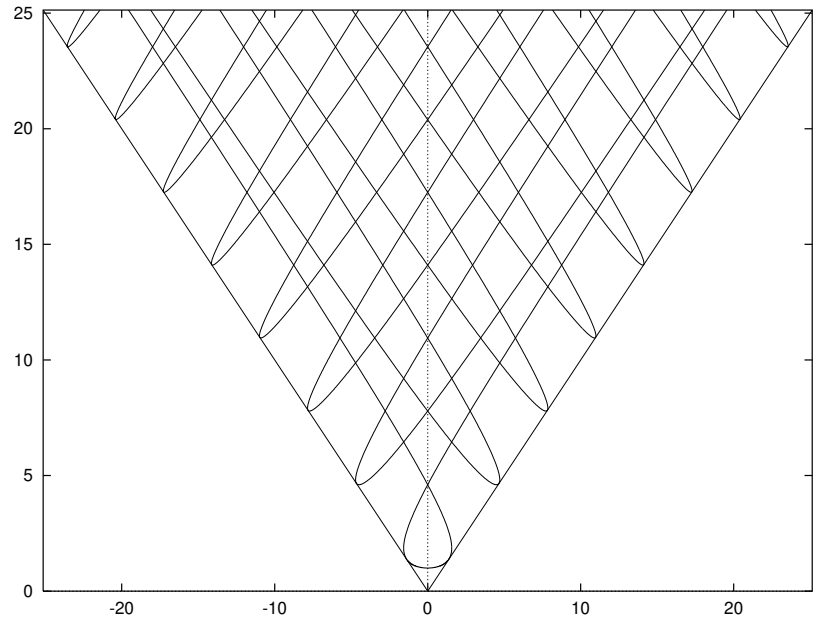

Figure 10. Curves of primary homo- and heteroclinic tangency in the (ω, α) plane for the Arnold circle map.

This whole discussion refers to 'primary' tangencies, in the sense that the image of the critical point x_c of $f_{\alpha,\omega}$ is a fixed point.

Hereafter, we shall confine our attention to the first component of the curve displayed in figure 10, that is, we restrict t to the interval $(-2\pi, 2\pi)$. For $t = 0$ one obtains the point $\alpha = 1, \omega = 0$. The values corresponding to $t \in (-2\pi, -t_0)$ will be denoted as $T_0^{1,0}$. Those for $t \in (t_0, 2\pi)$ will be denoted as $T_0^{2,0}$. Finally, for $t \in (-t_0, t_0)$, excluding the degenerate case $t = 0$, we shall use the notation $\bar{T}_0$.

In figure 11 we depict the curves $\Gamma_{0,i}^0$ and $T_0^{i,0}$. The broken curve $\bar{T}_0$ is the continuation of the curves $T_0^{i,0}$ when the fixed point is attracting. Moreover, we have drawn the curve C_0 of values of the parameters for which the unstable invariant manifold of the repellor has a cubic tangency with the strong stable foliation.

The idea behind this is that, when transferring from the 'trivial' 2D situation to the 'perturbed' case with $|\beta|$ small, we remain on a fold line throughout.

To this end we have to (re-)introduce the parameter β in our considerations, so obtaining maps which can be denoted by $G_{n,\omega,\beta}$. Several remarks are now in order. First, this map is differentiable with respect to the parameters. Second, e.g. see [39], there exists a strong stable foliation $\mathcal{F}^{ss}(p_{\omega,\beta})$ with leaves that are at least C^1. We note that we do not need more differentiability in order to define quadratic and cubic tangency, with respect to the foliation, at least in the topological sense. Third, both $\mathcal{F}^{ss}(p_{\omega,\beta})$ and the strong stable invariant manifold $W^{ss}(p_{\omega,\beta})$ depend continuously on β in the C^1 topology. The latter statement follows from Perron's existence proof (cf [44]).

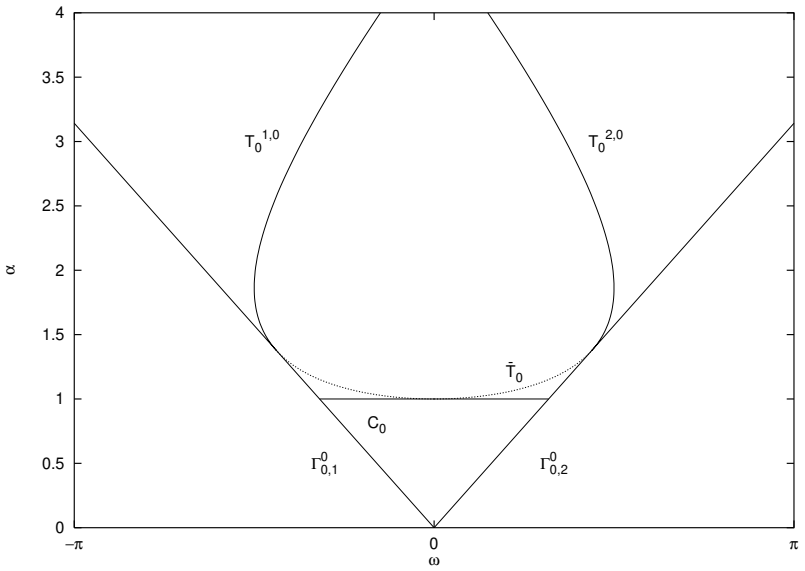

Figure 11. Homoclinic bifurcation curves in I_0^0.

3. Scenarios to complicated dynamics

We discuss various theoretical mechanisms by which the dynamics gets more complicated when the parameter α becomes larger. At first we are concerned with the destruction of the invariant circle. For related numerical studies, see Aronson *et al* [3], Feigenbaum *et al* [20] and Ostlund *et al* [43] (also cf Broer *et al* [10]). The second subject deals with the onset of chaos. (For bibliographical references see below.) We also note that all the possibilities sketched in this section occur in our example of the fattened Arnold family.

3.1. Loss of smoothness and destruction of invariant circles

In view of the destruction of the invariant circle, several theoretical scenarios are possible. One scenario involves the transition, on the circle, from a node to a focus. At this moment the circle only persists as a continuous curve. Briefly before the focus comes into existence, the eigenvalues of the node approach each other, until they coincide at the moment of transition. Let us discuss the differentiability of the invariant circle at the node. Generically this order is given by

$$\log|\lambda|/\log|\mu|,$$

where λ and μ denote the minimum and maximum eigenvalues (in absolute values) at the node. An exception occurs when the quotient is an integer, say n. The resonance between the eigenvalues gives rise to logarithmic terms in the local equation of the invariant circle, implying that this curve is only $(n-\epsilon)$-times differentiable for any positive value of ϵ. Hence, variation of a parameter will induce a gradual loss of differentiability.

After creation of the focus, the invariant circle is just continuous (note that the length is finite). In this form it can persist until a period-doubling bifurcation occurs (then the length would be infinite). However, in principle, up to the value of the parameter for which the flip occurs (with this value include) it can be homeomorphic to S^1. Before that it could

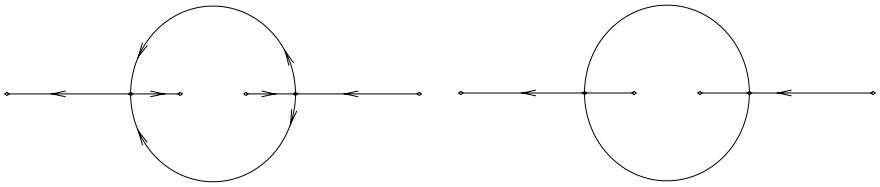

Figure 12. Typical transition in $\mathbb{C}$ of the eigenvalues at an attracting point in the orientation-preserving (left) and reversing (right) cases. The transition is from the fold to the flip, following the arrows.

already be destroyed by heteroclinic tangencies. Figure 12 displays the transition from fold to flip regarding the eigenvalues in the complex plane. The orientation-reversing case is simpler, since then the eigenvalues are always real.

Another possible scenario involves the occurrence of a cubic tangency between an unstable manifold with the strong stable foliation of a node or fold (saddle node), again yielding an invariant circle that is only continuous (see, e.g. figure 13(a), which refers to the fattened Arnold family).

In this case, at the moment of bifurcation, there is a sudden loss of differentiability, from C^r to C^0. It may even occur that, if the invariant circle consists of two branches of periodic saddles, both of these enter the node from the same side. Now we refer to figures 13(c) and (d). The reader can easily imagine intermediate cases. For instance consider figure 13, in which there is an occurrence of transversal intersections of the unstable manifold of the saddle and the strong stable manifold of the node (between (b) and (c) above), quadratic tangencies with the strong stable foliation of the node (between (c) and (d) above) or without any tangency with the mentioned foliation (between (d) and (e)). After such a cubic tangency, a homoclinic tangency may occur. In that case, the circle, which up to then persisted only as a continuous curve, is destroyed.

Depending on the region of the parameters these scenarios all seem to show up in this problem of the fattened Arnold family, as can be seen from figures 13(e) and (f), also see section 5.3. Similar situations are found in the case $\beta < 0$ as displayed in figure 14. In figures 15 and 16 similar pictures are given for the fold cases.

Another important point is what happens after the *last* homoclinic tangency. This behaviour is displayed in figure 15(e), for the fold case. In this problem such a tangency only occurs for positive β. Indeed, after the tangency the whole scenario is in some sense reversed. We mean that the unstable manifold of the saddle can, in turn, have a cubic tangency to the stable foliation of the same saddle. In that case a smooth invariant circle may be born (see the passage in figure 17 from the case (c) to (d)). The difference with the above scenario is that the rotation number of this curve changes with the parameter, while in the earlier case it had a fixed rational value. This curve can again be destroyed in various ways. Between the *first* and *last* homoclinic tangencies several interesting phenomena occur, with creation and destruction of sinks and the subsequent accumulation of 'secondary' fold curves. Also see the end of sections 4.3 and 5.3.2.

From proposition 2.7 and the previous considerations, we expect that the subset of the (α, ω)-plane, where the circle $C_{\alpha,\omega,\beta}$ is of class C^r, but not of class C^{r+1}, has a complicated geometry. This also holds for the boundary of the total parameter domain of invariant circles.

A matter which is not quite understood is how the quasiperiodic circles disappear into Denjoy or Aubry–Mather sets. It is suspected that some *obstruction phenomenon* as in the conservative case (see [42]) plays an important role.

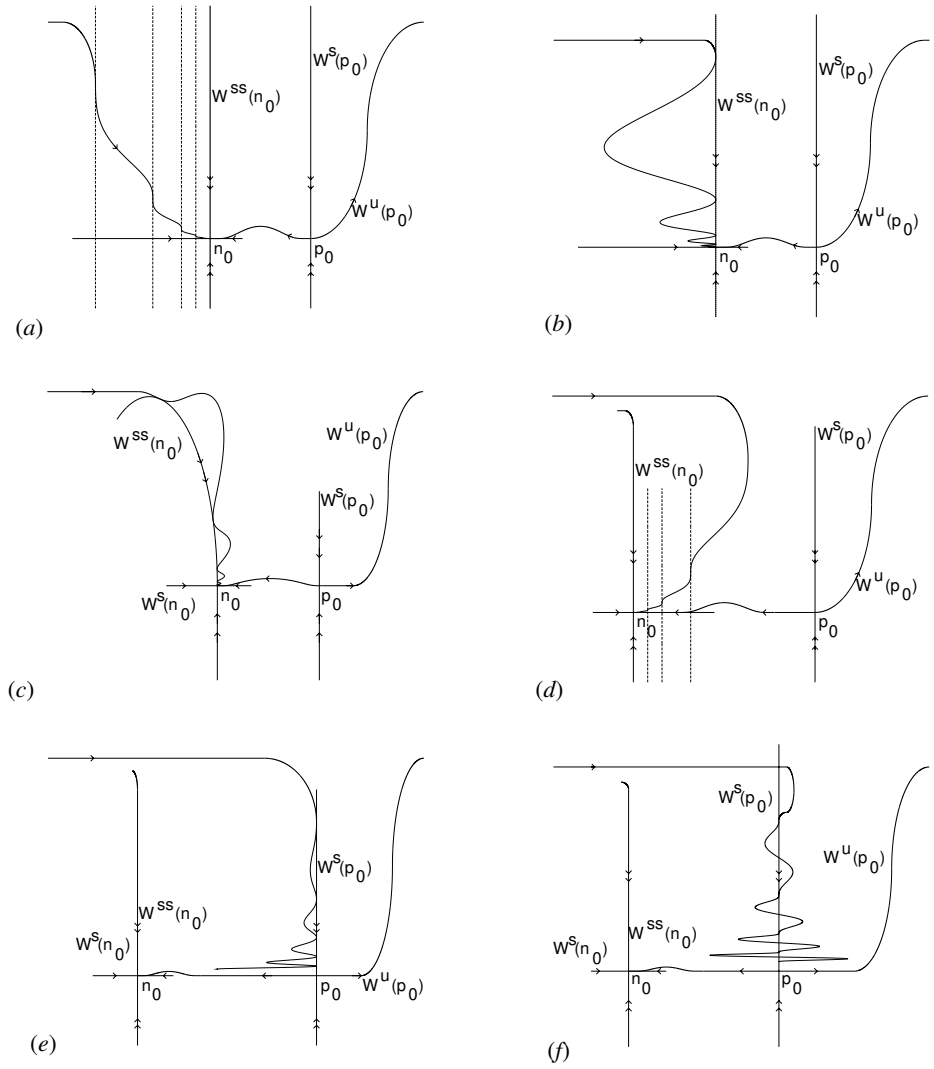

Figure 13. Some configuration of the invariant manifolds of a saddle for values of the parameters near a fold bifurcation. Case $\beta > 0$. (*a*) Left cubic tangency to $\mathcal{F}^{ss}$, (*b*) left quadratic tangency to W^{ss}, (*c*) right quadratic tangency to W^{ss}, (*d*) right cubic tangency to $\mathcal{F}^{ss}$, (*e*) left quadratic tangency to W^s and (*f*) cubic tangency to W^s.

3.2. Birth and death of chaos

Consider again the above scenarios by which the invariant circle loses differentiability. We claim that in both cases strange attractors (and chaos) can be brought about.

In the first scenario a node turns into a focus. After this the eigenvalues can go to the negative half-plane, where one of them can 'cause' a flip bifurcation (see figure 12). After this bifurcation the invariant circle, should have 'infinite length' and, furthermore, it is not homeomorphic to S^1. Then, repetition of a flip may lead to a cascade: a familiar method for obtaining chaos. This is exactly the mechanism that creates the Hénon attractor (cf Simó

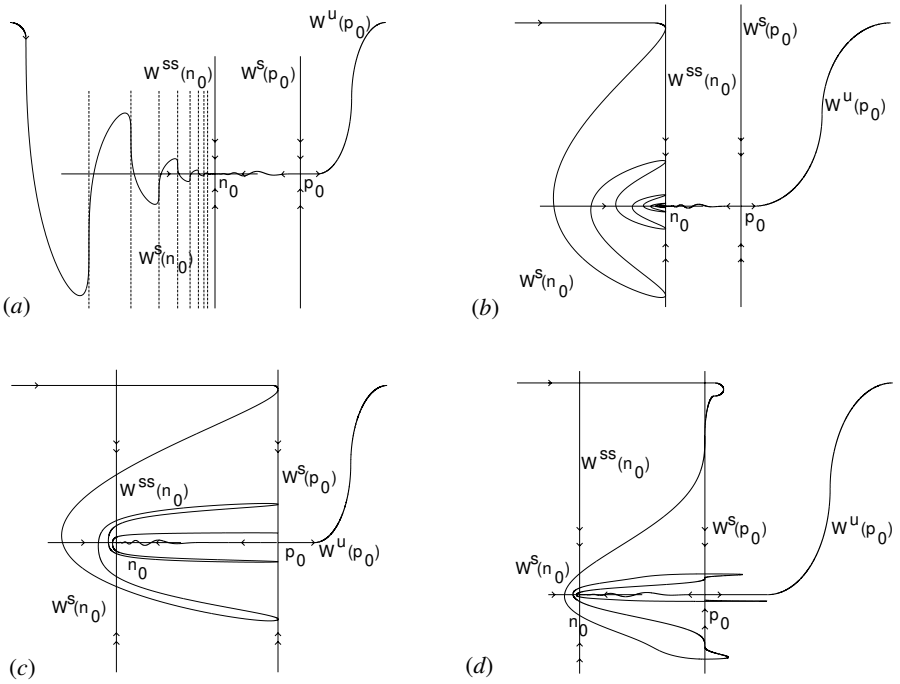

Figure 14. Some configurations of the invariant manifolds of a saddle for values of the parameters near a fold bifurcation. Case $\beta < 0$. (a) Cubic tangency to $\mathcal{F}^{ss}$, (b) quadratic tangency to W^{ss}, (c) quadratic tangency to W^s and (d) cubic tangency to W^s.

[50], Benedicks and Carleson [5], Palis and Takens [45], Mora and Viana [36] and Tatjer [57, 56]).

In the second scenario, involving the behaviour of the unstable manifold of the saddle and tangencies to stable manifolds or foliations, different kinds of attractors can occur. After a quadratic homoclinic tangency related to the saddle (that, for definiteness, we assume takes place to the left of the stable manifold), if one has transversality, a small piece of the unstable manifold goes to the right of the stable manifold. The situation is similar to the Hénon case. Theoretically one can expect creation of periodic orbits and then again the flip cascade and a usual road to chaos (see figures 17(a) and (b)). But the strange attractors created in this way should be named 'small' attractors. Suppose, however, that the 'last homoclinic tangency' occurs, i.e. that the unstable manifold completely goes to the right of the stable manifold of the saddle (or the fold), two quadratic tangencies occur with the stable foliation, see figure 17(b). This can again give rise to periodic orbits, but also to 'large' strange attractors. There is no way to avoid the 'folds' of the unstable manifold, and if this one accumulates to some invariant set, this set will inherit a similar 'folding'. It is only after a possible cubic tangency to the stable foliation when one can recover a smooth invariant curve (see figure 17(d)). Both types of phenomena occur inside an Arnold tongue. Another possible situation appears when one has quadratic tangencies to the strong stable foliation in the saddle-node case (to the left of the stable manifold) and a perturbation destroys the periodic orbit. Then again 'large' attractors may occur, but the parameters are outside the Arnold tongue (cf Díaz *et al* [19], Viana [60]). An illustration of this last situation is shown in figure 4, section 1.

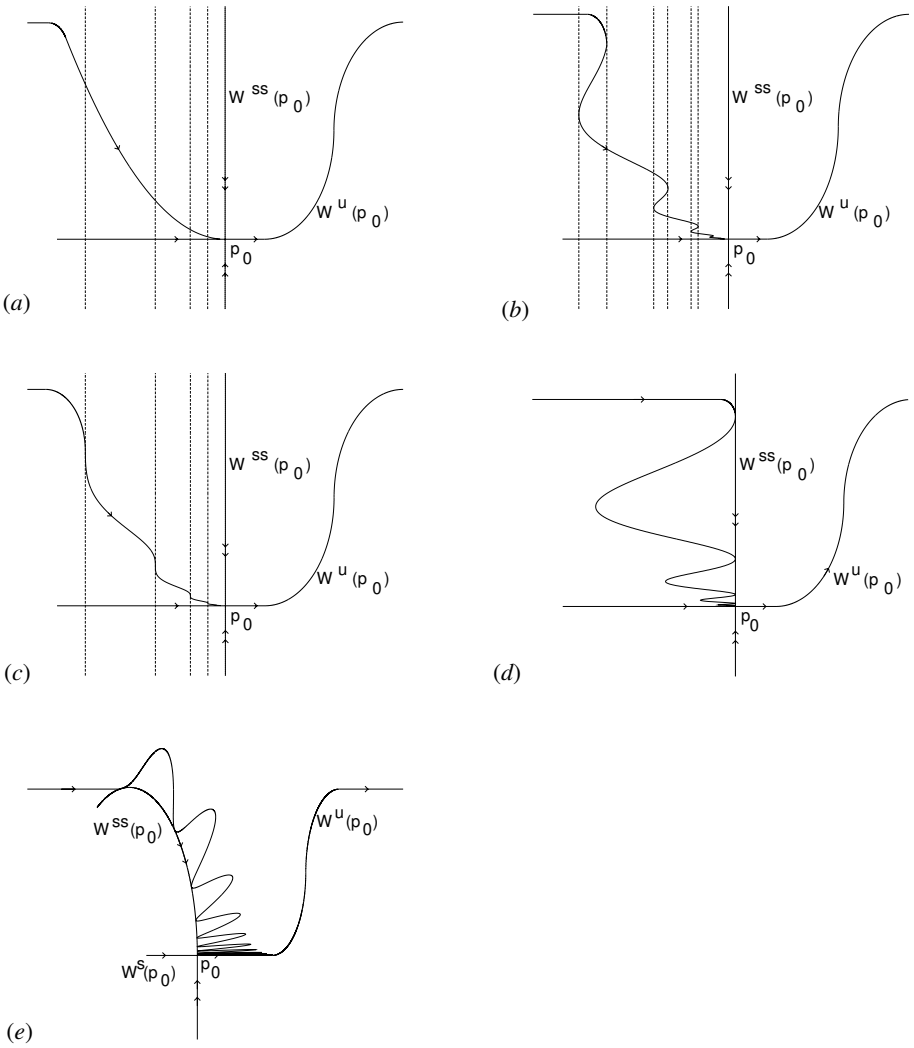

Figure 15. Several configurations of the invariant manifolds of a saddle-node fixed point. Case $\beta > 0$. (*a*) Fold cycle, (*b*) quadratic critical cycle, (*c*) cubic critical cycle, (*d*) fold homoclinic tangency and (*e*) fold homoclinic tangency from outside.

There is a simple way to see why in our case 'small' strange attractors do occur in some extreme situation. Indeed, we carry out the following change of variables and parameters on the map $F_{\alpha,\omega,\beta}$:

$$x = \frac{1}{\omega}\bar{x} + \frac{3}{2}\pi, \qquad y = \frac{1}{\omega^2}\bar{y} + \frac{\beta}{\beta - 1}, \qquad \alpha = \omega(1-\beta) + \frac{\gamma}{\omega},$$

where we transform (x, y) into $(\bar{x}, \bar{y})$ and (α, β) into (γ, β). The new map reads

$$\begin{pmatrix} \bar{x} \\ \bar{y} \end{pmatrix} \mapsto \begin{pmatrix} \bar{x} + \bar{y}(1-\beta) + (1 - \cos(\bar{x}/\omega))\omega^2(1-\beta) + \gamma(\bar{y}/\omega^2 - \cos(\bar{x}/\omega) + \beta/(\beta-1)) \\ \beta(\bar{y} + (1 - \cos(\bar{x}/\omega))\omega^2) \end{pmatrix}.$$

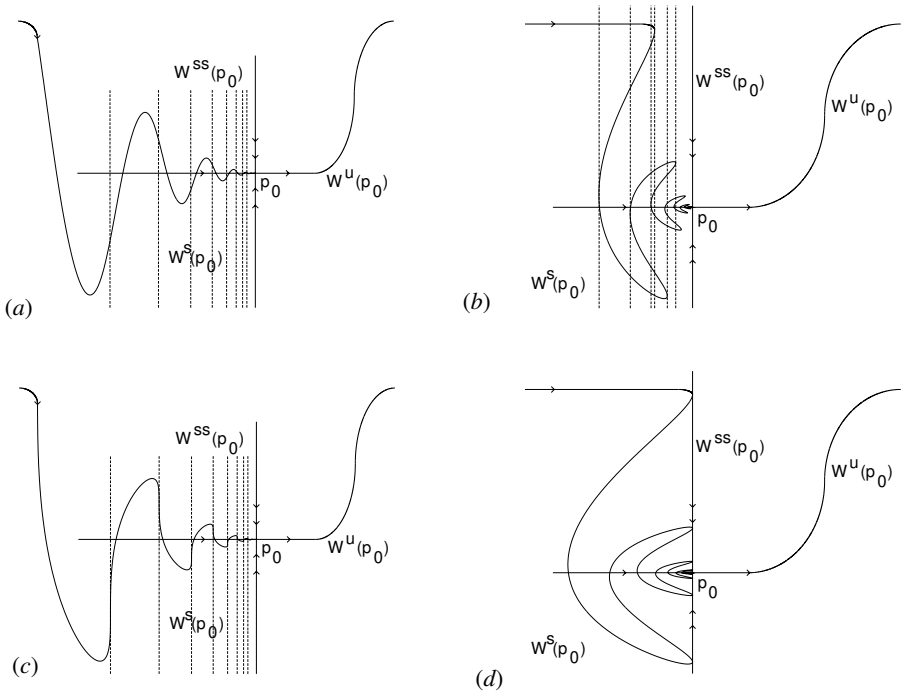

Figure 16. Several configurations of the invariant manifolds of a saddle-node fixed point. Case $\beta < 0$. (*a*) Fold cycle, (*b*) quadratic critical cycle, (*c*) cubic critical cycle and (*d*) fold homoclinic tangency.

It is easy to see that for $\omega \to \infty$ this map tends to

$$\begin{pmatrix} \bar{x} \\ \bar{y} \end{pmatrix} \mapsto \begin{pmatrix} \bar{x} + \bar{y}(1-\beta) + \frac{1}{2}(1-\beta)\bar{x}^2 - \gamma(\frac{\beta}{1-\beta} + 1) \\ \beta(\bar{y} + \frac{1}{2}\bar{x}^2) \end{pmatrix}.$$

So, the map under study can also be related to the Hénon map in a limit case. Then, using the results of Benedicks and Carleson [5] and Mora and Viana [36], we obtain the following.

Proposition 3.1. *There exist $\beta_0 > 0$ and $\omega_0 > 0$ such that if β and ω satisfy $|\beta| < \beta_0$ and $|\omega| > \omega_0$, then there is a subset $A \subset \mathbb{R}$ of positive measure such that, for all $\alpha \in A$ the map $F_{\alpha,\omega,\beta}$ has a strange attractor. Moreover, if $\alpha \in A$ then $\alpha = \mathrm{O}(\omega)$ and $|A| = \mathrm{O}(1/\omega)$.*

Remark. Note that the 'small' strange attractors as found in [45] occur in a different parameter domain.

3.3. On genericity

At this point it is appropriate to add some remarks on genericity. When dealing with a concrete example, one can always ask whether it has a given generic property or not. As an example consider the Kupka–Smale property, requiring that all periodic points are hyperbolic, while their stable and unstable manifolds meet only transversally. The C^r-theory ($r \geqslant 1$) is reviewed in Palis and de Melo [44]. For a real analytic analogue see Broer and Tangerman [13].

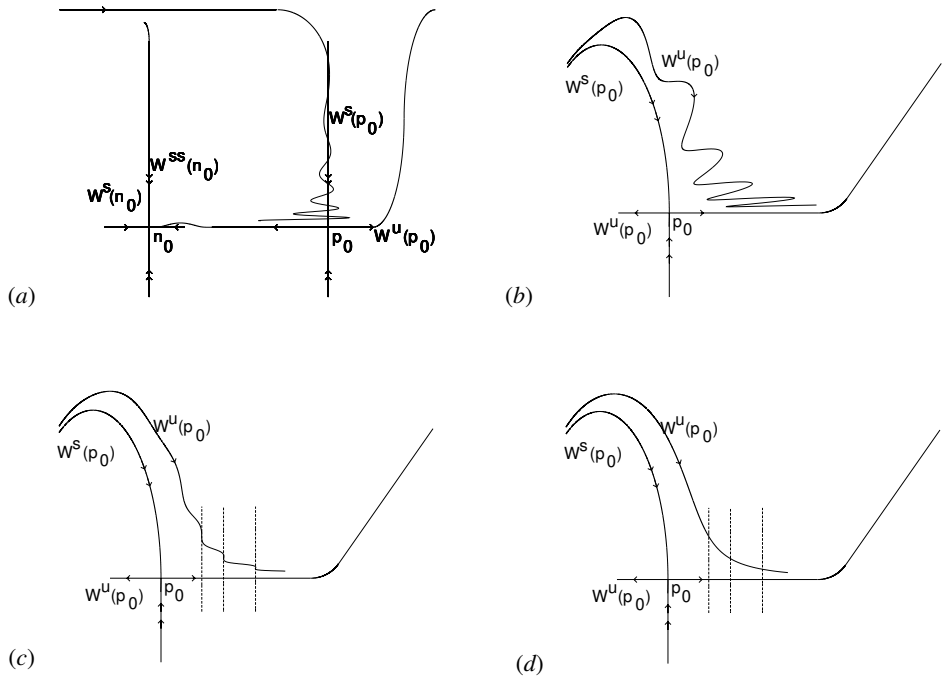

Figure 17. Several configurations of the unstable manifold of a saddle fixed point with respect to the stable manifold. Case $\beta > 0$. (The case $\beta < 0$ is not given.) (*a*) Just after inner (first) tangency, (*b*) just after external or outer (last) tangency, (*c*) cubic external tangency and (*d*) after the cubic external tangency.

It may be clear that for any given system such a property is almost impossible to verify. A similar situation to that which we met when considering the generic property $\mathcal{A}$ for circle maps. In general, the problem is that an infinitude of checks has to be made. However, note that in both of the above properties, any reasonable, finite amount of such checks in principle can be made with the help of a computer (cf appendix B).

In this predicament our approach is simply to assume 'genericity', or rather 'persistence', of the example in some wide sense, and to interpret the numeric evidence from this. Below, in some cases symbolic and numeric checks for such assumptions are made.

In view of the generic phenomena mentioned in this paper, in particular bifurcations and scenarios for transition to chaos, we repeat that all of these seem to occur in the fattened Arnold family under consideration.

We recall that our example $F_{\alpha,\omega,\beta}$, for $\alpha = \beta = 0$, boils down to the family of rigid rotations $x \mapsto x + \omega$ (cf the original Arnold family). This degeneracy even has codimension ∞. Nevertheless, as we saw above, the property that quasiperiodic dynamics occurs with positive measure in the parameter space, is persistent. Another special feature of our example is that y only occurs in a linear way. At the moment, beyond simplifying the normal-form computations, are not clear to us the consequences of this fact.

We close this section by listing a few other properties that play a role in this respect.

(1) Consider the normally hyperbolic invariant circle $C_{\alpha,\omega,\beta}$ as before. Generically r-normal hyperbolicity implies that the circle only is of class C^r, but in exceptional cases the circle may be C^∞, or even analytic. These exceptions are again degenerate of codimension

∞. Also in this case certain numerical checks can be made, at least partially, see below.

(2) Our example depends on the parameters α, ω and β. As said earlier, we mostly keep β fixed, unfolding with the pair (α, ω). Apart from the degeneracies occurring at $\alpha = 0$, see above, one expects that our map is 'Kupka–Smale as a family'. Among other things this means that only generic codimension 2 bifurcations occur. In section 4 we shall explore various theoretical possibilities of this.

4. A theoretical survey of bifurcations

In this section we briefly review some generic bifurcation theory as far as relevant for our purposes, namely for interpreting the numerical output concerning the fattened Arnold family. We consider elements from the local theory and from the global theory of homoclinic bifurcations.

4.1. Local bifurcations

We start with the bifurcations of periodic points in 2D maps, looking for codimension 1 and 2 phenomena, where a restriction is given by the dissipation. This leaves us with the fold, the flip, the cusp and the codimension two flip, while, for example, Hopf bifurcations are excluded. Particularly various semiglobal scenarios near the cusp will have our attention. For simplicity, all considerations will be held only for the case of fixed points.

So let $f_{a,b} : M \to M$ be a general two-parameter family of diffeomorphisms of a surface M. Assume that for $(a, b) = (a_0, b_0)$ the map has a fixed point $p_0 \in M$. Since our interests are local, we may assume that $M = \mathbb{R}^2$, for simplicity putting $(a_0, b_0) = 0 = p_0$. Let λ and μ be the eigenvalues of $Df_0(0)$. By dissipation at least one of the eigenvalues is inside the complex unit disk. Hereafter we may assume that $|\lambda| < 1$, non-hyperbolicity of the fixed point then meaning that $|\mu| = 1$, and hence, $\mu = 1$ or $\mu = -1$.

4.1.1. The cases of codimension not exceeding 2. First we consider the generic codimension 1 bifurcations. The corresponding cases are the well known fold ($\mu = 1$) and flip ($\mu = -1$). For a description of fold and flip, see, for example, Guckenheimer and Holmes [25], Devaney [18] or Newhouse *et al* [39]. We only recall that there are two possible classes of flip bifurcations: (a) subcritical, where one node of period 1 becomes a saddle and there appear two nodes of double period, and (b) supercritical where one saddle of period 1 becomes a node and there appear two saddles of period 2. Explicit necessary and sufficient conditions for their occurrence in this 2D case can be found in Tatjer [57] and Carcassès *et al* [16]. We recall that in the 2D parameter space these cases correspond to smooth curves, while the bifurcations occur upon transversal crossing of these.

Next we turn to the less well known, generic codimension 2 cases. These bifurcations occur in isolated points of the parameter plane. The only possibilities now are the so-called cusp ($\mu = 1$) and the codimension 2 flip ($\mu = -1$). Here dissipation excludes, among other things, the Bogdanov–Takens bifurcation.

We shall now give a brief outline of the two cases. For details, also concerning the explicit conditions for occurrence in 2D maps, we refer to [57, 16].

(1) *The cusp bifurcation.* As a representative example we consider $f_{a,b}(x, y) = (\lambda x, b + (1 + a)y \pm y^3)$, for some $\lambda \in \mathbb{R}$, $0 < |\lambda| < 1$, either positive or negative. The bifurcation diagram is given in figure 18. Here we exhibit the fixed points and their invariant manifolds, where arrows indicate the sense of the dynamics: more arrows signifying stronger attraction, namely repulsion.

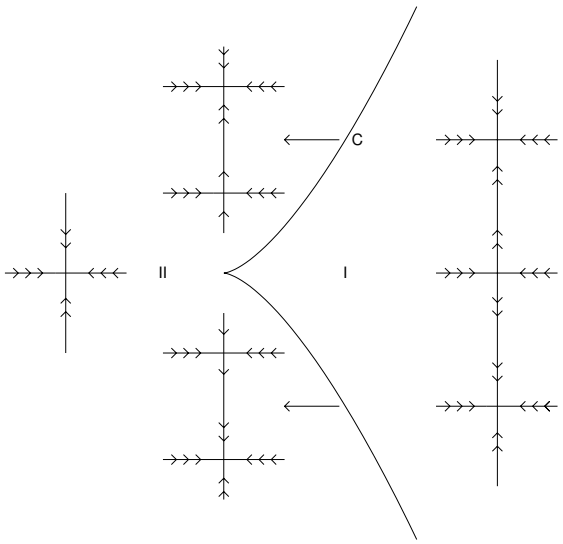

Figure 18. Bifurcation diagram of the cusp. More arrows indicate a stronger eigenvalue. The horizontal (vertical) axis corresponds to variable a (b). The cusp is at the origin and C denotes the saddle-node locus.

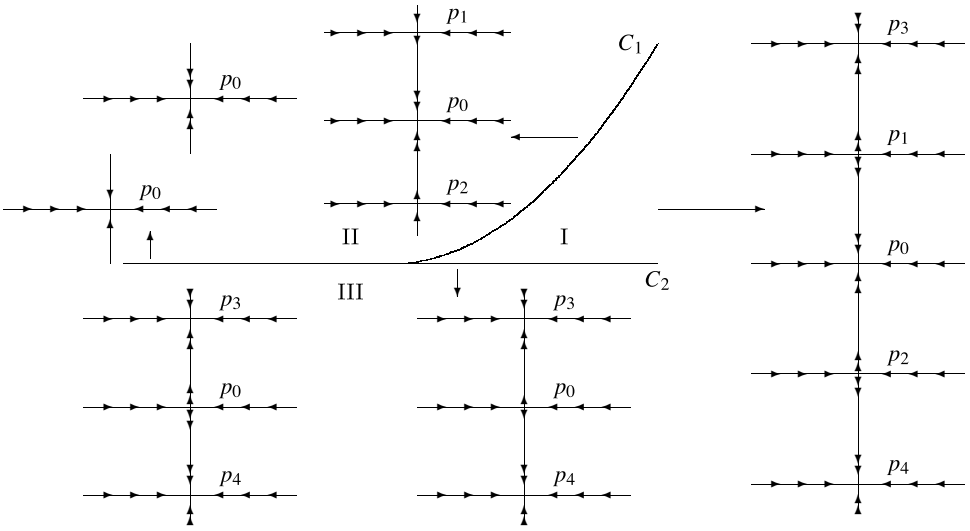

Figure 19. Bifurcation diagram of the codimension 2 flip. The point p_0 is fixed, whereas p_1, p_2, p_3, p_4 are 2-periodic: $f_{a,b}(p_3) = p_4$ and $f_{a,b}(p_1) = p_2$. More arrows indicate a stronger eigenvalue. The a and b axes are as in the previous figure. The codimension 2 flip is located at the origin.

(2) *The codimension-2 flip bifurcation*. Here a representative example is given by $f_{a,b}(x, y) = (\lambda x, (1 + a)y + by^3 \pm y^5)$. For a bifurcation diagram, see figure 19. Upon crossing of the curve C_1 into region II, the 2-periodic orbits disappear by a fold bifurcation of period 2. Therefore in region II only the sink p_0 remains. The crossing from region

I into region III over the curve C_2 gives a collapse of p_0, p_1 and p_2 into the fixed point saddle p_0. This happens in a flip bifurcation of fixed points.

Remark. The equations for the periodic point in the product of phase space and parameter space, with coordinates (x, y, a, b), determine a submanifold of codimension 2. In Carcassès *et al* [16, 17] the geometry of this submanifold is shown near a cusp and a codimension 2 flip.

4.1.2. Organization of the parameter plane near a cusp. One natural question arising from the previous section is as follows. How is the organization of the bifurcation curves near a cusp? Below we shall see how to obtain several possibilities for this.

Hereafter, we assume that we have a two-parameter family of smooth maps $f_{a,b} : V \subset \mathbb{R}^k \longrightarrow \mathbb{R}^k$, where $k = 1$ or $k = 2$, and V is an open set, where $(a, b) \in U \subset \mathbb{R}^2$ also open. First, we need to introduce the concept of generalized eigenvalue and of the level sets associated to such an eigenvalue.

Definition 4.1. Suppose that $S \subset U \times V$ is a regular surface, such that for $(a, b, x) \in S$, $f_{a,b}(x) = x$ holds, where $x \in \mathbb{R}^k$. Given $\lambda \in \mathbb{R}$, the level set of λ with respect the surface S is:

$$L_\lambda(f, S) = \{(a, b, x) \in S | \Lambda(a, b, x) = \lambda\},$$

where

$$\Lambda(a, b, x) = \begin{cases} \dfrac{\operatorname{tr} Df_{a,b}(x)}{\det Df_{a,b}(x) + 1} & \text{for } k = 2 \\ f'_{a,b}(x) & \text{for } k = 1. \end{cases}$$

$\Lambda(a, b, x)$ is called the generalized eigenvalue of $f_{a,b}$ at x.

If $(a, b, x) \in L_{\pm 1}(f, S)$, $x \in \mathbb{R}$ or $x \in \mathbb{R}^2$, then x is a fixed point of $f_{a,b}$ with one eigenvalue equal to ± 1. Moreover, if $k = 1$ the generalized eigenvalue is exactly the derivative of the map in this fixed point.

Using this concept there is a simple way of building various examples of configurations of bifurcation curves near a cusp. For $n = 2$ or 3, consider 1D families of $(n + 1)$-degree polynomial maps, having a codimension n bifurcation of eigenvalue 1.

First, let us consider the following two two-parameter families of 1D cubic maps that unfold the cusp bifurcation:

$$g^{\pm}_{a,b}(y) = (1 + a)y \pm y^3 + b.$$

We call the cusp bifurcation corresponding to $g^+_{a,b}$ a *cusp of saddle type* and the one corresponding to $g^-_{a,b}$ a *cusp of spring type* (these names are suggested by the patterns of the bifurcation locus in the parameter plane). Conditions for the existence of such types of cusps for a general 2D family of 1D or 2D maps having a cusp bifurcation were given in [6] and [57].

For these examples one easily identifies the fixed-point surface $S \subset \mathbb{R}^3$, in the a, b, y variables. Indeed, we obtain

$$S = \{(a, b, y) \in \mathbb{R}^3 : b = -ay \mp y^3\},$$

where the plus sign corresponds to $g^-_{a,b}$ and the minus sign corresponds to $g^+_{a,b}$. So, in this case, the level sets of (generalized) eigenvalue $\lambda \in \mathbb{R}$ are given by

$$L_\lambda(g^{\pm}, S) = \{(a, b, y) \in S : 1 + a \pm 3y^2 = \lambda\} = \{(a_\pm(y, \lambda), b_\pm(y, \lambda), y), y \in \mathbb{R}\},$$
$$(a_\pm(y, \lambda), b_\pm(y, \lambda)) = (\lambda - 1 \mp 3y^2, \pm 2y^3 + (1 - \lambda)y).$$

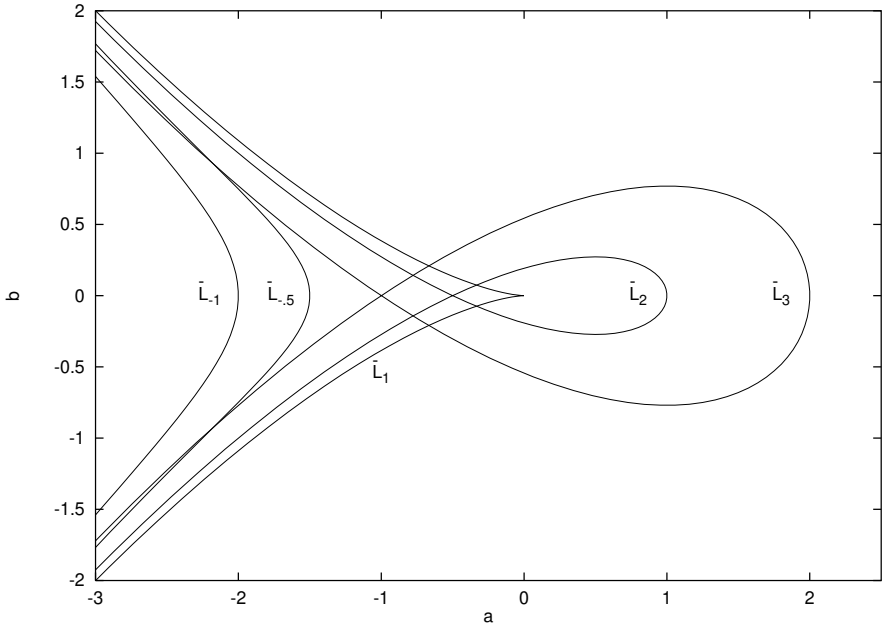

Figure 20. The cusp of saddle type corresponding to $g^+_{a,b}$.

In figures 20 and 21, for several values of λ, we depict the projection on the (a, b)-plane of some of these level curves $\bar{L}_\lambda$. In figure 21 there are two parameter points on the curve $\bar{L}_{-1}$, indicating the occurrence of codimension 2 flip bifurcations.

For any family of maps having a cusp bifurcation, a similar level set can be identified if $|\lambda - 1|$ is small enough.

Next we define the following configurations of bifurcation curves near a cusp.

Definition 4.2. Let $(f_{a,b})_{(a,b)\in U}$ be as before, having a cusp bifurcation at $x = x_0 \in \mathbb{R}^k$ ($k = 1$ or 2) for $(a, b) = (a_0, b_0)$. Suppose that the fixed-point surface S in the (a, b, x)-space has (a_0, b_0, x_0) as a regular point. We say that $f_{a,b}$ displays a *saddle area* (respectively a *spring area*) near $(a, b) = (a_0, b_0)$ if there exists a connected neighbourhood W of (a_0, b_0, x_0) in S such that:

(1) the cusp in x_0 is of saddle type (resp. spring type).

(2) The set of fixed points W satisfies:

$$W = \{(a, b, x) \in \mathbb{R}^{k+2} : (a, b, x) = (a(t, \lambda), b(t, \lambda), x(t, \lambda)), (t, \lambda) \in T\},$$

where T is an open and connected set in $\mathbb{R}^2$.

(3) There exist an open interval $I \subset \mathbb{R}$ containing $[-1, 1]$, such that for all $\lambda \in I$, the level set $L_\lambda(f, W)$ of the generalized eigenvalue λ satisfies:

$$L_\lambda(f, W) = \{(a, b, x) \in \mathbb{R}^{k+2} | (a, b, x) = (a(t, \lambda), b(t, \lambda), x(t, \lambda)), t \in T_\lambda\},$$

where $T_\lambda = \{t \in \mathbb{R} | (t, \lambda) \in T\}$.

(4) Let $\pi : W \subset \mathbb{R}^{k+2} \longrightarrow \mathbb{R}^2$ be the natural projection on the two first components. Then $\pi(W)$ is an open neighbourhood of (a_0, b_0), and $\pi(W) = W_1 \cup W_2 \cup \bar{L}_1(f, W)$, where $\bar{L}_1(f, W) = \pi(L_1(f, W))$, such that:

(a) W_1 and W_2 are open and connected, and W_1, W_2 and $\bar{L}_1(f, W)$ are disjoint,

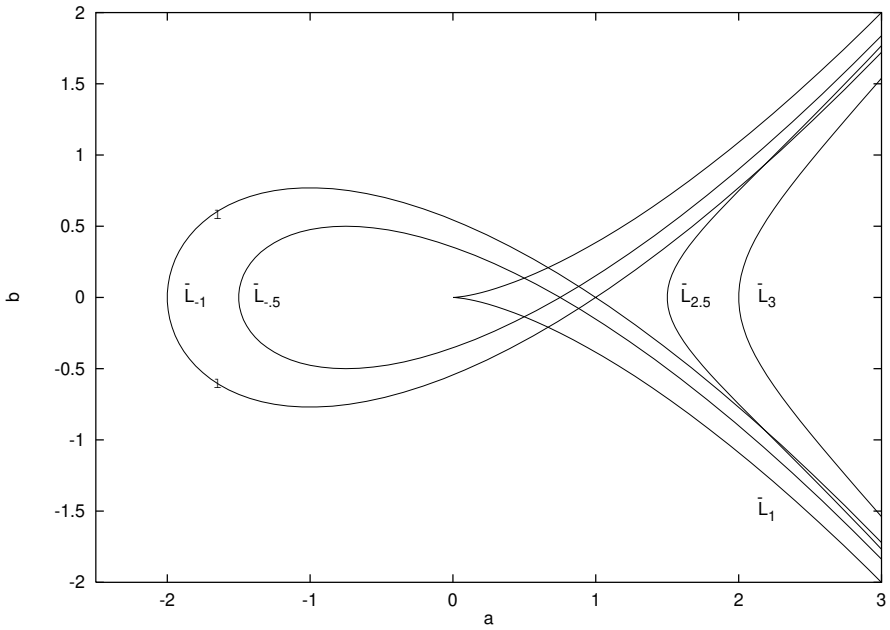

Figure 21. The cusp of spring type corresponding to $g^{-}_{a,b}$.

(b) if $(a, b) \in \bar{L}_1(f, W)$ there exists exactly one $(t, \lambda) \in T$ such that $\lambda \neq 1$ and $(a, b) = (a(t, \lambda), b(t, \lambda))$,

(c) if $(a, b) \in W_1$ there exist exactly three values $(t_i, \lambda_i) \in T$, $i = 1, 2, 3$, such that $(a, b) = (a(t_i, \lambda_i), b(t_i, \lambda_i))$

(d) if $(a, b) \in W_2$ there exists exactly one value $(t, \lambda) \in T$ such that $(a, b) = (a(t, \lambda), b(t, \lambda))$

(e) for all $\lambda \in I$ such that $\lambda > 1$ (resp. $\lambda < 1$) there are exactly two values t_1, $t_2 \in T_\lambda$ such that $(a(t_1, \lambda), b(t_1, \lambda)) = (a(t_2, \lambda), b(t_2, \lambda))$.

It turns out that the global organization around a cusp point can be different from the *saddle* and *spring* areas just defined. To see this, we consider the following three-parameter family of quartic 1D maps

$$g_{a,b,c}(x) = (1 + a)x + bx^2 + x^4 + c,$$

which is a local model of a codimension 3 cusp. Following the previous notation, the hypersurface of fixed points is given by

$$S = \{(a, b, c, y) \in \mathbb{R}^4 | c = -ay - by^2 - y^4\},$$

while the level sets of the eigenvalue λ are

$$L_\lambda = \{(a, b, c, y) \in \mathbb{R}^4 | a = -2by - 4y^3 + \lambda - 1, c = (1 - \lambda)y + by^2 + 3y^4\}.$$

Then the projection of this set on the (a, b, c)-space is

$$S_\lambda = \{(a, b, c) \in \mathbb{R}^3 | a = -2by - 4y^3 + \lambda - 1, c = (1 - \lambda)y + by^2 + 3y^4, y \in \mathbb{R}\}.$$

In figures 22 and 23 we depicted the surfaces S_1 corresponding to fold, and S_{-1} to flip bifurcation. In the fold surface S_1, we have two important curves, namely, $\gamma : \mathbb{R} \longrightarrow \mathbb{R}^3$ corresponding to codimension 2 cusps of period 1, such that

$$\gamma(s) = (a(s), b(s), c(s)) = (8s^3, -6s^2, -3s^4),$$

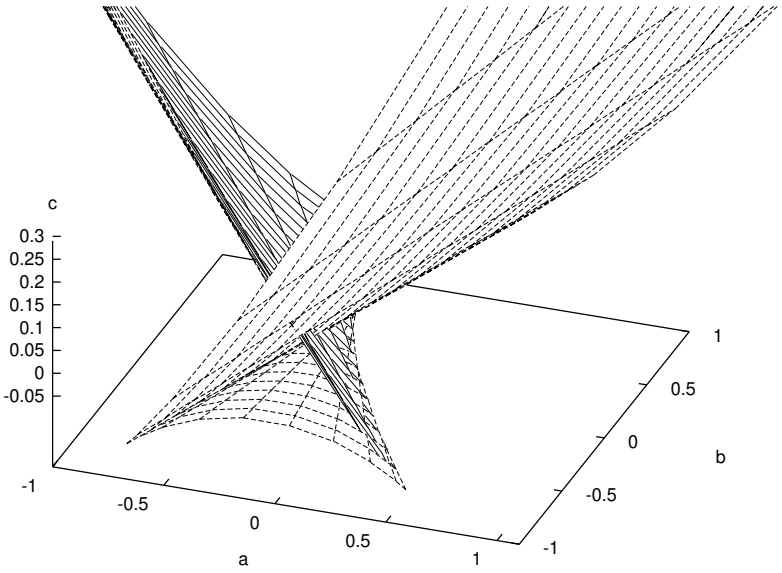

Figure 22. The S_1 surface of saddle-node bifurcation for the quartic map.

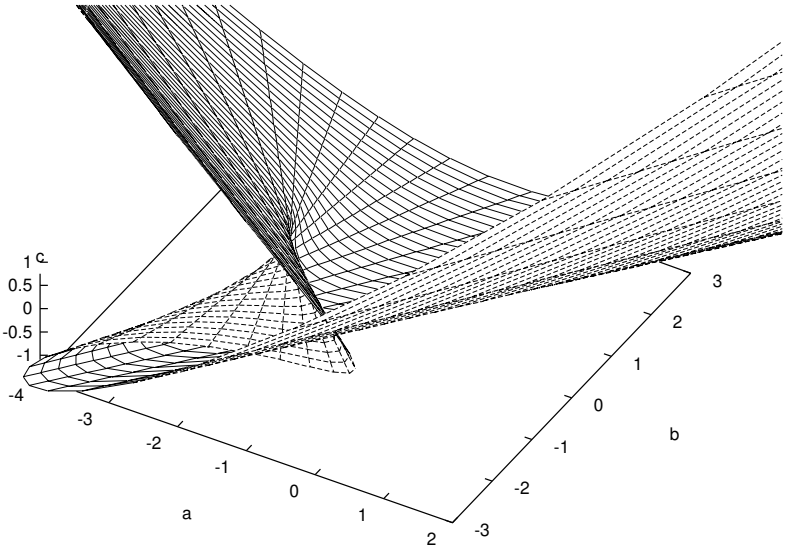

Figure 23. The S_{-1} surface of flip bifurcation for the quartic map.

and the self-intersection curve, $\bar{\gamma}$, defined by:

$$\bar{\gamma}(s) = (0, -2s^2, s^4).$$

In the flip surface there is also the curve of self-intersections, $\bar{\varphi}$, defined by

$$\bar{\varphi}(s) = \left(-8s^6, -6s^4 - \frac{1}{2s^2}, -3s^8 + \frac{5}{2}s^2 - \frac{2}{s^2} + \frac{1}{16s^4}\right),$$

while the curve

$$(a, b, c, y) = (-8s^6 + 4s^3 - 2, -6s^4 + 2s, -3s^8 + 2s^5 - 2s^2, -s^2)$$

corresponds to points with a codimension 2 flip bifurcation. Moreover, there are two points with codimension 3 flip bifurcations, namely, $(a, b, c) = (-2, 0, 0)$, for $y = 0$, and $(a, b, c) = (-\frac{49}{32}, (\frac{7}{16})(\frac{3}{2})^{1/3}, (\frac{9}{1024})(\frac{3}{2})^{2/3})$ for the point $y = -3^{2/3}/2^{8/3}$.

In order to create other configurations of bifurcation curves near a codimension 2 cusp, we only have to consider two-parameter families like $f_{u,v} = g_{a(u,v),b(u,v),c(u,v)}$, such that for some (u_0, v_0), the map f_{u_0,v_0} has a codimension 2 cusp. The simplest case occurs when the maps a, b and c are affine. Below, we need some of these configurations.

We do not know whether this procedure exhausts all possibilities, but it seems that it does for the more 'frequent' ones. A heuristic argument for this runs as follows. It is well known that, given any one-parameter family of 2D maps f_a having a dissipative saddle with a quadratic homoclinic tangency, the family of iterates, f_a^n, for n sufficiently large and after a change of scale, behaves, near the tangency, as a one-parameter family of 1D quadratic maps. The same is true for a two-parameter family with a cubic tangency: a high iterate behaves like a cubic family (see Tatjer [58]). It is plausible that the same is true when considering three parameters, a quartic tangency and a quartic family.

This would mean that, at least if the considered family is near a family having a homoclinic tangency of order 2 or 3, the expectedly most frequent configurations of the bifurcation curves of periodic points near a cusp, are those obtained before using the cubic and quartic families of maps. This may even be true if the family is near, but not too near, a family having a quartic homoclinic tangency.

We now proceed by giving two more definitions, that may involve many subcases.

Definition 4.3. Let $(f_{a,b})_{(a,b)\in U}$ be as before, having a cusp bifurcation at $x = x_0 \in \mathbb{R}^k$ ($k = 1$ or 2) at (a_0, b_0). Suppose that the fixed-point surface S in the (a, b, x)-space has $(a_0, b_0, x_0) \in S$ as a regular point.

(1) We say that $f_{a,b}$ displays a *cross-road area* near (a_0, b_0, x_0) if:

(a) the cusp bifurcation in x_0 is of spring type;

(b) there exist a connected neighbourhood W of (a_0, b_0, x_0) in S such that the map $\Lambda : W \subset S \longrightarrow \mathbb{R}$ has one and only one non-degenerate critical point of saddle type $(a_1, b_1, x_1) \in W$ such that $-1 < \Lambda(a_1, b_1, x_1) < 1$;

(c) there is only one cusp bifurcation (a_0, b_0, x_0) in W.

(2) Suppose that there is another cusp bifurcation for f_{a_1,b_1} in $x_1 \in \mathbb{R}^k$. We say that $f_{a,b}$ displays a *dovetail area* near the two cusps if there exists an open set W in S such that:

(a) $(a_i, b_i, x_i) \in W$ for $i = 0, 1$;

(b) the projection of the level set $L_1(f, W)$ on the (a, b)-plane can be parametrized by a differentiable map $\gamma : [-3, 3] \longrightarrow \mathbb{R}^2$ such that it has points of self-intersection for $t = -1$ and $t = 1$. Furthermore, the two cusps occur for $t = -\frac{1}{2}$ and $t = \frac{1}{2}$;

(c) one cusp is of saddle type and the other is of spring type;

(d) the curve $\gamma_{|[-1,1]}$ is a Jordan curve such that the region bounded by it does not contain any point of the curve γ.

Finally, we present some examples of the configurations described above. Here we use the following notation for the bifurcation curves: fol^n indicates a fold of period n, fl^n a flip of period n, c^n a cusp of period n and $\overline{\text{fl}}^n$ a codimension 2 flip of period n. Moreover, subscripts are used in order to distinguish different curves of the same type, and the broken lines indicate level sets $\bar{L}_\lambda$ corresponding to various values of λ.

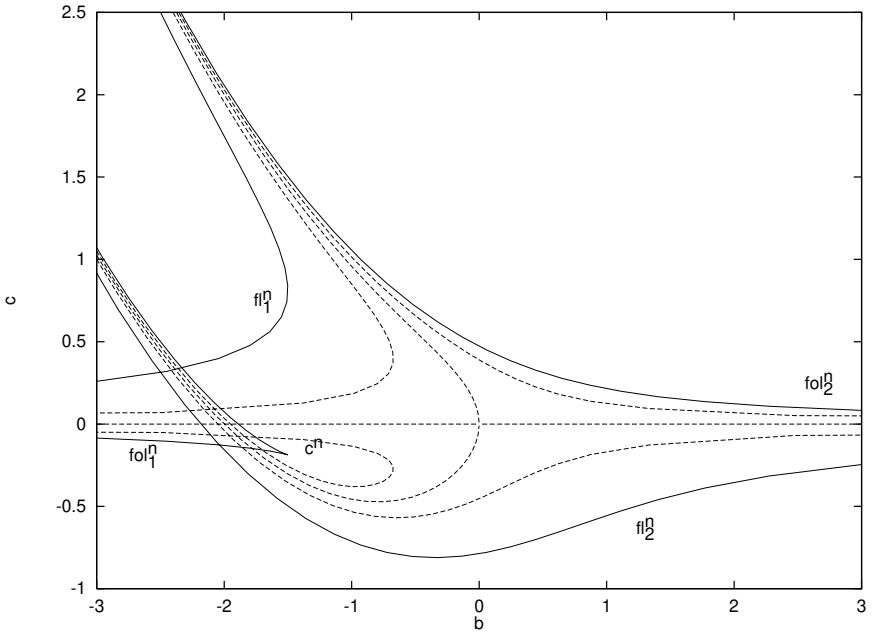

Figure 24. Cross-road area. The dotted curves correspond to level lines of Λ.

So, as before, let $f_{a,b}$ be a two-parameter family of diffeomorphisms having a cusp bifurcation for $(a, b) = (a_0, b_0)$. Then we have the following configurations of bifurcation curves near the origin of the parameter plane.

(1) *Cross-road area*. In figure 24 the configuration is depicted for the model $x \mapsto bx^2 + x^4 + c$, where we consider the fixed-point case $n = 1$. The flip curves fl_1^n, fl_2^n approach different fold curves in different regions of the (b, c)-plane.

(2) *Spring area*. In figure 25 we show the configuration for the model map $x \mapsto -2x + bx^2 + x^4 + c$. Again we took $n = 1$. The curve fl_1^n loops around c^n. On this curve the points between $\overline{\mathrm{fl}}_1^n$ and $\overline{\mathrm{fl}}_2^n$ are supercritical flips, the remaining ones being subcritical. At the codimension 2 flips, folds of double period are born.

(3) *Saddle area*. Figure 26 shows the configuration for the model map $x \mapsto 2x + bx^2 + x^4 + c$ in the case $n = 1$. The reader may observe that in some part a cross-road area structure shows up.

(4) *Dovetail area*. In figure 27 we can see that this family displays a spring area near one cusp and a saddle area near the other. The model map is $x \mapsto (1 + a)x - 3x^2 + x^4 + c$, while $n = 1$.

Most of the terminology has been introduced by Mira and co workers (see, e.g., Mira [34])

In figure 28 we display some cases of relative positions of the fold and flip curves. They are obtained by intersection of the surfaces displayed in figures 22 and 23 with some suitable planes. From cases A–C the fold and flip curves have only one component, from D–F they have two, and the remaining ones have three. Case A shows a dovetail area with self-intersections of both the fold and flip curves. Case B is obtained by evolution of A, and the fold curve contains two cusps associated to spring and saddle areas, respectively. Case C shows no cusps but self-intersections. Cases D and E illustrate a transition from

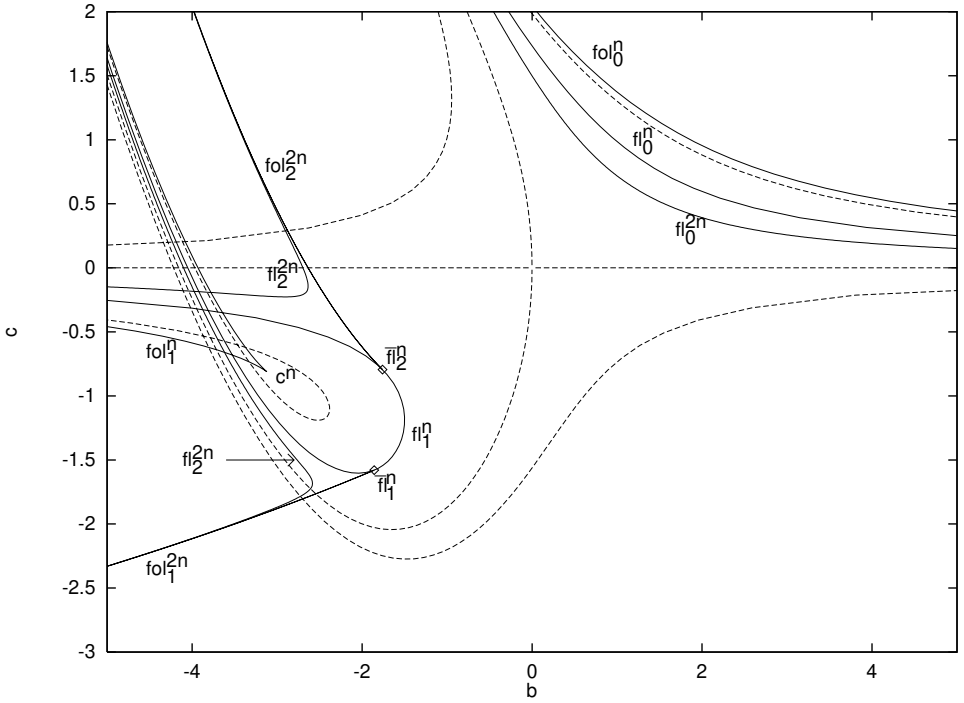

Figure 25. Spring area. The dotted curves correspond to level lines of Λ.

spring area to cross-road area. Case F is, in fact, a cross-road area example, but shortly after a dovetail area meets a spring area. Cases G and H, with three components, have no cusps and they illustrate a transition from no changes to a cross-road area situation. In case I a saddle area, a spring area and a fold curve without cusp, appear simultaneously, which evolve to a saddle area plus a cross-road area in case J. Case K displays a triple exchange of the flip curves with respect to the fold ones. Finally, case L is similar to case J but with four cusps in all, two of them associated to a small dovetail area.

4.2. Cascades of bifurcations

We close this section with a sketch of a cascade of bifurcations, associated to the cusp, in particular a cross-road area. In figure 29 we display the corresponding organization of the parameter plane by bifurcation curves, using the same convention as before. Figure 30 enlarges the rectangle A in figure 29. The behaviour of the bifurcation curves in the rectangle B is similar. In these figures we observe that associated to the main cusp, c_1^n, two more cusps of period $2n$ appear (c_1^{2n} in B and c_2^{2n} in A). These, in turn, are centres of cross-road areas of double period. This doubling repeats itself, giving cusps of period 4, 8, 16 etc, all these cusps being centres of cross-road areas. The model map used here is $x \mapsto bx^2 + x^4 + c$, and again $n = 1$.

Remarks.

(i) When following the broken line l in figure 29, we undergo an ordinary Feigenbaum cascade of flips.

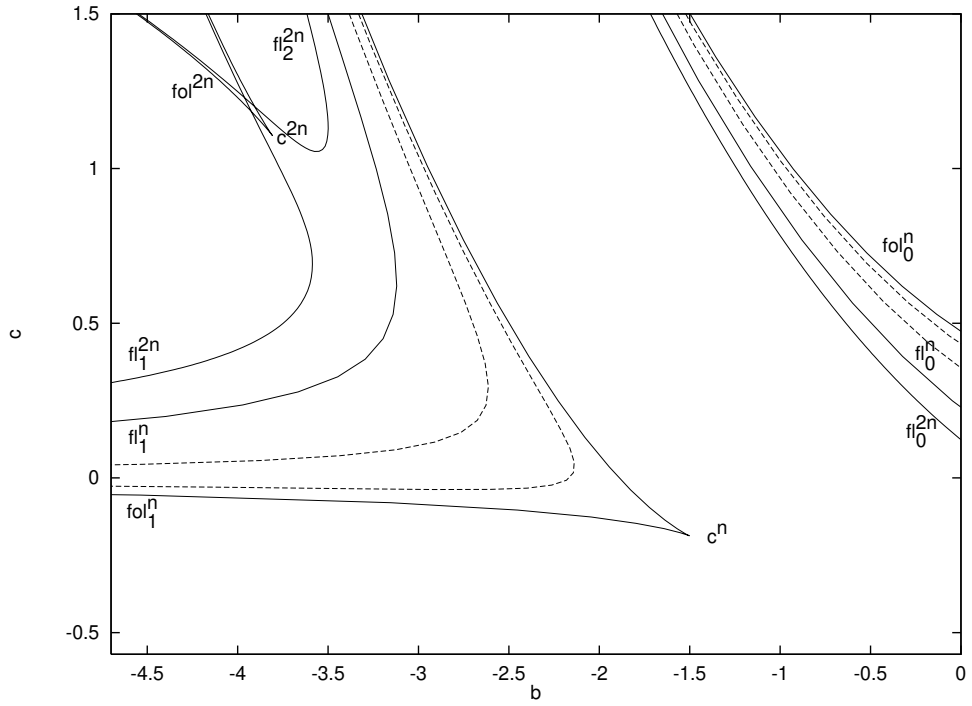

Figure 26. Saddle area. The dotted curves correspond to level lines of Λ.

(ii) The occurrence of cusp cascades in the Arnold family was studied by Bélair and Glass [4].

(iii) The concept of generalized eigenvalue has been used before in Carcassès [15] (where it is called reduced multiplier) to obtain information on the configuration of bifurcation curves near a cusp.

(iv) In Carcassès *et al* [16] the concept of cross-road area is more restrictive than here and corresponds to the example we have described above.

(v) The name dovetail area was first used in Mira *et al* [35]. There one considers, moreover, other possibilities of dovetail areas, some of these with more cusps.

(vi) The dovetail area can appear when the two-parameter family is near a codimension 3 fold bifurcation (see section 5.1.1).

4.3. Homoclinic bifurcations related to saddles and folds

In this section we treat homoclinic phenomena, as far as relevant to us, both related to saddle points and to fold points (saddle nodes). Apart from transverse homoclinic points we also have to consider homoclinic tangencies. As before, we simply restrict ourselves to the case of fixed points. Reference will be made to some figures (mainly figures 13–17) from section 3. We recall that these illustrations are taken from the fattened Arnold family. Hence, the plots are on a cylinder (one should identify the left- and right-hand sides) and that the cases $\beta > 0$ and $\beta < 0$ are orientation preserving and reversing, respectively.

So we again consider a general two-parameter family $f_{a,b}$ of 2D diffeomorphisms having a fixed point, p_0, for $(a, b) = (0, 0)$. We distinguish between the following two cases.

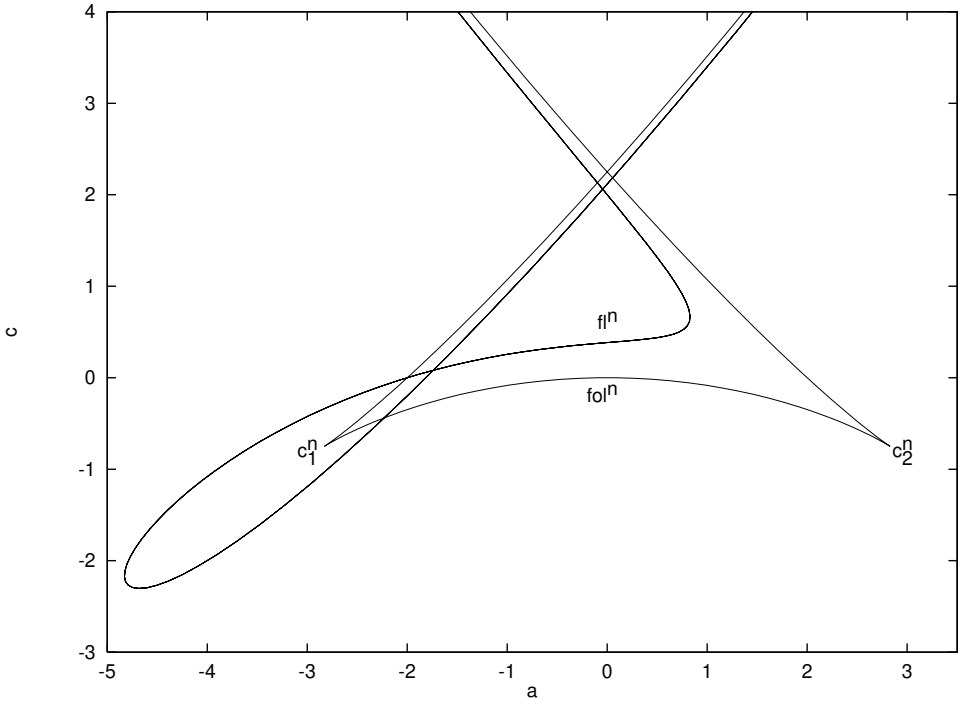

Figure 27. Dovetail area.

(1) p_0 *is a saddle point*. Homoclinic dynamics then means that $W^u(p_0) \cap W^s(p_0) \neq \{p_0\}$. Since the saddle is persistent, for parameter values $(a, b) \approx (0, 0)$ the map $f_{a,b}$ has a nearby saddle, say $p_{a,b}$, together with its stable and unstable manifolds $W^s(p_{a,b})$ and $W^u(p_{a,b})$. In the corresponding figures n_0 denotes the companion node, created together with the saddle at a fold bifurcation.

There are several possibilities for the generic behaviour of $W^s(p_{a,b})$ and $W^u(p_{a,b})$. First, they can intersect transversally. This case is well known and will not be discussed here. In our two-parameter context there are two further generic cases to consider.

(a) *Quadratic tangency of* $W^s(p_0)$ *and* $W^u(p_0)$. This is a codimension 1 phenomenon, so generically taking place along a curve Γ in the parameter plane. This case has also been widely studied, e.g. see Newhouse [38], Palis and Takens [45], Tatjer and Simó [59], Mora and Viana [36].

Among other things, it can be proven that, for any sufficiently large n, there exists an n-periodic fold curve Γ_n, where $\Gamma_n \to \Gamma$ as $n \to \infty$. Moreover, for suitable values of (a, b) near Γ there are infinitely many periodic attractors. Finally, for appropriate values of (a, b) near Γ, strange attractors exist. According to Mora and Viana [36], the corresponding set of parameter values has positive measure.

(b) *Cubic tangency of* $W^s(p_0)$ *and* $W^u(p_0)$. This is a codimension 2 bifurcation and therefore generically taking place only in isolated points of the parameter plane. In this case, it has been shown that for any n there exist parameter values for which n-periodic cusps and codimension 2 flips occur, where these parameter values tend to $(a, b) = (0, 0)$ as $n \to \infty$ (see Tatjer [58]).

Furthermore, we consider the position of the manifold $W^u(p_0)$ with respect to the stable

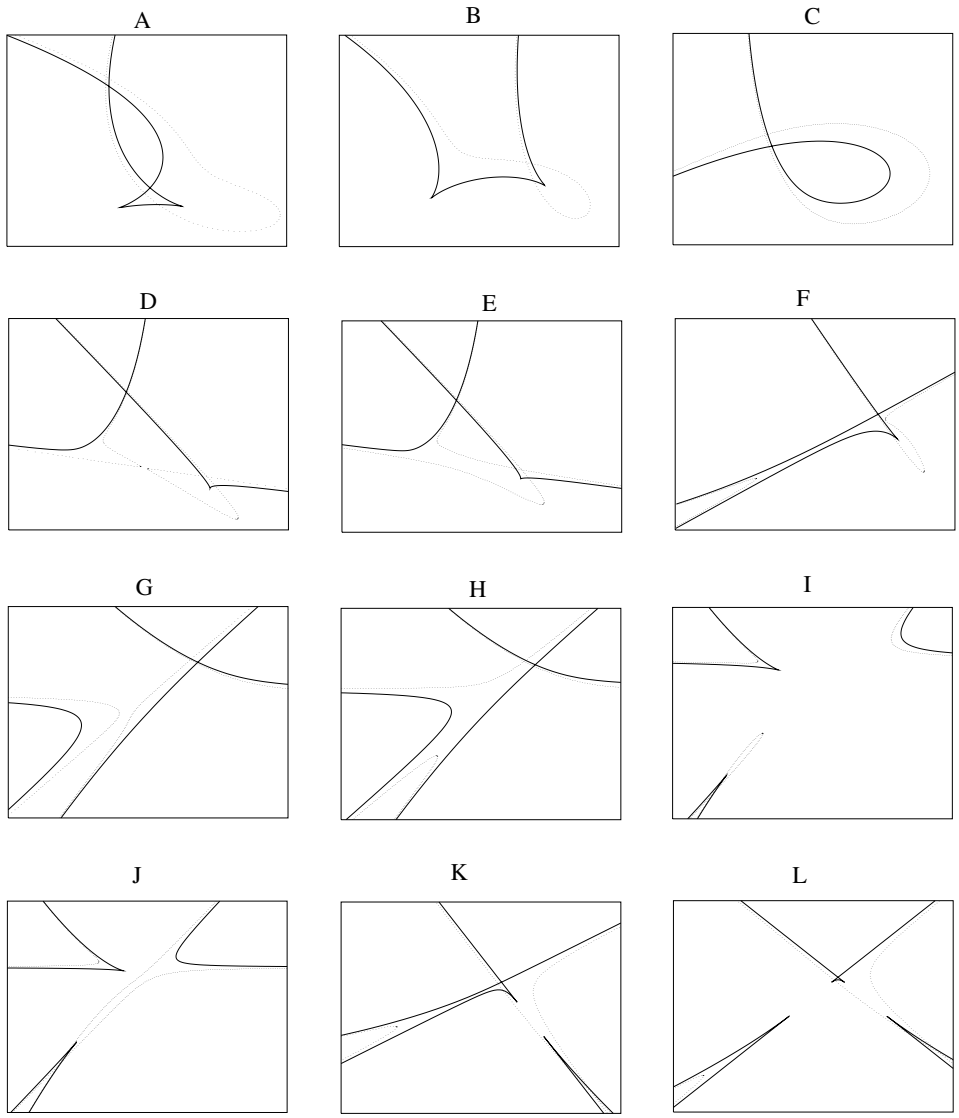

Figure 28. Some configurations of fold (lines) and flip (dots) bifurcations curves obtained by intersection of the corresponding surfaces by planes. See additional explanation in the text.

and strongly stable manifolds $W^s(n_0)$ and $W^{ss}(n_0)$ of the companion node n_0 (think of the saddle-node bifurcation). Codimension 1 bifurcations appear at the homoclinic quadratic tangencies of $W^u(p_0)$ with some of the manifolds of n_0 and at the cubic tangencies of $W^u(p_0)$ with the strong stable foliation $\mathcal{F}^{ss}$ associated to n_0 (see later). Figures 13 and 14 display some of these possibilities, both for the $\beta > 0$ and $\beta < 0$ cases. Some of these situations can coexist, giving phenomena of higher codimension. For instance, an 'external' heteroclinic tangency between $W^u(p_0)$ and $W^{ss}(n_0)$ (as in figure 13(c)) can coexist with an 'internal' homoclinic tangency between $W^u(p_0)$ and $W^s(p_0)$ (as in figure 13(e)), giving a codimension 2 case.

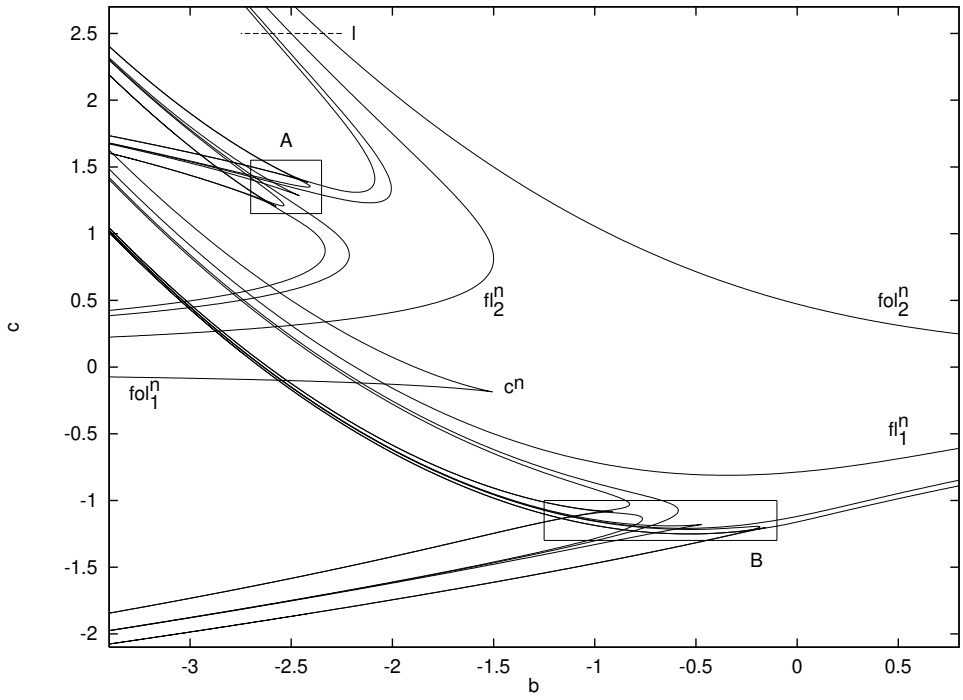

Figure 29. First steps of a cascade of cusp bifurcations.

(2) p_0 *is a fold point*. First, we note that associated to this fold we have a weak unstable invariant manifold $W^u(p_0)$, a strong stable invariant manifold $W^{ss}(p_0)$ and an invariant strong stable foliation $\mathcal{F}^{ss}$ (cf Newhouse *et al* [39]). See figure 15, where $\mathcal{F}^{ss}$ is represented by vertical lines. A weak (and non-unique) stable manifold, $W^s(p_0)$, also appears. Both $W^u(p_0)$ and $W^s(p_0)$ are on the centre manifold $W^c(p_0)$ and both consist of only one branch. In this case we have four possibilities, two of codimension 1 and two of codimension 2.

(a) *Fold cycle*. This is a codimension 1 case. As we can guess from figure 15(a), $W^u(p_0)$ is a smooth invariant circle. This case has been studied in [39].

(b) *Quadratic critical cycle*. This is again a codimension 1 case, occurring whenever there are points in $W^u(p_0)$ belonging to the basin of attraction of p_0, that have quadratic tangency with $\mathcal{F}^{ss}$. It has been proved by Díaz *et al* [19] that for values of the parameter near $(0, 0)$ there exist strange attractors, again for a parameter set of positive measure [36] (see figure 15(b)).

(c) *Cubic critical cycle*. This case is like the previous one but now the tangency is cubic. Therefore, it is a codimension 2 bifurcation (see figure 15(c)).

(d) *Fold homoclinic tangency*. This bifurcation occurs when $W^u(p_0)$ has a quadratic tangency with W^{ss}. This is again a codimension 2 bifurcation (see figures 15(d) and (e)). Note that, despite the length of the unstable branch of the fold is infinite, this branch is still homeomorphic to a circle.

We note that the cases β positive and β negative are different as is shown in the figures. In figure 15 we have $\beta > 0$ and in figure 16 $\beta < 0$.

As far as we know, cases (c) and (d) have not been studied theoretically. In particular one would like to know the structure of the codimension 1 and 2 bifurcations of periodic

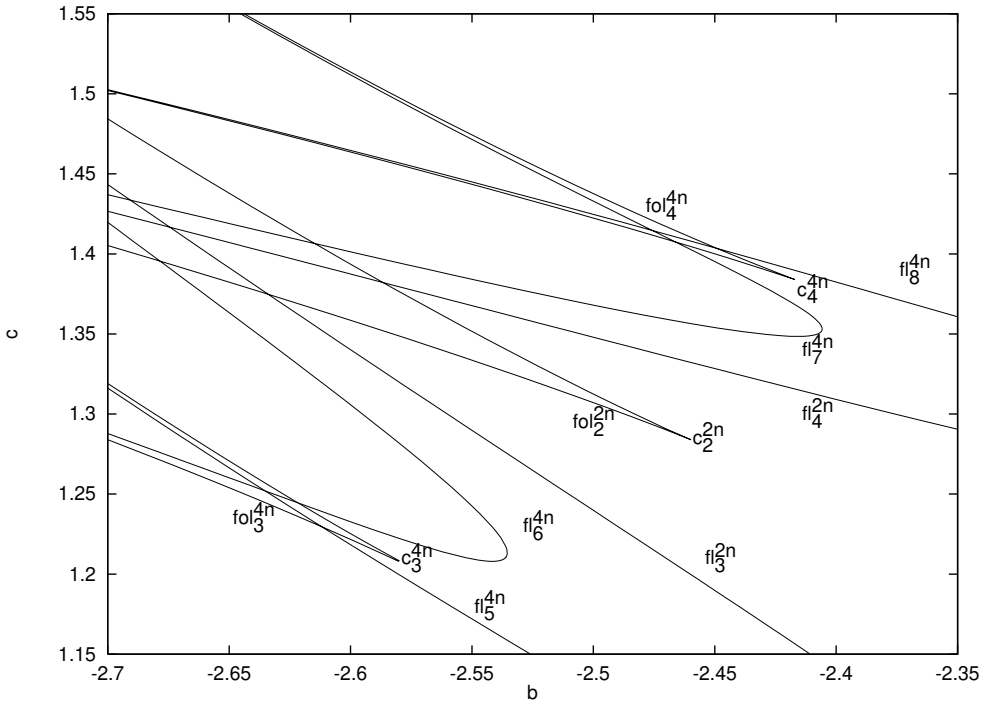

Figure 30. Amplification of rectangle A of figure 29.

points near $(a, b) = (0, 0)$.

When considering a one-parameter family having a fold point, the four possibilities are found in the following order: fold cycle, cubic tangency to $\mathcal{F}^{ss}$, quadratic tangencies to $\mathcal{F}^{ss}$ and then a quadratic homoclinic tangency. After the quadratic homoclinic tangency, generically, transversal homoclinic intersections appear. Later, another quadratic homoclinic tangency can occur and then the homoclinic points disappear. This happens in our problem for β positive when increasing the parameter ω. We refer to these tangencies as inner and outer. In the case $\beta < 0$ outer tangencies cannot appear, because the change of orientation forces us to have homoclinic points in both branches of $W^{ss}(p_0)$, forcing $W^u(p_0)$ to have points in $W^s(p_0)$. Cubic homoclinic tangencies to the fold can also occur, but this is a codimension 3 phenomenon (see the next section).

Remark. We give some additional explanation related to section 3.1. Assume that in the case of figure 17(a) we take a small 'vertical' rectangle, $\mathcal{R}$, to the right of $W^s(p_0)$ and with left boundary rather close to $W^s(p_0)$ ('parallel' to it). After, say, n iterates the image of $\mathcal{R}$ intersects $\mathcal{R}$, giving rise to a horseshoe-like behaviour. In the horseshoe we find two fixed points of the return map (n-periodic points of the initial map f). In our geometrical situation one of these is a saddle and the other is a saddle with reflection. By moving parameters we can go back to the 'first' homoclinic tangency and even before this occurs. At some moment $f^n(\mathcal{R})$ has no intersection with $\mathcal{R}$ (say, $f^n(\mathcal{R})$ is confined to the left of $W^s(p_0)$).

Between these values of the parameters and those of the previously described horseshoe a fold bifurcation occurs. Typically the saddle created at the fold bifurcation remains a saddle all the time, while the node goes to a flip (see figure 12) and then to a saddle with

reflection. In the (a, b) space there will be a line close to (and 'after') the line of first homoclinic tangency for which an n-fold bifurcation is produced. Taking $\mathcal{R}$ closer and closer to $W^s(p_0)$ the value of n increases, because the iterates spend more time close to p_0, and a sequence of fold bifurcation curves, with increasing period, accumulates to the first homoclinic tangency in the parameter space (to the 'right').

Similar to the case of the line of 'last' homoclinic tangency. Consider the situation shown in figure 17(b). If $\mathcal{R}$ is close to $W^s(p_0)$ it cannot intersect any of its iterates. By moving $\mathcal{R}$ to the right a sufficiently large amount we may again have some horseshoe. Hence a fold curve will be created. Then, by letting the parameters approach the line of the last homoclinic tangency, the periods of the folds will increase, as before, and that line will be accumulated, by a sequence of fold bifurcation curves (to the 'right' of it). The behaviour just described appears in the case of the fattened Arnold family, and further numerical evidence will be presented in section 5.3.2.

4.4. General remarks

We conclude this section on bifurcations by a few remarks.

4.4.1. Transversality. Transversal intersection of all stable and unstable manifolds of fixed and periodic saddles is an open property. As observed before it may be hard to know (and difficult to prove) in which cases our family of maps has this property and what can be said about the set of parameter values where transversality does not hold.

A typical numerical computation of a homoclinic tangency starts at a fold point (saddle node), after which the line of tangencies is obtained by a continuation method. As usual we fix β. Along the continuation checks are made for extra degeneracies. The only extra cases we detected correspond to β negative and are geometrically related to cubic tangencies. At these tangencies new lines of tangencial homoclinics are born, which can be followed as in the previous case. The full tools to develop and implement this methodology are given in [51].

4.4.2. The role of heteroclinic intersection. Heteroclinic intersection plays an important role, since it couples dynamics arising from different saddles. Let us consider the case where a saddle has a transversal homoclinic point. In that case the closure of the unstable invariant manifold is a good candidate to be a strange attractor [50, 5]. Heteroclinic tangencies can destroy such an attractor by 'pulling out' points. Indeed, it may well be called a *potential strange attractor*.

Also a 'coupling' of two strange attractors may occur. Indeed, let $\mathcal{S}_1$ and $\mathcal{S}_2$ be two different strange attractors, occurring as the closure of the unstable manifolds ${W_1}^u$ and ${W_2}^u$. If the related stable manifolds, ${W_1}^s$ and ${W_2}^s$ intersect ${W_2}^u$ and ${W_1}^u$, respectively, a larger potential attractor will be born. In the process of changing parameters to obtain these transversalities, periodic sinks will certainly appear and will destroy, locally in parameter space, the strange attractors.

4.4.3. Preservation versus reversion of orientation. The original motivation for the study of our family is its occurrence as a model of the return map of a near-the-identity map. Since the initial map preserves orientation, so does the return map. However, in some cases, due to the special geometry of the problem, the initial map can be seen as the composition of a

near-the-identity map with a symmetry. In this case the return map is orientation reversing, and should also be considered. This motivates our interest for the case $\beta < 0$. Main differences with the case $\beta > 0$ are the non-existence of foci (see section 3.1), that, as said before, a *last* homoclinic tangency never occurs (see, for instance, section 3.1), and the very wild character of the 'last' invariant curves in the anticonservative case (see appendix C). This is reflected in some attractors of the fattened Arnold family (see section 5.3.4).

5. Numerical study of the fattened Arnold family

In this section we return once more to the fattened Arnold family F, given by (1):

$$\begin{aligned} \bar{F}_{\alpha,\omega,\beta} : \mathbb{S}^1 \times \mathbb{R} &\to \mathbb{S}^1 \times \mathbb{R} \\ (x, y) &\mapsto (x + \omega + \alpha(y + \sin x) (\mathrm{mod}\, 2\pi), \beta(y + \sin x)). \end{aligned}$$

As announced several times, we now perform perturbations corresponding to larger values of the parameter α. Our results are partly conjectural and based on numerical computation which are interpreted against the theoretical background of the previous sections. The results mostly concern the bifurcation set in the (α, ω)-plane but also aspects of the corresponding dynamics are shown. As before we mostly fix $|\beta| < 1$, but sometimes a codimension 3 phenomenon is observed, in which case β is taken into account as an extra parameter. Our exposition chiefly restricts us to the main tongue I_0^β, but almost all our statements and speculations directly translate to the other tongues.

We divide this section into four parts. The first part deals with bifurcations of periodic points, mainly restricting us to one Arnold tongue. In this exploration we find all the phenomena described in section 4.1, including strong evidence of infinite cascades of cusp (cf section 4.2). Another aspect is the geometry of the tongue boundary. We shall see that for $\beta < 0$ this boundary no longer needs to consist of two smooth curves. In section 5.2 homoclinic bifurcations are studied, again using the main tongue I_0^β as a representative case. Our special interest is with homoclinic bifurcations near the tongue boundary. It appears that all the complexity of section 4.3 is met. The third part is concerned with global aspects of the dynamics. As announced before, we study the accumulation of tongue boundaries on certain curves of homoclinic tangency. We also consider the invariant circle, certain types of strange attractors and the coexistence of attractors. Finally, in a conclusive section, we present a sample of attractors, some bifurcation diagrams and the corresponding dynamical scenarios, as observed numerically.

5.1. Local bifurcations

First we obtain the different structures of bifurcation curves, analysed in section 4. However, there is one difference, namely that in the diagrams the role of the fold curves is played by the boundary curves $\Gamma^\beta_{p/q,i}$, $i = 1, 2$, the 'cusp' then being the tongue tip $(\omega, \alpha) = (2\pi p/q, 0)$. We shall conclude that it is easy to detect many examples of saddle area, spring area and cross-road area. Second the boundary of the tongues $I^\beta_{p/q}$ is studied further. We shall see that this boundary is not always the union of the $\Gamma^\beta_{p/q,i}$, $i = 1, 2$. Finally an example is given of (the beginning of a) cascade of cusp bifurcations (cf section 4.2).

5.1.1. Cusps inside one tongue. We found all three: the saddle, the cross-road and the spring area associated to the fold curves $\Gamma^\beta_{p/q,i}$, $i = 1, 2$, but with the tongue tip $(\omega, \alpha) = (2\pi p/q, 0)$ replacing the cusp point.

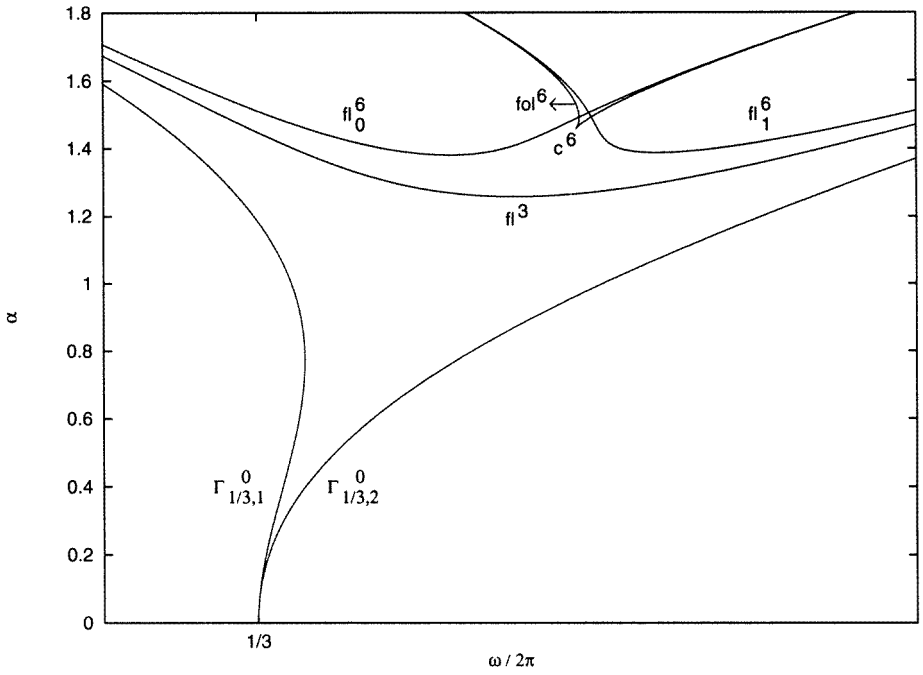

Figure 31. Saddle area in $I^0_{1/3}$.

(1) *Saddle area*. We find this type of behaviour for all $\beta \geqslant 0$, and also for $\beta < 0$ not too close to -1. Admittedly this does not exactly correspond to the definition of section 4, since in the ω-axis no cusp bifurcation takes place. Nevertheless, the pattern of bifurcation curves is strikingly similar.

In this case we have only level sets of a generalized eigenvalue less than 1, which means that there are at most two periodic points inside one tongue. However, by analogy we also call this type of behaviour a saddle area. In figure 31 we show an example for $\beta = 0$, $p/q = \frac{1}{3}$, displaying bifurcation curves corresponding to periods 3 and 6 (cf the above figure 26).

(2) *Cross-road area*. We have found this phenomenon only for $\beta < 0$. Again, the difference with its analogue in section 4 is that now there does not exist a fold curve of period q without cusps. We detected three different cases:

(a) without codimension 2 flips. In figure 32 we depict the bifurcation curves of period 4 (cf figure 24, above);

(b) with two codimension 2 flips in one of the flip curves of period 4, see figure 35. We show the same curves as in case (a) and also fold curves of period 8 leaving from the codimension 2 flips;

(c) with two codimension 2 flips in each flip bifurcation curve of period 4 (cf figure 36).

(3) *Spring area*. This is again similar to the case studied in section 4, with the same difference as noted before. Moreover, in the case presented in figure 37, there are two codimension 2 flips in each of the flip curves of period 4.

(4) *Transition cross-road area–saddle area*. The transition we find from cross-road area to saddle area occurs through codimension 3 bifurcations (see figures 32–34). The behaviour of the bifurcation curves is as follows. There exist two negative values of β, β_1

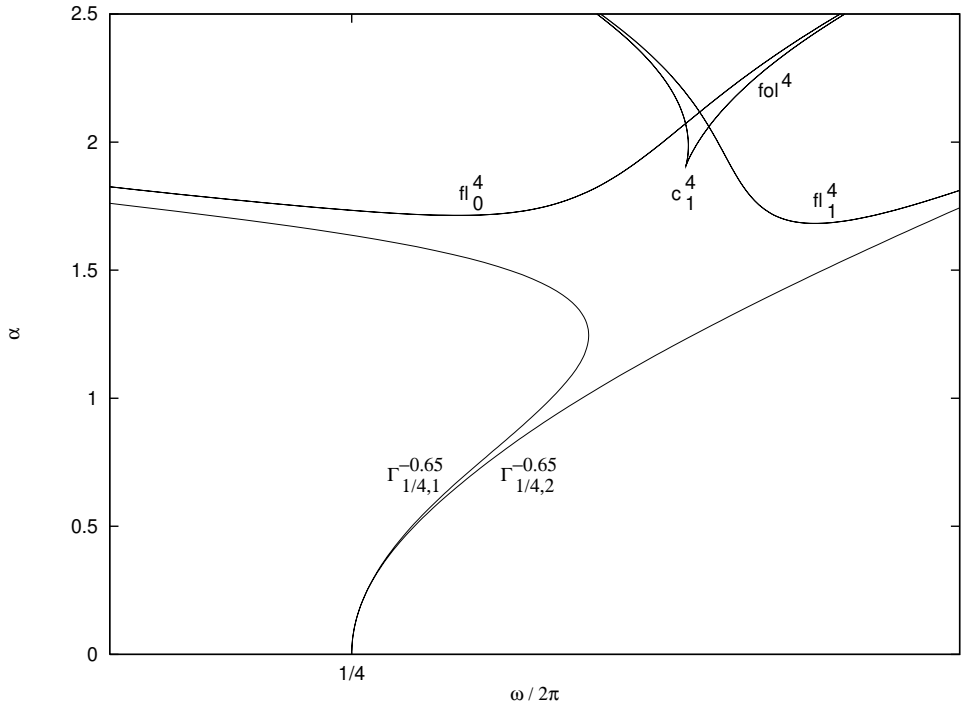

Figure 32. Cross-road area in $I^{-0.65}_{1/4}$.

and $\beta_0 < \beta_1$, where the following properties hold.

(a) For $\beta < \beta_0$ there is a cross-road area with centre in c^q_1 (cf figure 32).

(b) For $\beta = \beta_0$ a 'double' cusp point appears on a fold line (this is the codimension 3 cusp bifurcation) and, then, the two cusp points go away from the fold line creating a dovetail area. In our example this occurs between figures 32 and 33.

(c) For $\beta \in (\beta_0, \beta_1)$ the dovetail area becomes apparent (see the magnification in figure 33). The cusps in the dovetail are named c^q_0 and c^q_2, and they are of saddle and spring type, respectively. The other cusp, c^q_1, already present in figure 32 as the organizer of the cross-road area, approaches c^q_2.

(d) For $\beta = \beta_1$ there is another codimension 3 fold bifurcation (different from the previous one). It is produced by the coincidence of the two cusps c^q_1 and c^q_2. In our example this occurs between figures 33 and 34. The two fold curves that at the moment of the bifurcation become tangent, go away from each other. This produces a global change in the fold curve which connects with one of the curves of $\Gamma^\beta_{p/q,i}$, $i = 1, 2$, of the tongue boundary for small values of α. In this example, this happens for $\Gamma^\beta_{1/4,1}$, and then, instead of going quickly to the left, as in figure 32, it continues as the previous left branch of fol^4.

(e) For $\beta > \beta_1$ there exist two saddle areas, one associated to the tongue boundary, as in the item 1, and the other in a neighbourhood of the cusp that was denoted as c^q_0. This is displayed in figure 34.

We note that in the process just described, one of the branches $\Gamma^\beta_{p/q,i}$ has undergone a strong modification. Moreover, it is possible to find a model of this type of transition using the quartic model of the codimension 3 fold that we presented in section 3, taking planes in the space of parameters a, b, c parallel to a plane $b = \alpha a + \beta c$ through $(a, b, c) = 0$.

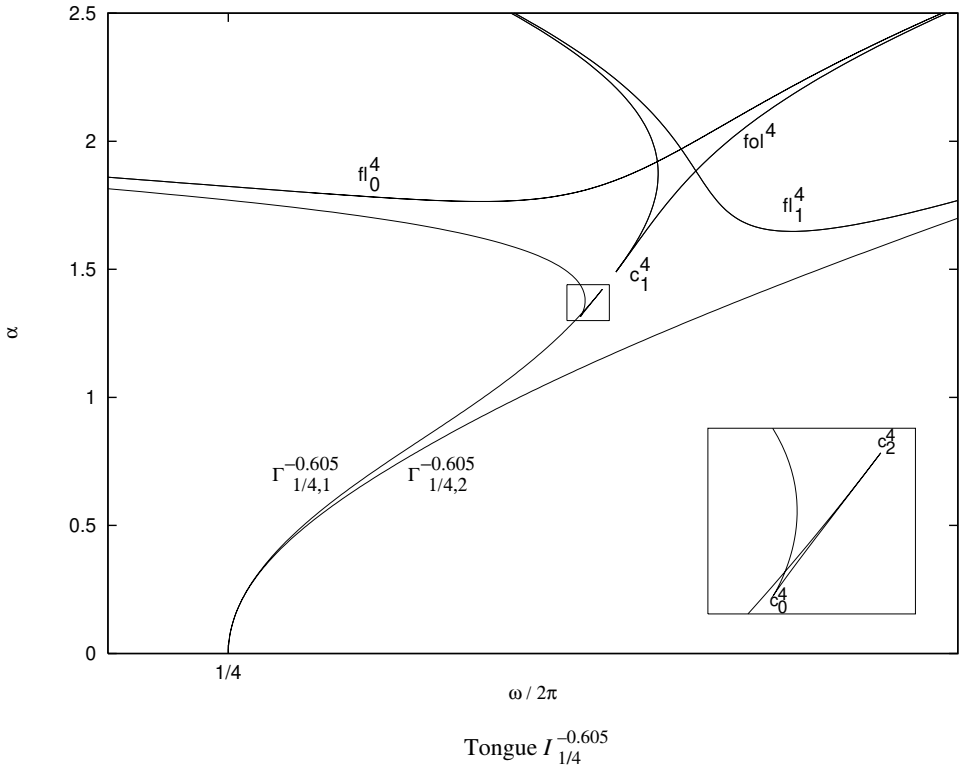

Figure 33. Transition cross-road area–saddle area. Between the two codimension 3 bifurcations ($\beta_0 < \beta < \beta_1$). The horizontal window is $[0.75/\pi, 1/\pi]$. The small rectangle, whose window is $[1.77, 1.795] \times [1.3, 1.44]$, is enlarged in the lower right corner of the figure.

The values of β_0 and β_1 in the example shown for $p/q = \frac{1}{4}$ are -0.6176 and -0.6046, approximately.

(5) *Transition cross-road area–spring area.* This transition is due to a transversal intersection between the two flip curves of period q.

Let $\beta = \beta_0 \approx -0.888\,638\,3860$ be the value for which this intersection occurs. In figure 37 we show the bifurcation curves for $\beta < \beta_0$, and in figure 36 for $\beta > \beta_0$. In other words, when $\beta = \beta_0$ the generalized eigenvalue map as defined in section 3 has a critical point of saddle type of critical value -1. When $\beta > \beta_0$ the corresponding critical point is larger than -1 and smaller than 1, so there is a cross-road area. When $\beta < \beta_0$ the critical value is less than -1 and therefore we have a spring area. We note that in this case there are four codimension 2 flips. By further increasing β we have a case like figure 35, where $\overline{\text{fl}}^4_2$ and $\overline{\text{fl}}^4_3$ have collapsed and disappear.

As before we can obtain a similar behaviour for the quartic map cited before. For example, we can take in the parameter space a, b, c, the planes $b = a + \gamma$. Then if we perturb γ from 1.5 we obtain the same situation of our example, by changing the parameter β by γ and β_0 by 1.5

All examples presented here seem to be persistent. According to our numerical simulations, the case $0 \leqslant \beta < 1$ is quite simple, since only the saddle area seems to occur. The case $-1 < \beta < 0$, however, is a lot more complicated, while this complexity

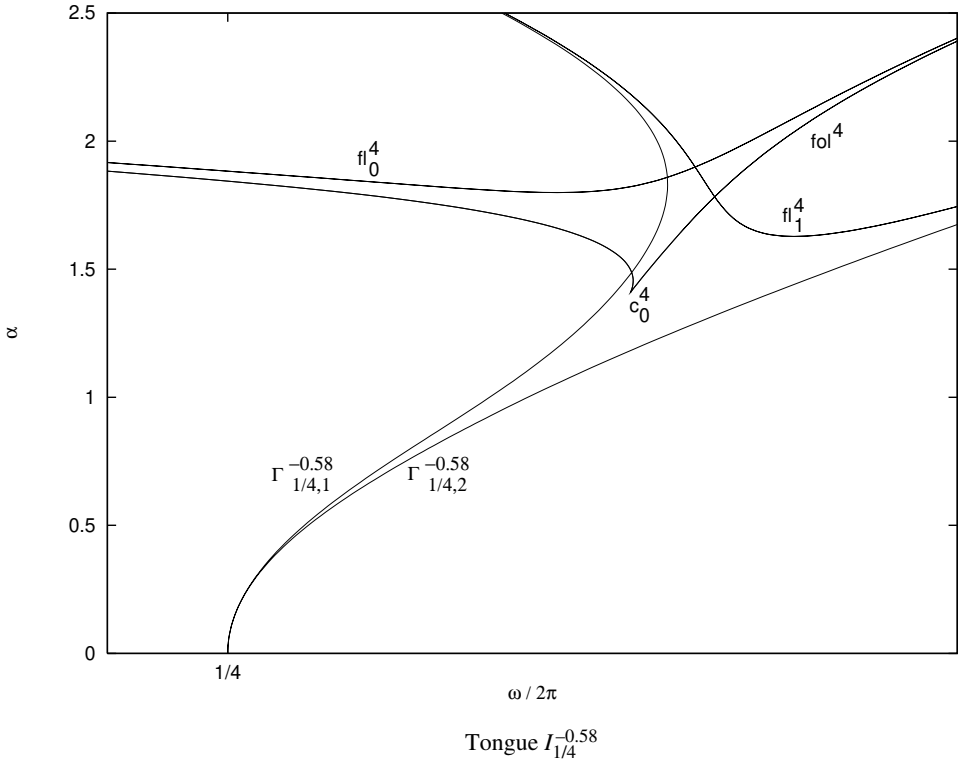

Figure 34. Transition cross-road area–saddle area. After the codimension 3 bifurcations ($\beta > \beta_1$). Same window as previous figure.

increases rapidly with decreasing β. We are not sure whether in this case all tongues display the three areas we have described.

5.1.2. The tongue boundary. In section 2 we studied the Arnold tongues $I^{\beta}_{p/q}$ for $|\beta| < 1$, conjecturing that for sufficiently small α_0, the straight lines $\alpha = \alpha_0$ intersect $I^{\beta}_{p/q}$ in an interval, with endpoints in the curves $\Gamma^{\beta}_{p/q,i}$, $i = 1, 2$. We shall see that for larger $|\alpha|$, the tongue boundary may be not so simple.

It seems that the boundary of $I^{\beta}_{p/q}$ is most complicated for $\beta < 0$. Indeed, figure 34 already suggests that the curves $\Gamma^{-0.58}_{1/4,i}$, $i = 1, 2$, are not the boundary of $I^{-0.58}_{1/4}$. This boundary seems even very complicated for β near -1. In figure 38 some 4-periodic fold curves are depicted, corresponding to the tongue $I^{-0.99}_{1/4}$. Beyond the curves $\Gamma^{-0.99}_{1/4,i}$, $i = 1, 2$, one observes several additional fold curves, each containing a cusp point close to $\Gamma^{-0.99}_{1/4,i}$ and a 'near cusp' close to $\Gamma^{-0.99}_{1/4,3-i}$. Here 'near cusp' indicates a point in the fold curve where the cusp condition (some function equal to zero) is not satisfied, but the related function has an extremum close to zero. The cusp point in a given curve is also close to the 'near cusp' point of the preceding one (going from bottom to top). See the magnifications in figure 39.

One complicating factor concerning the boundary of $I_{p/q}$, is related to codimension 3 bifurcations in the curves $\Gamma^{\beta}_{p/q,i}$, $i = 1, 2$, as described before (again see figure 33). The behaviour of the map $F_{\alpha,\omega,\beta}$ for values of the parameters in $I^{-0.99}_{1/4}$ seems very complicated.

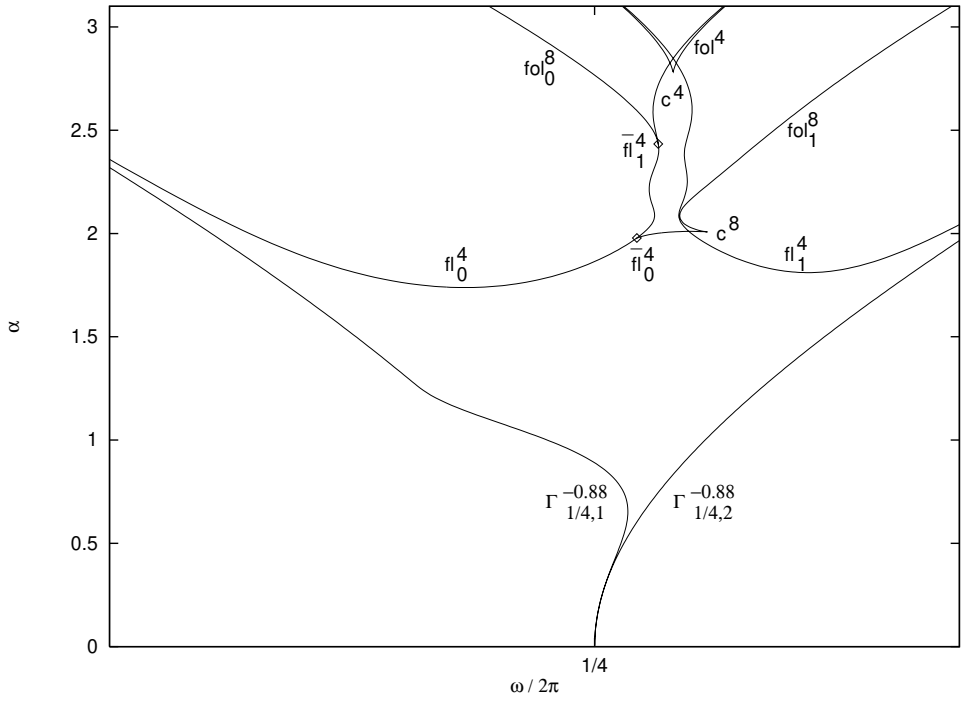

Figure 35. Cross-road area with two codimension 2 flips in $I_{1/4}^{-0.88}$.

As we will see in section 5.3, it is possible to obtain coexistence of a quasiperiodic attractor and several attracting periodic orbits of period 4, and also coexistence of a 'large' strange attractor and attracting periodic orbits. We note that at least for values of the parameters (α, ω) in $I_{1/4}^{-0.99} \cap \{(\alpha, \omega) : 0 \leqslant \alpha \leqslant 1.2\}$ there exists some attracting periodic orbit.

However, there are also many cases in which the curves $\Gamma^{\beta}_{p/q,i}$ do seem to be the boundary of $I^{\beta}_{p/q}$. We expect this to be the case anyway for all $0 \leqslant \beta < 1$, and for all $|\beta| < 1$ only in the special cases I^{β}_{p} and $I^{\beta}_{1/2+p}$, for $p \in \mathbb{Z}$.

5.1.3. Cascades of bifurcations. We have detected cascades of cusp bifurcations as described in section 4. In figures 40 and 41 there is an example inside $I^{0.2}_{1/3}$, showing bifurcation curves of periods 3, 6, 12, 24 and 48. It was conjectured by Tatjer [57], that in any parameter region with cross-road areas, saddle areas or spring areas, subregions exist with a cusp cascade. In particular, it seems that there is always a cusp cascade associated to the saddle area. From all this we now conjecture that the corresponding behaviour is the same as above for all tongues with $\beta > 0$ and also for $\beta < 0$ with $|\beta| \ll 1$.

5.2. Homoclinic bifurcations and cubic tangencies to the strong stable foliation

As we saw in the theoretical considerations of sections 2–4, the behaviour of the stable and unstable manifolds is of importance for the global geometry of the Arnold tongues of our family $F_{\alpha,\omega,\beta}$. As stated there, we first consider the simpler case $\beta = 0$, and present some conjectures in the case $0 < |\beta| \leqslant 1$, based on numerical simulations.

We now divide into two sections. First, the homoclinic bifurcations in the boundary

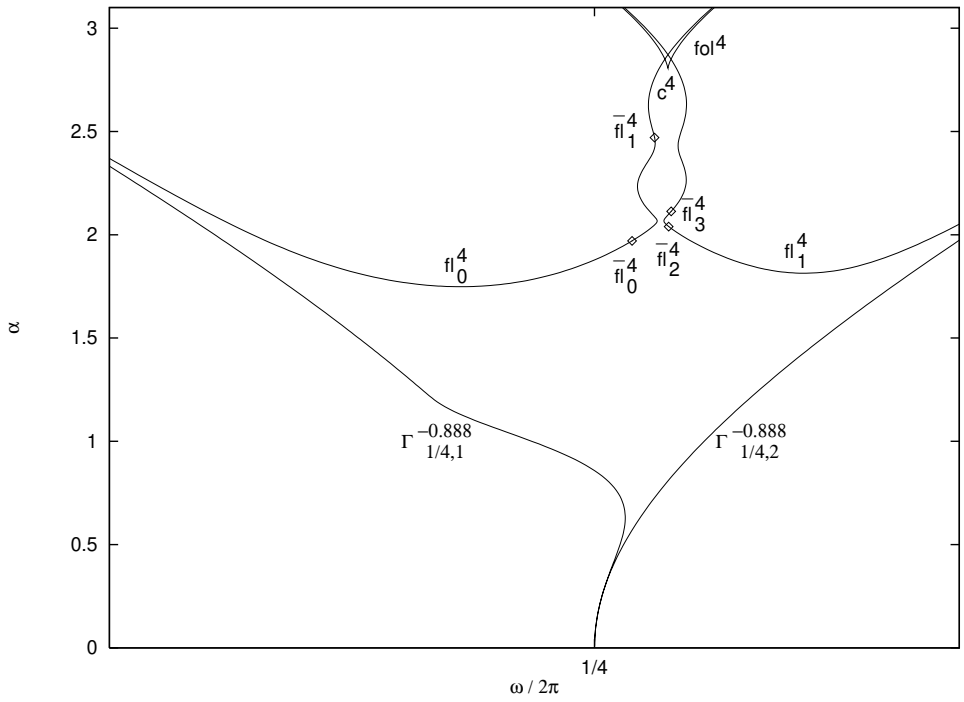

Figure 36. Cross-road area with four codimension 2 flips in $I^{-0.888}_{1/4}$.

of the tongue I^{β}_0 are considered. When perturbing from the case $\beta = 0$, we conjecture all homoclinic phenomena listed in section 4 to be persistent. As a remarkable fact, however, we here announce that for $\beta > 0$ a fold homoclinic bifurcation seems to occur, which is not persistent for $0 \geqslant \beta \gg -1$. See conjecture 5.1, below, in what refers to the 'last' tangency. In a second section we shall find two curves of homoclinic bifurcation inside the tongue I^0_0, symmetric with respect to $\omega = 0$. These curves emanate from the boundaries $\Gamma^0_{0,i}$, probably with a quadratic order of contact. We expect this phenomenon also to be persistent for $|\beta| \ll 1$. Moreover, as said before, we found the main tongue I^{β}_0 quite representative for the others.

Hereafter, we restrict ourselves to $\omega > 0$, the case $\omega < 0$ being similar. The following will be necessary throughout both sections.

The fold curves $\Gamma^{\beta}_{0,i}$, $i = 1, 2$ are given by $\alpha = \pm(1 - \beta)\omega$. As before, we have to distinguish between $\bar{F}$ and its lift F. Indeed, we study the family $F_{\omega(1-\beta),\omega,\beta}$, associated to the right-hand tongue boundary. Let $p_{\omega,\beta,k} = (x_{\omega,\beta,k}, y_{\omega,\beta,k})$, $k \in \mathbb{Z}$ be the fold fixed points of this. It is easy to see that $x_{\omega,\beta,k} = x_{\omega,\beta,0} + 2\pi k$ and $y_{\omega,\beta,k} = y_{\omega,\beta,0}$, all these points being representatives of one fixed point $\bar{p}_{\omega,\beta}$ of $\bar{F}_{\omega(1-\beta),\omega,\beta}$.

5.2.1. Homoclinic bifurcations and cubic tangencies to the strong stable foliation on the tongue boundary. In the previous section we described the perturbation programme from the case $\beta = 0$, i.e. from the unperturbed map $F_{\omega,\omega,0}(x, y) = (x + \omega(1 + \sin x + y), 0)$ on the tongue boundary $\Gamma^0_{0,2}$. Based on the results described in section 4 (see also appendix D) and on our numerical computations (mainly figure 42), we now formulate for the case $|\beta| \leqslant 1$ and the saddle-node fixed point, $\bar{p}_{\omega,\beta}$.

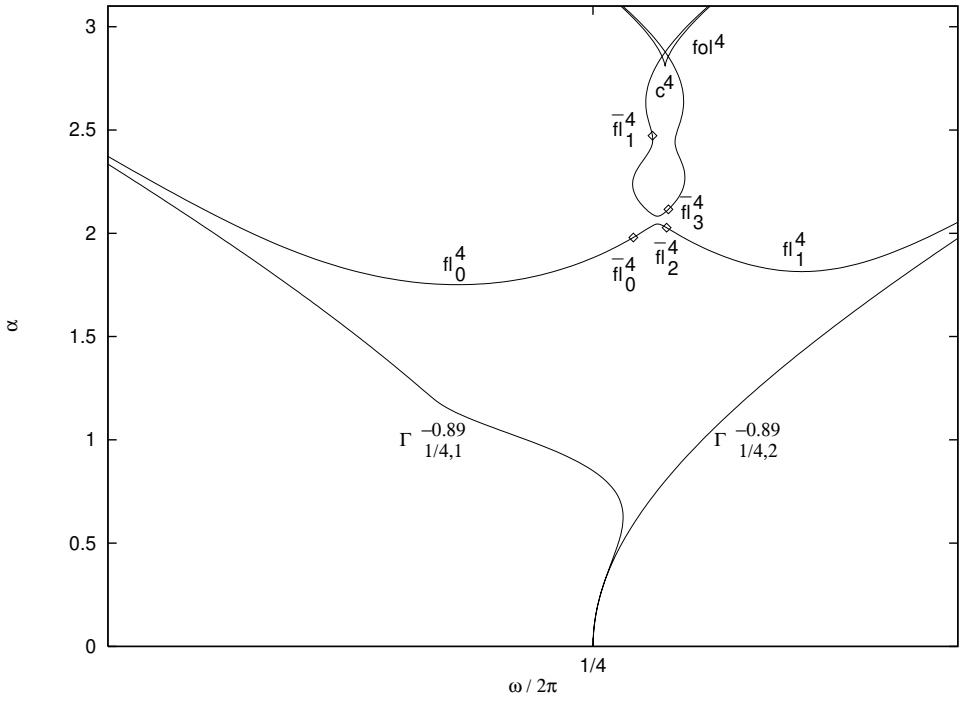

Figure 37. Spring area with four codimension 2 flips in $I_{1/4}^{-0.89}$.

Conjecture 5.1. *Figure 42 displays an accurate configuration of the global bifurcation curves where the following properties hold.*

(1) For parameter values (ω, β) *inside the region A no critical cycle exists, while the curve* ω_0 *corresponds to the first or inner (cubic) tangency to the strong stable foliation.*

(2) All the homoclinic bifurcations are quadratic, except at the point of contact between the curves ω_3 *and* ω_4*, which is a cusp point of cubic tangency.*

(3) The parts of the curves ω_2 *and* ω_3 *in the border of the region* $B \cup C$ *correspond to the first homoclinic tangency, while at the curve* ω_1 *the last homoclinic tangency occurs (as* ω *increases from* 0 *to* ∞*).*

(4) For $\beta < 1$ *and close to* 1*, all the differences between* $\omega_0(\beta)$*,* $\omega_3(\beta)$ *and* $\omega_1(\beta)$ *are exponentially small in* $1 - \beta$*.*

(5) For $\beta > -1$ *and close to* -1*, the functions* $\omega_0(\beta)+1$ *and* $\omega_2(\beta)+1$ *are exponentially small in* $1 + \beta$*.*

(6) $\omega_1(\beta) \uparrow \infty$ *as* $\beta \downarrow 0$ *and* $\omega_2(\beta), \omega_4(\beta) \uparrow \infty$ *as* $\beta \uparrow 0$*.*

The numerical values of the cusp point in item 1 and the point of intersection of the curves ω_1 and ω_2 are, respecively, $(\omega_3(\beta_0), \beta_0) = (1.5110, -0.3907)$ and $(\omega_2(\beta_1), \beta_1) = (1.5301, -0.2832)$.

In figures 43 and 44 one can see the behaviour of the unstable invariant manifold of the saddle-node point near values corresponding to a cubic critical cycle. Finally, in figure 45 pictures are shown of the invariant manifolds of the saddle-node fixed point corresponding to several zones in the (ω, β) plane.

The computation of the curve ω_0 has been carried out in a simple way. Starting with a local approximation of the unstable branch of the fold, it has been globalized numerically,

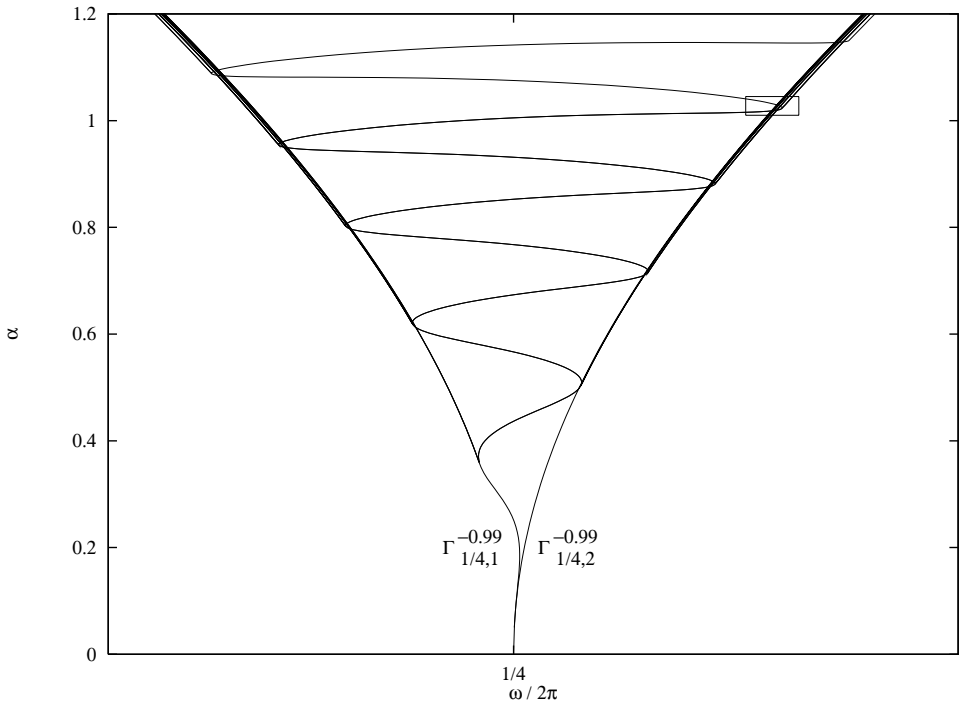

Figure 38. Some 4-periodic fold curves of the tongue $I^{-0.99}_{1/4}$.

until it is close enough to the 'node part' of the fold. A change of variables puts the invariant manifolds as the horizontal and vertical axes, locally. Assume the vertical axis corresponds to the strong stable manifold. Then, points on a fundamental domain have been taken, and the projection on the horizontal axis of the return close to the node part of the fold has to preserve the order before the cubic tangency, while after this tangency there are points whose projections have reversed order. It is easy to implement routines detecting the critical situation, but one should be very careful with the arithmetic error.

The following question is also of interest. The curves ω_3 and ω_1 correspond to first (or inner) and last (or outer) homoclinic tangencies, respectively. The curve ω_0 corresponds to the inner cubic tangency to the strong stable foliation of the saddle node. What about an outer cubic tangency to this foliation? The experimental results are shown in figure 46, where for completeness, we also include the parts of the ω_0, ω_1, and ω_3 curves in the window $(\omega, \beta) \in [0, \pi] \times [0, 1]$. The new curve is denoted by ω_5, despite the fact that it cannot be represented as the graph of a single-valued function of β. For the computations around the saddle node it is convenient to use a different representation of the map (1), namely

$$\begin{pmatrix} u \\ v \end{pmatrix} \mapsto \begin{pmatrix} u^* \\ v^* \end{pmatrix} = \begin{pmatrix} u + \frac{\alpha}{2}(v + 2\sin^2(\frac{u}{2})) \\ \beta(v + 2\sin^2(\frac{u}{2})) + 2\sin^2(\frac{u^*}{2})) \end{pmatrix}, \tag{4}$$

where $\alpha = \omega(1 - \beta)$. Now the saddle node is at the origin and the centre manifold has a representation $v = g(u) = \sum_{n \geqslant 2} g_k u^k$, where the coefficients g_k depend on ω and β.

Before going into detail we must clarify the exact meaning of the ω_5 curve. For small values of ω it is certainly related to cubic tangency to the strong stable foliation of $\bar{p}_{\omega,\beta}$. Between the outer homoclinic tangency and the outer cubic tangency to this foliation, the

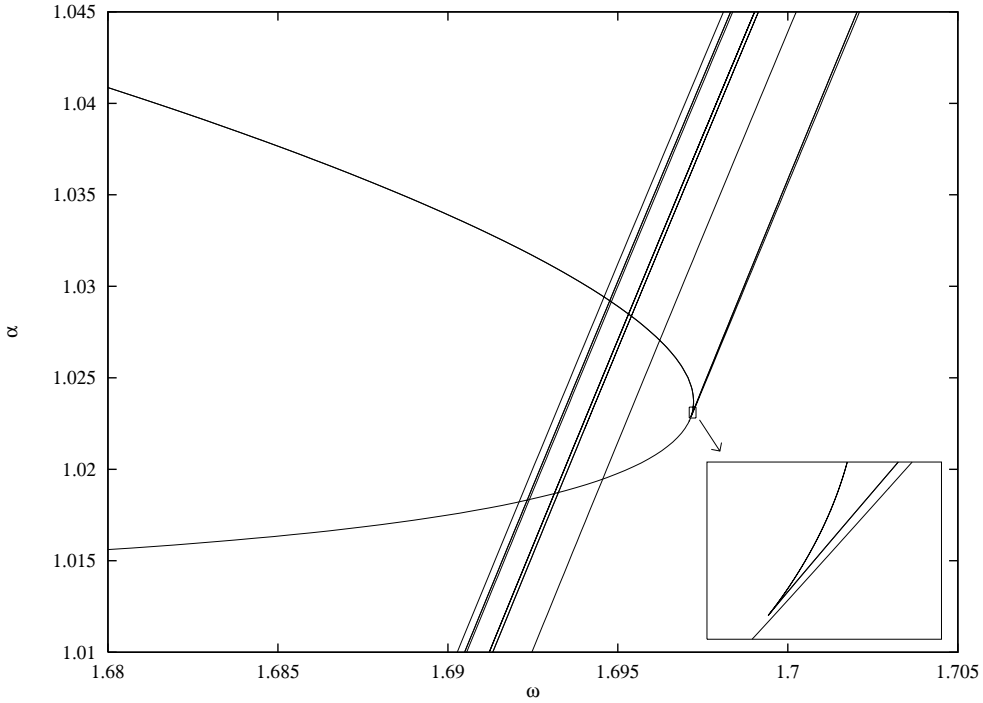

Figure 39. Magnification of the rectangle of the previous figure. As the arrow shows, in the lower right corner there is a magnification of the small rectangle, using the window $[1.6971, 1.6973] \times [1.0228, 1.0234]$.

branch $W^u(\bar{p}_{\omega,\beta})$ (W^u for short) is 'folded', and the 'folds' are preserved under iteration. What we have followed, to obtain the curve ω_5, is the boundary of the set in the (ω, β)-plane for which there are 'folds' in W^u. To detect the 'folds', after W^u has been approximated in a fundamental domain using g, it has been continuated with controlled distance between any two consecutive points and controlled angle between any three consecutive points. The 'folds' show up if two points, having $u_1 < u_2$ in the fundamental domain, have iterates under (4) such that the order of the first components is reversed (mod 2π). This has been checked allowing for some tolerance to account for the rounding errors.

As can be seen in figure 46, for small values of ω the curve ω_5 seems to also have a exponentially flat contact with ω_1 and the other two curves. For $\omega > 1$ it goes away from ω_1 and several 'soft' peaks appear, related to resonances. The sources of the existence of 'folds' in W^u can be of different kinds. The following points have been observed.

- A quadratic tangency to the strong stable foliation at the saddle node.
- W^u spirals approaching an invariant curve with rational rotation number. The attracting periodic orbit inside this curve goes from a node to a focus.
- The same as in the previous case, the periodic attractor being still a node, but the points of W^u approach the node entering close to only one of the branches of the unstable manifold of the node (see figure 13(d)).
- W^u spirals approaching a periodic saddle and becomes tangent to the stable foliation of that saddle. Eventually, by moving parameters, W^u has points going to the saddle and later they go to an attracting focus. This seems to be the main mechanism for values of β close to 1.

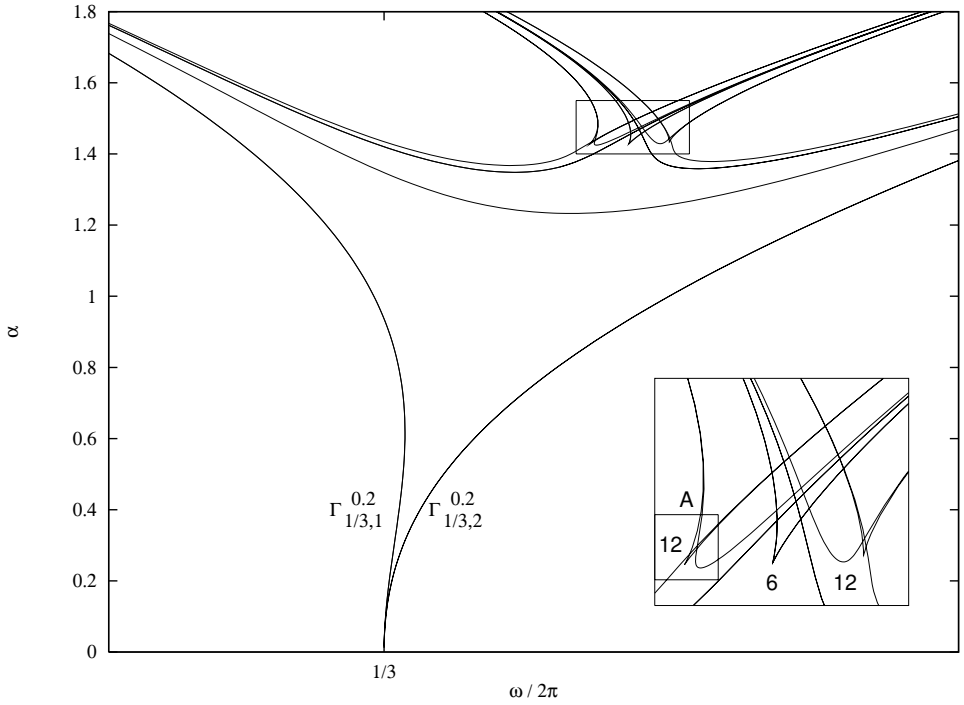

Figure 40. First steps of a cusp cascade for $I^{0.2}_{1/3}$. In the lower right corner there is a magnification of the rectangle $[2.23, 2.31] \times [1.4.1.55]$ marked in the upper part.

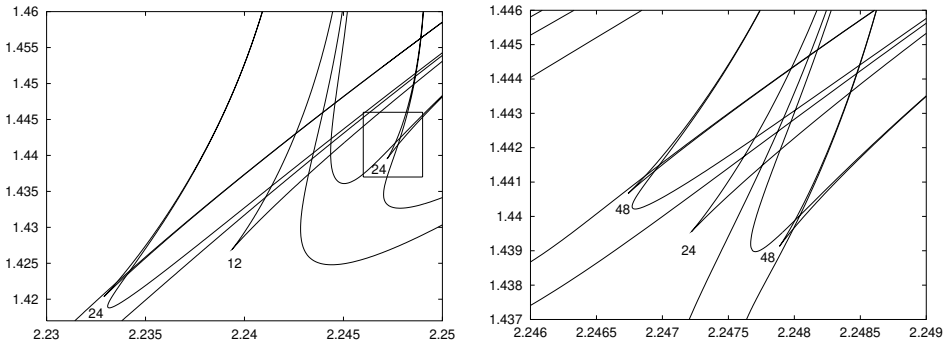

Figure 41. Cusp cascade (details). On the left we show a magnification of the rectangle A of the previous figure. This figure includes cusps of period 12 and 24. The small rectangle of this picture is magnified on the right. The right picture includes cusps of periods 24 and 48.

It is clear that the source of 'folds', in the first case, is due to the proximity of a homoclinic situation and, in the other cases, to the proximity to a heteroclinic one.

5.2.2. Homoclinic bifurcations originating from a tongue boundary. Although one can find many curves of homoclinic bifurcation inside the tongue $I^{\beta}_{0,i}$ (for example, cf Ostlund *et al* [43]), our main interest is with curves originating from a fold point on the boundary. This is concerned with our preoccupation with the tongue boundaries and the accumulation property

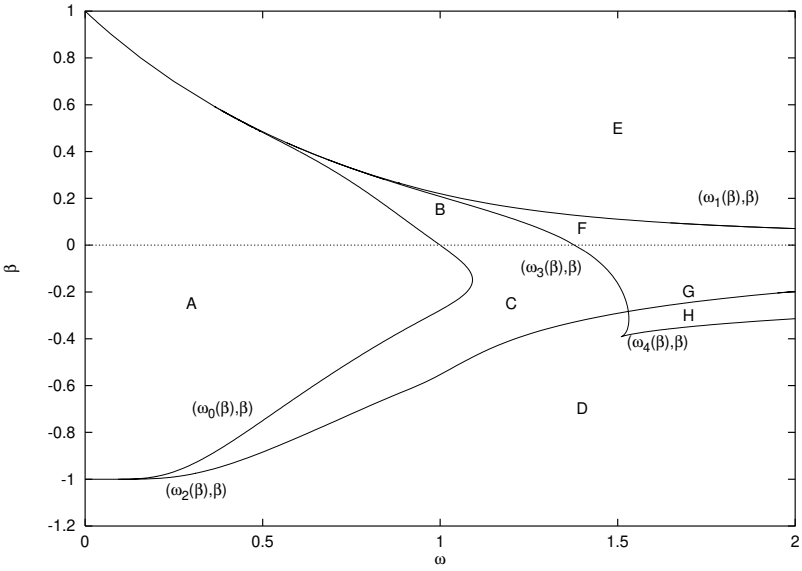

Figure 42. Curves of cubic critical cycles (ω_0) and saddle-node homoclinic bifurcations ($\omega_1, \ldots, \omega_4$), corresponding to the saddle-node fixed point in the parameter plane (ω, β).

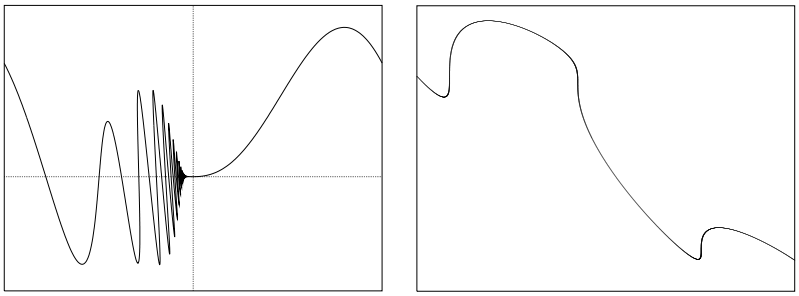

Figure 43. W^u_{sn} for $\beta = -0.7$, $\omega = 0.547\,341$. The origin is at the *sn* and the axes are eigenspaces. Near the *sn* the foliation $\mathcal{F}^{ss}$ is almost vertical. Left: the full manifold in the window $[-3.2, 3.2] \times [-0.5, 0.75]$. Right: magnification using the window $[-0.08, -0.075] \times [0.0044, 0.0005]$, containing two complete fundamental domains; the vertical tangencies are easily seen.

to be illustrated in section 5.3.2 and which was sketched at the end of section 4.3. In this respect the two curves of homoclinic bifurcation, to be presented here, also are of special interest. In fact, again we restrict ourselves to considering the main tongue I^0_0, generalizing from this.

The new curves are denoted $T^{i,\beta}_{p/q}$, so presently we shall deal with $T^{i,\beta}_0$, $i = 1, 2$. Their definition is by continuation, indeed, they represent homoclinic bifurcation curves of rotation number p/q originating from a fold homoclinic bifurcation. The case with $\beta = 0$ was displayed in section 2. In figures 47–51 we give several configurations of the homoclinic bifurcation curves, in the (ω, α)-plane, that are born in the saddle-node bifurcation curve $\Gamma^{\beta}_{0,2}$. Moreover, in each picture there are the curves corresponding to the cubic tangency of the unstable invariant manifold of the saddle fixed point to the strong stable foliation of its corresponding node (born by saddle-node bifurcation). Also, we depict

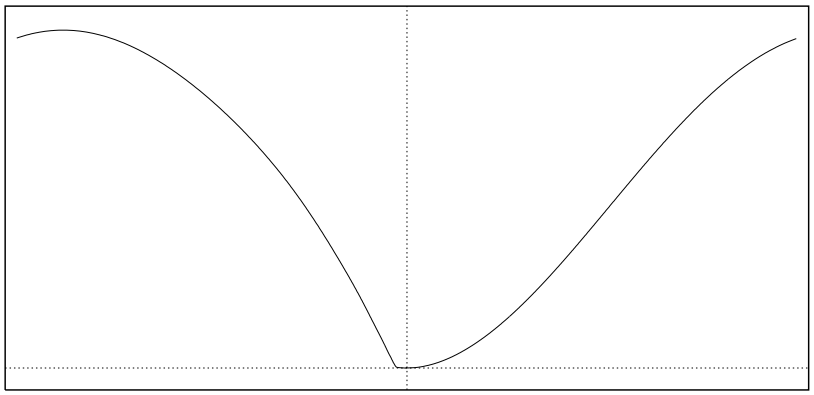

(*a*)

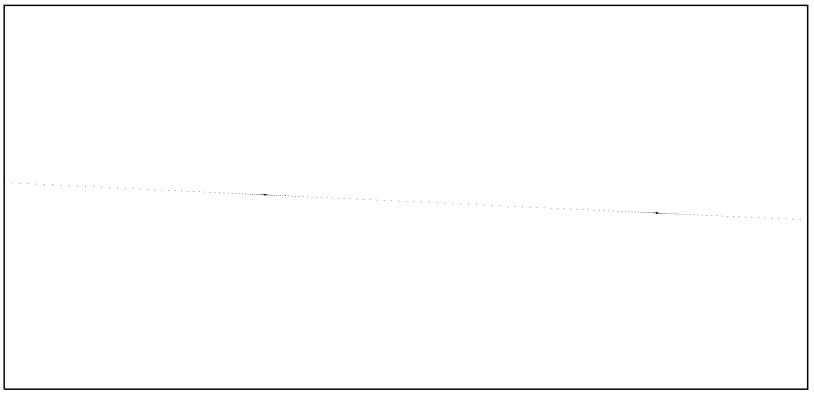

(*b*)

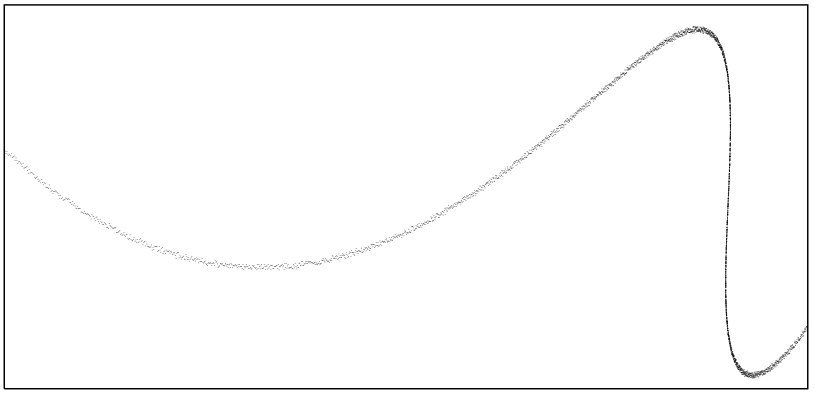

(*c*)

Figure 44. The unstable manifold W^u_{sn} of the saddle-node (sn) for $\beta = 0.3$, $\omega = 0.718\,8724$ (slightly after the cubic tangency to $\mathcal{F}^{ss}$). Origin and axes as in figure 43. (a) The full manifold. Window: $[-3.2, 3.2] \times [-0.2, 3.45]$. ($b$) Magnification of window $[-0.052, -0.05] \times [0.0015, 0.0035]$ using 100 points per fundamental domain. Roughly two fundamental domains are displayed. One can see an accumulation of points where the tangencies with $\mathcal{F}^{ss}$ occur. (c) Figure (b) enlarged, using 10^5 points per fundamental domain, to the window $[-0.051\,3437, -0.051\,3436] \times [0.002\,5126, 0.002\,5127]$. The value of the regression line has been substracted from the ordinates and the difference is displayed. The vertical window in (c) is $[-3 \times 10^{-15}, 3 \times 10^{-15}]$. One can see the effect of the rounding errors and the shape of W^u_{sn} near a cubic tangency to the (vertical) $\mathcal{F}^{ss}$.

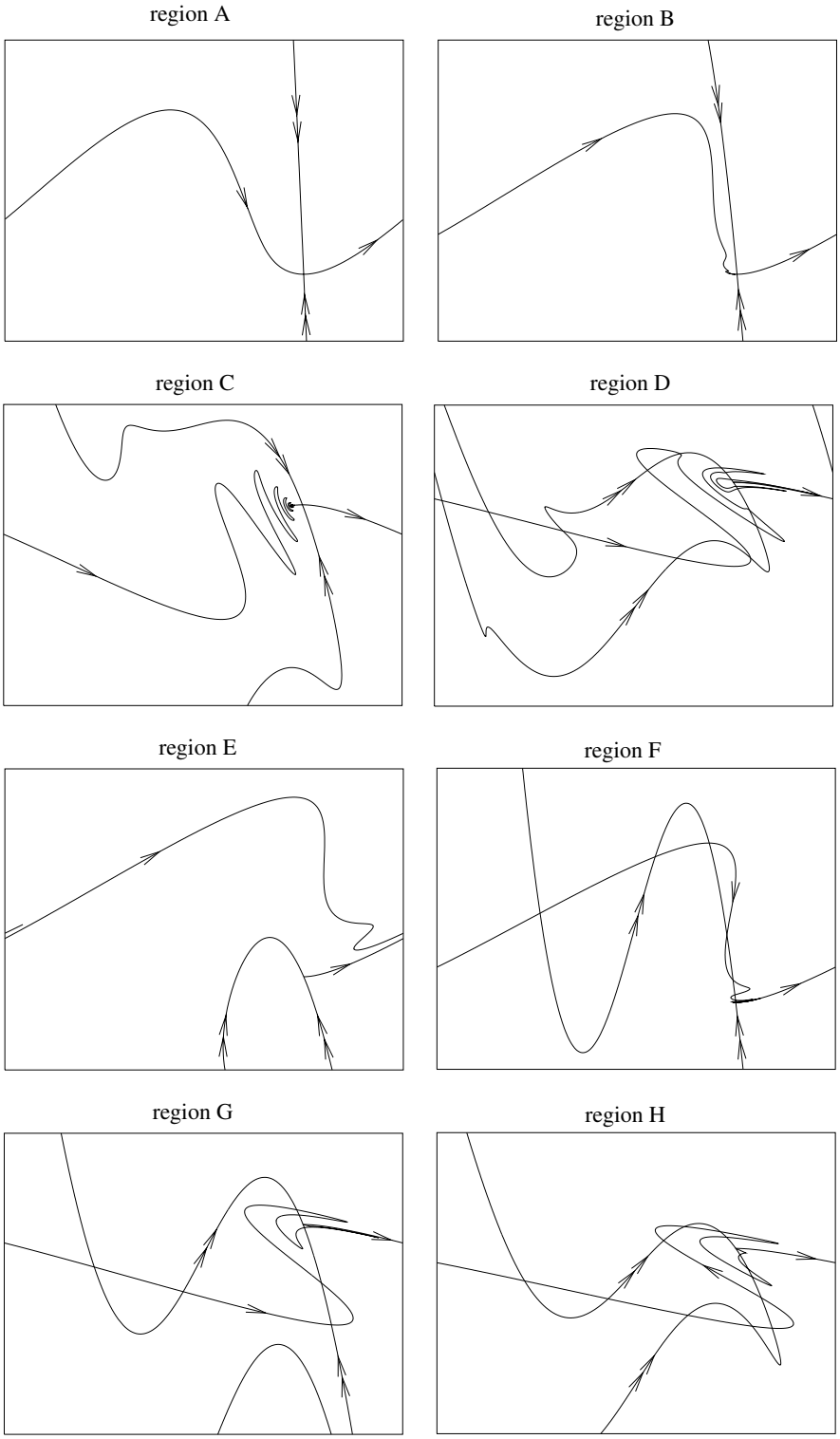

Figure 45. Configuration of the invariant manifolds of the saddle-node fixed point in the regions indicated in figure 41.

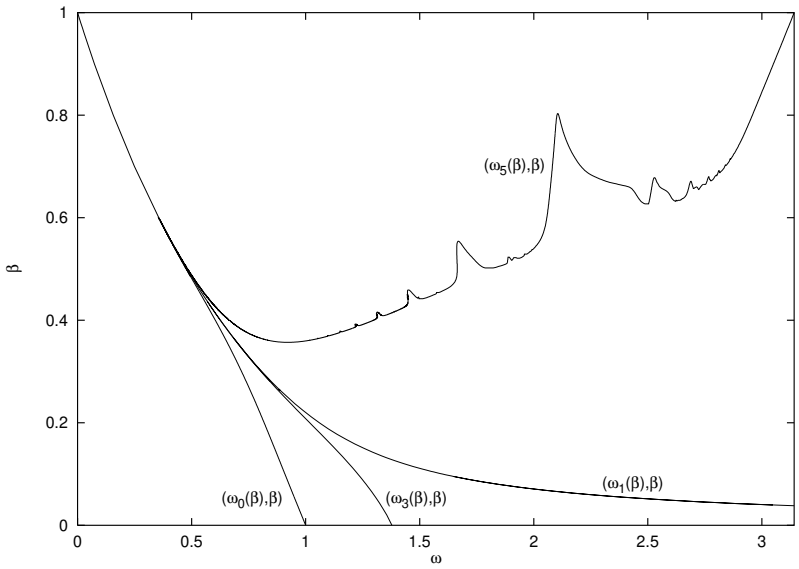

Figure 46. The curves of inner (ω_0) and outer (ω_5) cubic tangency to the strong stable foliation at the saddle node, together with the curves of inner (ω_3) and outer (ω_1) homoclinic tangency.

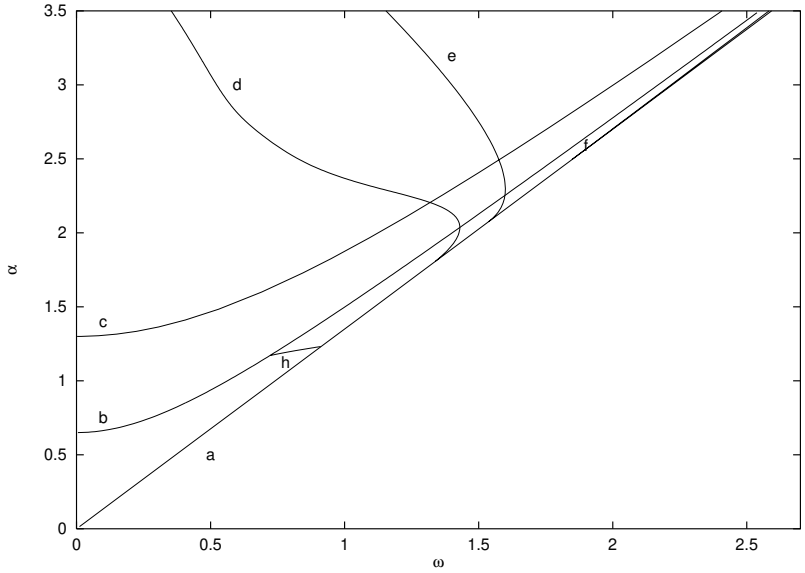

Figure 47. Several bifurcation curves for $\beta = -0.35$.

the curves corresponding to equal absolute value of the eigenvalues ($\Sigma_{2\beta^{1/2}}$ in the notation of section 2.4 for $\beta > 0$ and Σ_0 for $\beta < 0$) and the curves $\Sigma_{-1-\beta}$ corresponding to the flip bifurcation of the fixed points. Apparently the behaviour of the curves is similar for $\beta > 0$ and there are several possible configurations for $\beta < 0$. This will be important when determining the smoothness and the destruction of the invariant circle.

To be more concrete, in figures 47–51 the lines labelled a, b and c correspond to

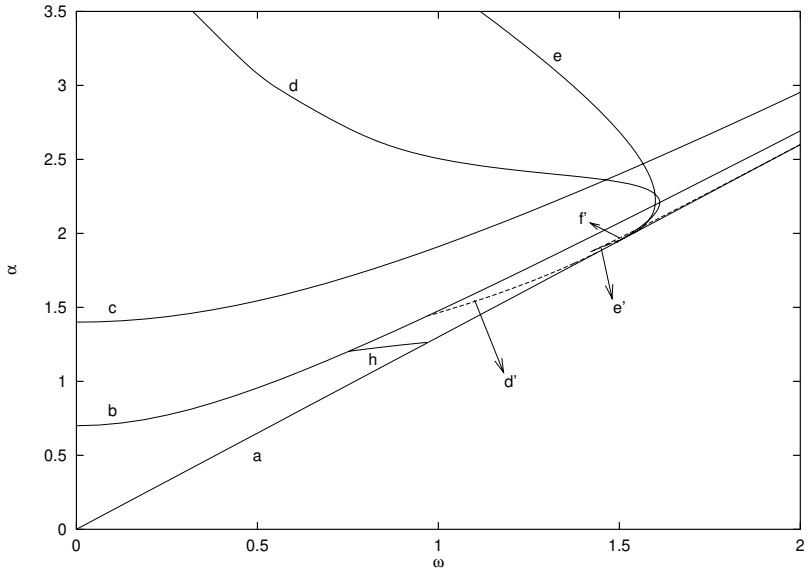

Figure 48. Several bifurcation curves for $\beta = -0.3$.

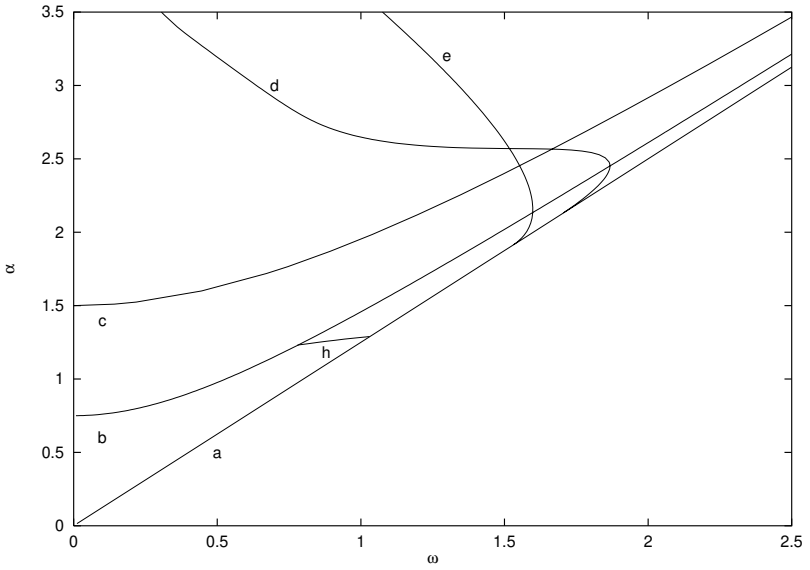

Figure 49. Several bifurcation curves for $\beta = -0.25$.

fold, equal eigenvalues (in absolute value) and flip bifurcations, respectively. That is, for simplicity, a stands for $\Gamma^{\beta}_{0,2}$, b stands for $\Sigma_{2\beta^{1/2}}$ (if $\beta > 0$) and for Σ_0 (if $\beta < 0$), and c stands for $\Sigma_{-1-\beta}$. Lines d, e and f (the latter displayed only in figure 47) denote quadratic homoclinic tangencies. For $\beta > 0$ the line g corresponds to the last homoclinic tangency. The line h denotes a cubic tangency to the strong stable foliation. In figure 48 consider lines d', e' and f'. They correspond to heteroclinic tangencies between the unstable manifold of the saddle and the strong stable one of the node. We note that e' and f' meet in a

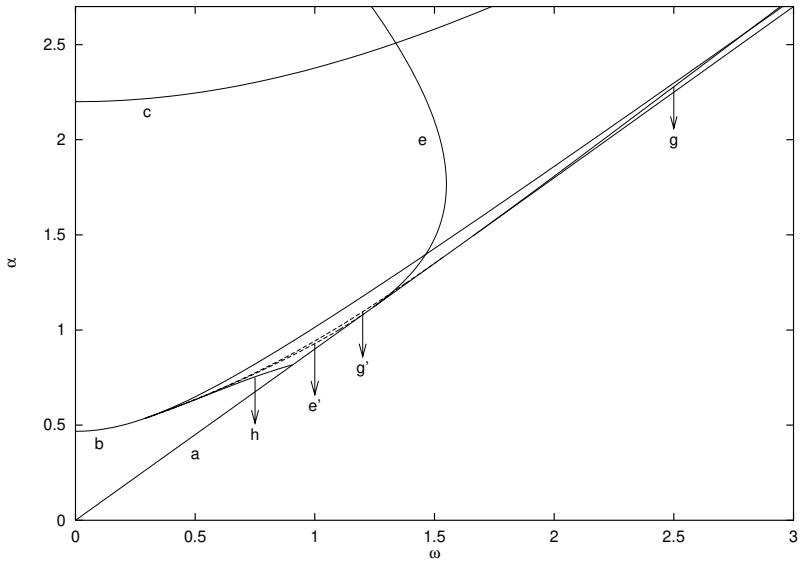

Figure 50. Several bifurcation curves for $\beta = 0.1$.

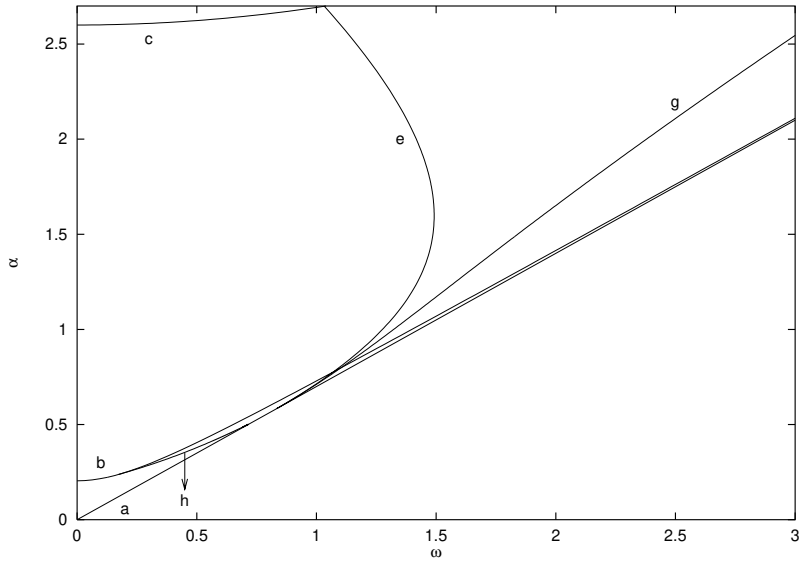

Figure 51. Several bifurcation curves for $\beta = 0.3$.

cusp point, corresponding to a cubic heteroclinic tangency. In figure 50 lines e' and g' are shown, which correspond to a first and last heteroclinic tangency of the type described in figure 48.

In view of the invariant circle, if it is not destroyed by phenomena related to other fixed or periodic points, we have the following scenario. Let us begin with figure 47. In the interior of the region bounded by a, b and h the circles are smooth curves, the degree of differentiability decreasing when going from a to b (see sections 2.4 and 5.3.1). When either b or h are reached, the invariant curve is just C^0 (with a sudden jump of differentiability if

h is reached). The curve persists while remaining in the region bounded by a, c and d. In figure 48 a part of the role of d is taken by e, whichever is reached first, and in figure 49 it is fully taken by e.

For $\beta > 0$, in figures 50 and 51, lines a, b and h have the same role as before, but the boundary of existence of C^0 invariant curves is now made by the corresponding parts of the lines a, c and e.

On the fold the curves h, g, d, e and f begin at $\omega_0(\beta), \ldots, \omega_4(\beta)$, respectively. See conjecture 5.1.

5.3. Global aspects

We now come to deal with several global phenomena appearing in the fattened Arnold family $F = F_{\alpha,\omega,\beta}$. We consider the loss of smoothness, namely the destruction of the invariant circle, accumulation of the tongues, the occurrence of strange attractors and the coexistence of various types of attractors.

5.3.1. The invariant circle. Two numerical tests have been (repeatedly) carried out involving the genericity property on the differentiability of the invariant circle when the rotation number is rational, that is, inside the Arnold tongue.

Both tests use the fact that the invariant circle exactly consists of the closure of the unstable manifold W^u_S of a periodic saddle S. Indeed, this is a piecewise analytic curve, where the smoothness is only lowered at the nearby periodic nodes, where different branches of W^u_S enter. Let N be such a node, with eigenvalues $0 < \lambda_1 < \lambda_2 < 1$. By W^{ss}_N, W^s_N we denote the strongly stable and the (weakly) stable invariant manifolds of N, associated to λ_1 and λ_2. According to the results of [14], if $r := \log(\lambda_1)/\log(\lambda_2) \notin \mathbb{N}$ then there exists an unique analytic W^s_N. Generically this does not coincide with the circle W^u_S, which is one of the things checked by the tests. Nevertheless we can use W^s_N as a local reference for the branches of W^u_S to be compared.

For both tests we select parameters such that $r \notin \mathbb{N}$ and we start as follows.

- First S is computed and W^u_S is obtained by means of local (Taylor) expansions.
- The manifolds (branches) are globalized by taking a suitable number of points in a fundamental domain and iterating under our map F.

Now we describe the first test. Up to an affine change of variables, we may assume N at the origin and the coordinate axes such that the tangents to W^s_N and to W^{ss}_N, at N, are in the x and y directions, respectively. The manifold W^s_N can either be generated as the graph of an analytic function, $y = g(x)$, or by means of a parametric representation $p(t) = (x(t), y(t))$ such that $F(p(t)) = p(\lambda_2 t)$. An advantage of the latter representation is that, as F is an entire function, the analyticity of W^s_N implies that p is entire.

Consider points in W^u_S close to N with coordinates $(\bar{x}, \bar{y})$. There is a value, $\bar{t}$, of t in the parametric representation, p, such that $x(\bar{t}) = \bar{x}$ and now we consider and compute the error in y:

$$\Delta y := \bar{y} - y(\bar{t}).$$

When genericity holds, $|\Delta y|$ must behave as $A|x|^r(1 + \mathrm{o}(1))$ as $x \to 0$. Taking logarithms yields $z := \frac{\log(|\Delta y|}{\log(|x|)} = r + \frac{\log(A)+\mathrm{o}(1)}{\log(|x|)}$. Therefore, by plotting z versus $\frac{1}{\log(|x|)}$ for the unstable branches of W^u_S entering N from the right and from the left, one must see lines tending to r as $1/\log(|x|)$ tends to zero. Furthermore, if the limit slopes, $\log(A_r)$ and $\log(A_l)$ are different, the invariant curves are just C^r. This is illustrated in figure 52 for $\omega = \pi/10, \beta = 0.1$ and α taking the values 0.54 and 0.545. In these cases N and S are fixed points. We note

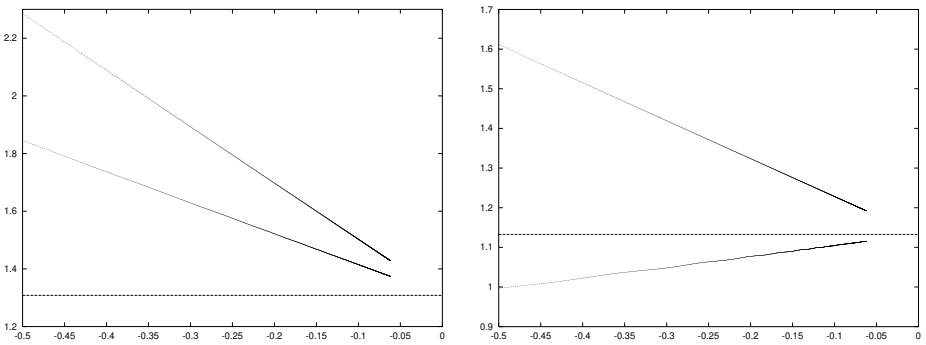

(*a*) (*b*)

Figure 52. Genericity test using the order of contact between the invariant circle and W^s_N at the node. $\omega = \pi/10$, $\beta = 0.1$. (*a*) $\alpha = 0.54$; (*b*) $\alpha = 0.545$. See the text for additional explanation.

that the rounding errors prevent taking $|x|$ too small. The horizontal lines correspond to the limit value r.

The second test concerns the Fourier expansion of the invariant circle $W^u_S \cup \{N\}$. As before it is analytic except at a finite number of points (the periodic nodes) where we test whether it is exactly of class $C^r, r \notin \mathbb{N}$. Let W^u_S be represented as $y = h(x)$, h being a 2π-periodic function. Let $\sum_{n\geqslant 0} h_{n,c}\cos(nx) + h_{n,s}\sin(nx)$ be the Fourier series of h, and define $h_n = (h^2_{n,c} + h^2_{n,s})^{1/2}$. Then one has $h_n = \frac{B(1+o(1))}{n^{r+1}}$ when $n \to \infty$. By taking logarithms one has $z := \frac{\log(h_n)}{\log(n)} = r + 1 + \frac{\log(B)+o(1)}{\log(n)}$. Therefore, the representation of z versus $\frac{1}{\log(n)}$ must tend to $r + 1$ as $\frac{1}{\log(n)}$ goes to zero. The steps to follow are as follows.

- It is convenient to have points (x, y) on the invariant circle for equally spaced values of x. This is obtained by interpolation from a suitable set of points produced by iteration from a fundamental domain of W^u_S.
- Then a Fourier analysis is carried out using a standard FFT procedure. The moduli of successive harmonics are obtained. The computations are stopped whenever h_n is below 10^{-14}, to prevent the effect of rounding errors. Otherwise, up to 2^{20} harmonics have been computed.

A small sample of results is displayed in figure 53 for $\omega = \pi/10$, $\beta = 0.1$ and α taking on the values 0.45, 0.50, 0.54 and 0.5463. The latter is rather close to the value of α giving $\lambda_1 = \lambda_2$ ($\alpha = 0.546\,389\,627\,623\ldots$). As in the previous figure, the horizontal lines correspond to the limit value $r + 1$.

In all the cases we obtained results as to be expected. Hence, there is strong evidence for generic behaviour of the smoothness of the invariant circle.

On the other hand, if we take a fixed value of β, there is a way to obtain an approximation of the set of parameter values (ω, α) for which an r-normally hyperbolic invariant circle exists.

Indeed, let $p_{\alpha,\omega}$ be a p/q-periodic attractor with $(\alpha, \omega) \in I^\beta_{p/q}$ and let λ_1 and λ_2 be its eigenvalues, such that $|\lambda_1| \leqslant |\lambda_2| < 1$. We know that $\lambda_1\lambda_2 = \beta^q$. If there exists an r-normally hyperbolic invariant circle then $|\lambda_1|/|\lambda_2|^r < 1$. So, let us consider the set $\tilde{\Sigma}_{p/q,r} \subset I^\beta_{p/q}$ defined as

$$(\alpha, \omega) \in \tilde{\Sigma}_{p/q,r} :\Leftrightarrow \operatorname{tr} DF^q_{\alpha,\omega,\beta}(p_{\alpha,\omega}) < \operatorname{sign}(\beta^q)|\beta|^{rq/(r+1)} + |\beta|^{q/(r+1)},$$

for the related p/q-periodic point. So for all $(\omega, \alpha) \notin \tilde{\Sigma}_{p/q,r}$ the global attractor Ω is not

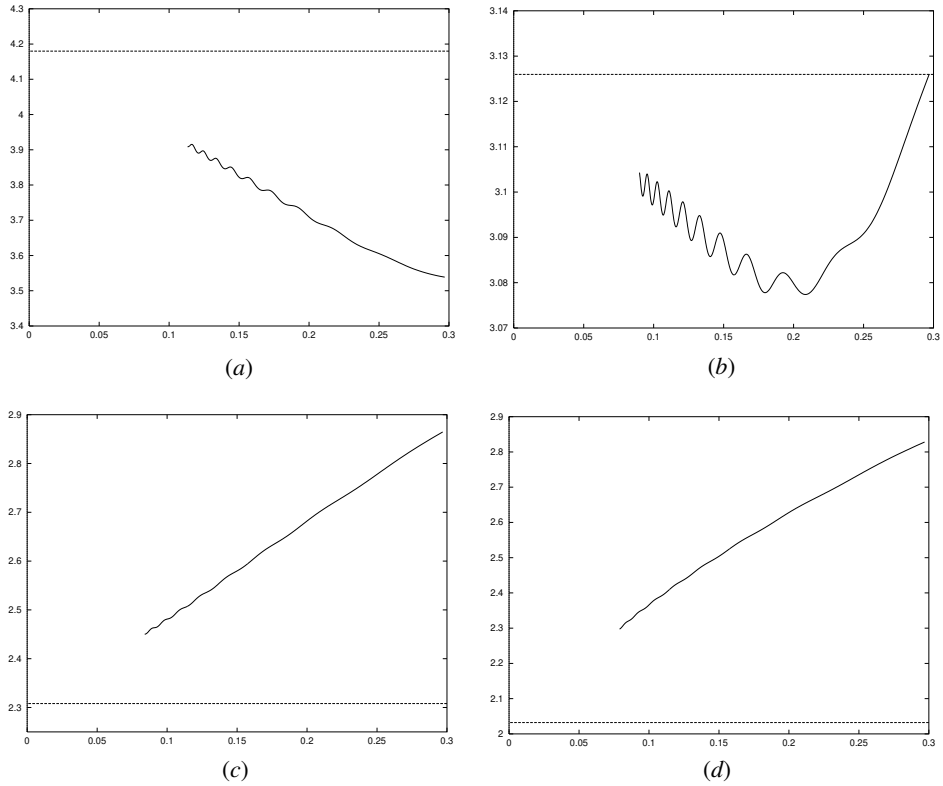

Figure 53. Genericity test using the asymptotic behaviour of the coefficients of the Fourier expansion of the invariant circle. $\omega = \pi/10$, $\beta = 0.1$. (*a*) $\alpha = 0.45$; (*b*) $\alpha = 0.50$; (*c*) $\alpha = 0.54$; (*d*) $\alpha = 0.5463$. See the text for additional explanation.

an r-normally hyperbolic invariant circle. Therefore the set of parameter values (α, ω) for which Ω is an r-normally hyperbolic invariant circle is contained in $\cap_{p/q\in\mathbb{Q}} \tilde{\Sigma}_{p/q,r}$.

In order to compute the set $\cap_{p/q\in\mathbb{Q}} \tilde{\Sigma}_{p/q,r}$ it is sufficient to compute for every tongue $I^{\beta}_{p/q}$ the curves $\Sigma_t \subset I^{\beta}_{p/q}$, as defined in proposition 2.10. We have performed these computations for all tongues of period less than or equal to 17. In figure 54 there is a representation in the (ω, α) plane of the set $\cap_{p/q\,|\,0<q\leqslant 17,\,0<p\leqslant q/2} \tilde{\Sigma}_{p/q,1}$ for the values of β 0.9, 0.3, -0.3 and -0.9. The curves are approximations of the upper boundary of the sets for which the global attractor can be just a continuous invariant circle. (These are obtained by first computing the corresponding flip curves.) However, the reader should be aware that for some regions below these curves, other mechanisms, such as homo/heteroclinic tangencies, can also destroy the invariant circle.

5.3.2. Accumulation of tongues. One of the interesting global phenomena is the accumulation of tongues on curves of homoclinic bifurcation. This accumulation phenomenon seems to take place for all $|\beta| < 1$.

Again, we present most of the results for the main tongue. The curves $\Gamma^{\beta}_{p/q,i}$, $i = 1, 2$ with $p = 1$ or at least p fixed, originating at $(\alpha, \omega) = (0, 2\pi p/q)$, seem to accumulate on two different curves: the left-hand curves ($i = 1$) accumulate on one curve and the right-hand ones on another. For this it is required that $q \to \infty$. We only consider $p/q > 0$,

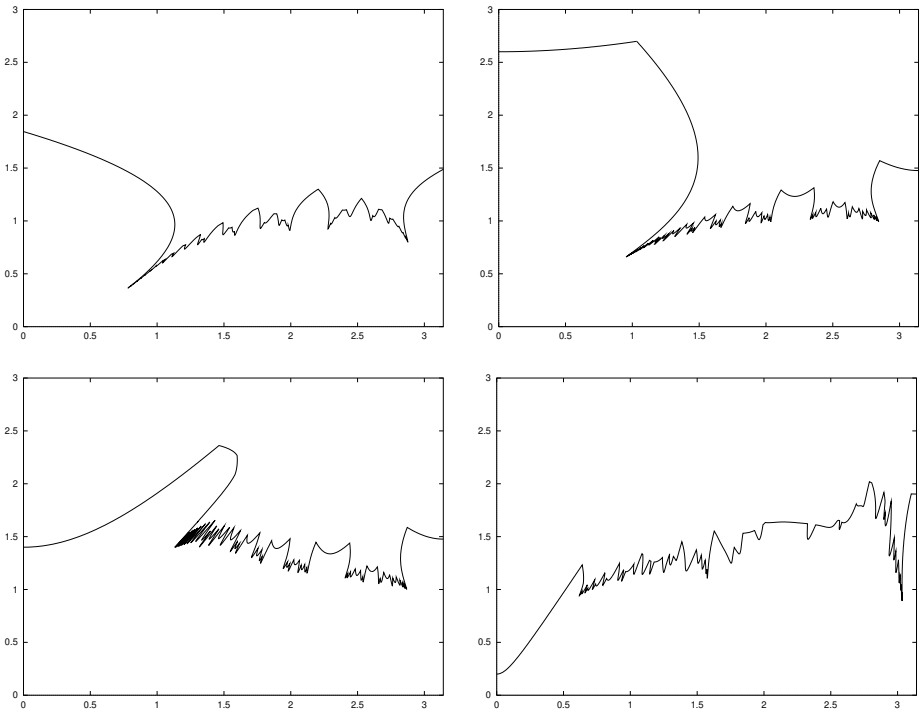

Figure 54. Existence of invariant circles. The curves shown are approximations of the upper boundary of the sets for which invariant circles exist. Top: left $\beta = 0.9$, right $\beta = 0.3$. Bottom: left $\beta = -0.3$, right $\beta = -0.9$. In the horizontal and vertical directions the variables are ω and α, respectively.

the other case being obtained by symmetry. We distinguish between the three cases $\beta = 0$, $\beta < 0$ and $\beta > 0$. There is an increasing complexity of the tongues when β approaches -1.

(1) Case $\beta = 0$. Here the behaviour of the tongues seems very simple. One of the branches of the boundary, $\Gamma^0_{p/q,1}$, accumulates on the homoclinic bifurcation curve called $T_0^{2,0}$ in figure 11. The other branches accumulate at the boundary of the (main) Arnold tongue corresponding to fixed points, that is at $\Gamma_0^{0,2}$. In figure 55 we show all the tongues corresponding to periods less than or equal to 10, as well as the flip bifurcation curves inside these tongues. Moreover, we give the curve of homoclinic tangency, denoted by $T_0^{2,0}$.

(2) Case $\beta > 0$. This case is more involved. As in the previous case, the curves $\Gamma^\beta_{1/q,1}$ appear to accumulate at $T_0^{2,\beta}$, the curve of first homoclinic tangency. However, the other curves $\Gamma^\beta_{1/q,2}$ now seem to accumulate at a homoclinic bifurcation curve starting at another fold homoclinic bifurcation, namely at the last homoclinic tangency. Following the notation of conjecture 5.1, the latter curve seems to begin at $(\alpha, \omega) = ((1-\beta)\omega_1(\beta), \omega_1(\beta)) \in \Gamma^\beta_{0,2}$. We shall denote this curve by S_1^β. In figure 2 the case $\beta = 0.3$ is shown, see section 1. One can recognize the curves $T_0^{2,0.3}$ and $S_1^{0.3}$ in figure 2 as the curves e and g in figure 51. In figure 3, also in section 1, two magnifications are presented of the rectangles in figure 2. Here the accumulation of the tongues is demonstrated more clearly.

(3) Case $\beta < 0$. We distinguish two cases: $\beta_0 < \beta < 0$ and $\beta < \beta_0$. The value β_0 is as defined in the previous section.

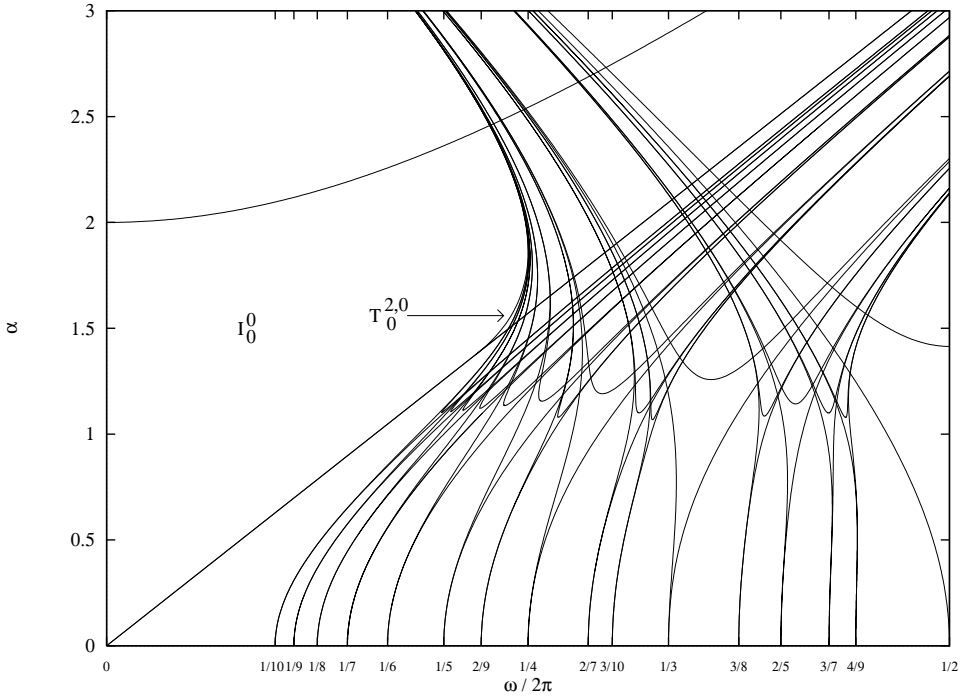

Figure 55. Arnold tongues for $\beta = 0$ and the curve of homoclinic tangencies $T_0^{2,0}$.

For $\beta > \beta_0$ (but not too close to 0) we computed tongues corresponding to rotation numbers $1/i$ from $i = 1$ to $i = 11$. The boundaries of these tongues have full curves in figure 56. Inside every tongue of period $\geqslant 4$ a fold (saddle-node) bifurcation curve appears of the same rotation number with an 'inner' cusp. We show these curves as broken curves. Moreover, three homoclinic bifurcation curves show up, that we call $T_1^{2,\beta}$, $T_0^{2,\beta}$ and $T_2^{2,\beta}$. Compare these curves with d, e and f in figure 47 for a nearby value of β. These curves are born at the saddle-node curve $\Gamma_{0,2}^{\beta}$ respectively in the points $\tau_1 = ((1-\beta)\omega_2(\beta), \omega_2(\beta))$, $\tau_0 = ((1-\beta)\omega_3(\beta), \omega_3(\beta))$ and $\tau_2 = ((1-\beta)\omega_4(\beta), \omega_4(\beta))$. We note that $\omega_2 < \omega_3 < \omega_4$.

In this case the branches $\Gamma_{1/q,2}^{\beta}$ tend to $\Gamma_{0,2}^{\beta}$ as $q \to \infty$. The left fold curves $\Gamma_{1/q,1}^{\beta}$ seem to approximate to the curve $T_0^{2,\beta}$ as in the case $\beta > 0$, for q not too large ($q \leqslant 7$), while for q large enough it seems that they tend to the homoclinic bifurcation curve $T_1^{2,\beta}$. For the other saddle-node bifurcation curves, born at the inner cusp, the left branches tend to $T_1^{2,\beta}$ as $q \to \infty$ and the right branches tend to $T_2^{2,\beta}$. In figures 57 and 58 one sees details of figure 56.

It is important to note that the first period q for which the left branch of the tongue boundary, $\Gamma_{p/q,1}^{\beta}$, is near the curve $T_1^{1,\beta}$ increases as β decreases. The behaviour of these curves is related to the existence of two codimension 3 bifurcations of fold type for any branch $\Gamma_{p/q,1}$. We described these types of bifurcations in section 5.1 in the item about the transition of saddle-area to cross-road area. The fold bifurcation curve with a cusp that played a role there, is the same we have considered here for every tongue. In table 1 we give the value of β for which the bifurcation corresponding to the tangency of the branches emanating from the cusps occurs. From table 1 it seems to follow that these values increase, as q tends to ∞, like $-c_1 - c_2 n^{-c_3}$ with constants $c_i > 0$. One can estimate the values of

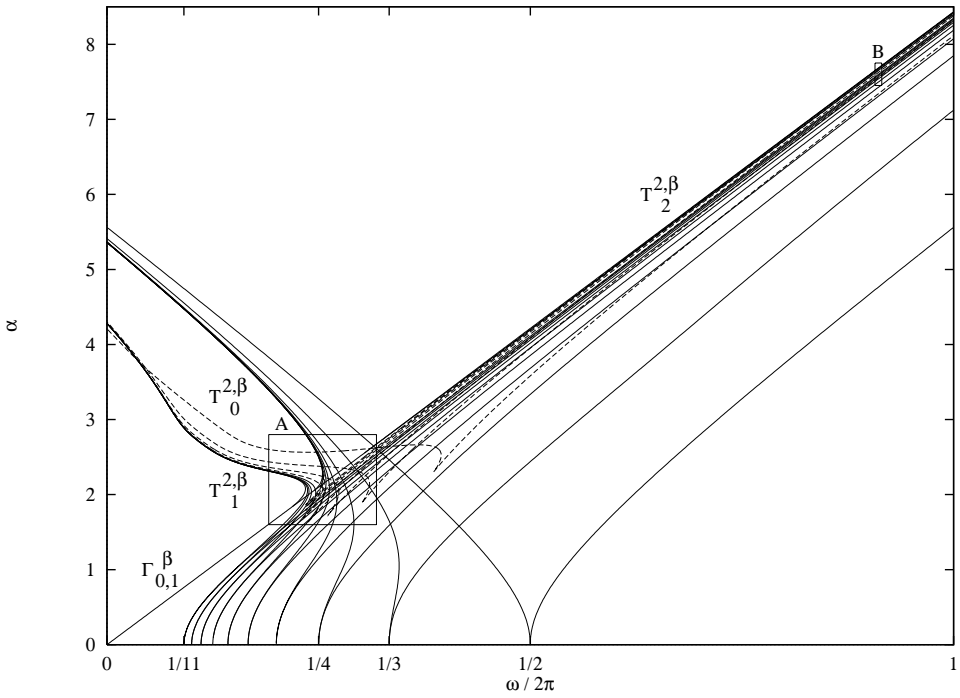

Figure 56. Arnold tongues for $\beta = -0.3365$. Also three homoclinic bifurcation curves are shown, all of these beginning in the saddle-node bifurcation curve.

Table 1. Values of β for which a codimension three cusp exist for rotation numbers $1/q$.

q	β	q	β	q	β	q	β
50	−0.2580	24	−0.2640	17	−0.2719	10	−0.3018
30	−0.2611	23	−0.2646	16	−0.2739	9	−0.3128
29	−0.2614	22	−0.2655	15	−0.2764	8	−0.3285
28	−0.2618	21	−0.2664	14	−0.2794	7	−0.3518
27	−0.2622	20	−0.2675	13	−0.2831	6	−0.3899
26	−0.2627	19	−0.2688	12	−0.2878	5	−0.4592
25	−0.2634	18	−0.2702	11	−0.2938	4	−0.6046

c_i as 0.2562, 4.5 and 2, respectively. We have no explanation for this phenomenon.

The behaviour of the tongues for $\beta < \beta_0$, and at least for β near β_0, seems to be quite similar. The main difference is that the curves $T_0^{2,\beta}$ and $T_2^{2,\beta}$ collide in a point in $\Gamma_{0,2}^{\beta}$ for $\beta = \beta_0$. (Recall that this value of β corresponds to a cubic tangency of the invariant manifolds of the saddle node.) For $\beta < \beta_0$ these two curves form one unique curve with a cusp point. The latter point corresponds to a cubic tangency of the saddle fixed point. If again $T_0^{2,\beta}$ denotes the left branch of the new curve and $T_2^{2,\beta}$ the right branch, then they play the same role as in the previous case.

Finally, we wish to emphasize that all these phenomena can also be observed for tongues of another rotation number. Figure 59, for example, shows tongues of rotation numbers $n/(3n-1)$ and $n/(3n+1)$ for $n = 1, \ldots, 10$, in the case $\beta = 0$. These exhibit accumulation of boundaries with respect to the tongue of rotation number 1/3, $I_{1/3}^0$, similar to what we

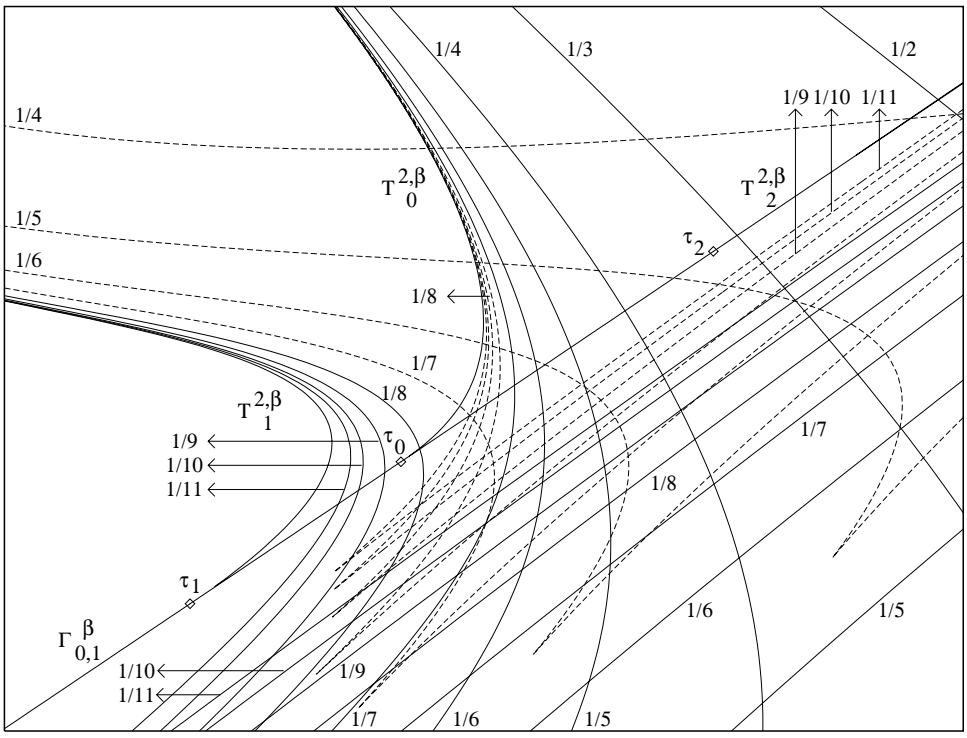

Figure 57. Magnification of rectangle A in figure 56. The rotation number associated to every bifurcation curve is shown. Window: $[1.2, 2.0] \times [1.6, 2.8]$.

described before regarding the tongue I_0^0. Now the symmetries of the I_0^0 case disappear, but the meaning of 'right' and 'left' curves of homoclinic tangencies is still clear.

5.3.3. 'Large' attractors. In this global model, next to 'small' strange attractors also 'large' attractors show up. We now discuss their occurrence. First, we define an attractor S to be 'large', if for each $x \in \mathbb{S}^1$ there exists an $y \in \mathbb{R}$ such that $(x, y) \in S$, so if it winds around the entire annulus.

One example of a 'large' attractor is the circle attractor $C_{\alpha,\omega,\beta}$ of section 2. In view of the creation of 'large' strange attractors we met several theoretical scenarios in section 3. The most familiar of these involves the transition of a node into a focus. At that moment the circle is only of class C^0. After that the eigenvalues can go to the negative half-plane, leading to a cascade of flips. We will not pursue this at this moment, but we shall return to it in section 5.4.1.

Another scenario develops near a quadratic critical cycle. Referring to section 4 for theoretical considerations and references, we here claim to have found such a 'large' strange attractor, see figure 4, section 1. We note that this attractor occurs for a parameter point near, but still outside, the tongue I_0^β.

In some scenarios strange attractors seem to exist close to the boundary of the parameter domain with invariant circles, perhaps even in its closure. This seems reasonable in several cases. Indeed, if the destruction of an invariant curve with rational rotation number is due to a homoclinic tangency, just after the tangency strange attractors should appear (cf the end of section 4.3). If, on the one hand, its occurrence is due to the leaving of a tongue,

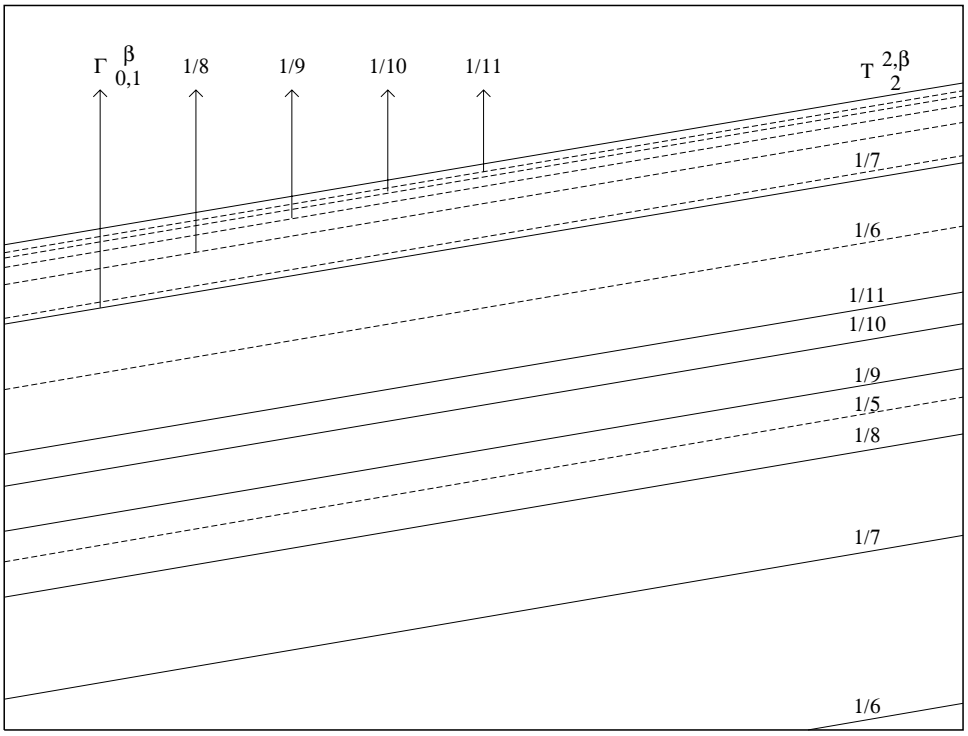

Figure 58. Magnification of rectangle B in figure 56. Window: $[5.7, 5.75] \times [7.45, 7.75]$.

its shape can be as in figure 4. If, on the other hand, the invariant curve has an irrational rotation number and is destroyed by an obstruction phenomenon (cf the end of section 3.1), the periodic orbits involved in the destruction can give rise to a homoclinic tangle creating a strange attractor.

It is also easy to find 'large' strange attractors that are in the tongue boundary corresponding to period 1 that display many 'turns' in terms of x as an angle variable. To obtain these we only have to consider larger values to ω. As an example, see figure 5, section 1.

5.3.4. Coexistence of attractors. By the work of Newhouse [38], also see Palis and Takens [45], it is known that for certain parameter values there is coexistence of infinitely many periodic attractors (sinks). Numerically one can see as many of these as the precision of the computer allows. An example of this in our map can be found near the homoclinic bifurcation line where tongues accumulate, see section 5.3.2. For the case of coexistence of infinitely many strange attractors see the nice results of [46] in a quite different context.

For the coexistence of invariant circles and periodic attractors, or strange attractors and periodic attractors for $\beta > 0$, we consider values of the parameters inside the tongue I_0^β and beyond the S_1^β curve of outer homoclinic tangencies. Here the invariant manifolds of the saddle fixed point can behave as those of figure 17 in cases (b), (c) or (d). In a case like figure 17(b) we have found coexistence of a 'large' strange attractor and an attracting fixed point for $\beta = 0.1$, $\alpha = 2.34$ and $\omega = 2.57$. In figure 60 we depict this strange attractor and, with broken curves, the invariant manifolds of the saddle fixed point. The corresponding

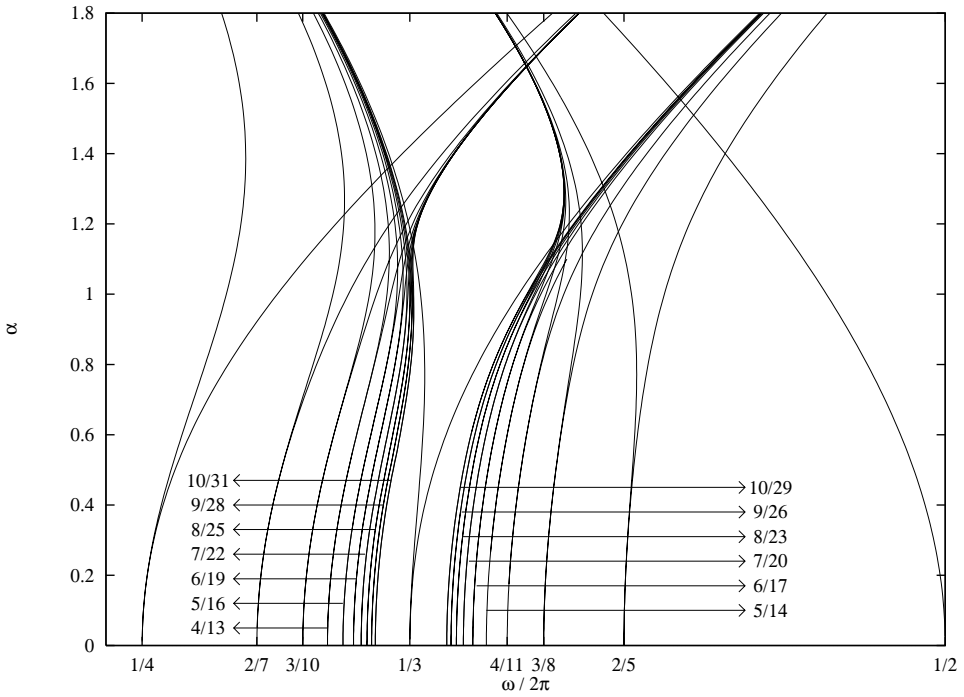

Figure 59. Accumulation of tongues in the tongue $I^0_{1/3}$.

node is at the end of the left branch of the unstable manifold. The right branch of the unstable manifold is in the basin of attraction of the strange attractor.

In a case like figure 17(d) we detected coexistence of an invariant circle and an attracting fixed point for $\beta = 0.9$, $\alpha = 0.12$ and $\omega = 0.7$ (see figure 61). Here an invariant curve is shown, and in broken curves also the invariant manifolds of the saddle fixed point. The left branch of the unstable manifold tends to the focus and the other branch is in the basin of attraction of the invariant circle.

We note that the strange attractor of figure 60 is destroyed when the parameters move to the other side of the curve S^β_1 and that the invariant circle of figure 61 will be destroyed for parameters corresponding to a cubic external tangency as in figure 17(c).

There is an easy way to see coexistence of quasiperiodic or strange attractors and periodic attractors, namely by taking values of β near the anticonservative case, $\beta = -1$ (see appendix C). In the first picture (case 1) of figure 62 we show the orbits of 10 points: $(0, -2)$, $(0, -4)$, $(3.8579, -4.3082)$, $(5.67, -1.97)$, $(0.95, -1.44)$, $(1.75, -4.48)$, $(1.82, -4.35)$, $(1.61, -4.57)$, $(0, 0.893\,04)$, $(0, 0.82)$. We distinguish two 4-periodic elliptic islands (one with three invariant circles displayed and the other with two), an invariant circle (of, say, 'snake' type) and a 24-periodic elliptic island near the invariant circle in the middle of the picture. Moreover, there are 24-periodic elliptic points in the two borders of the external chaotic region. In the next picture we see the invariant circle in more detail as well as the small invariant circles that surround the 24-periodic elliptic orbit. We remark that the chaotic zones generated from $(0, -2)$ and $(0, -4)$, as well as the two families of large islands and the period 24 small external islands, go up and down jumping over the snake curve because of the reversion of orientation. A 'period two' very wild invariant

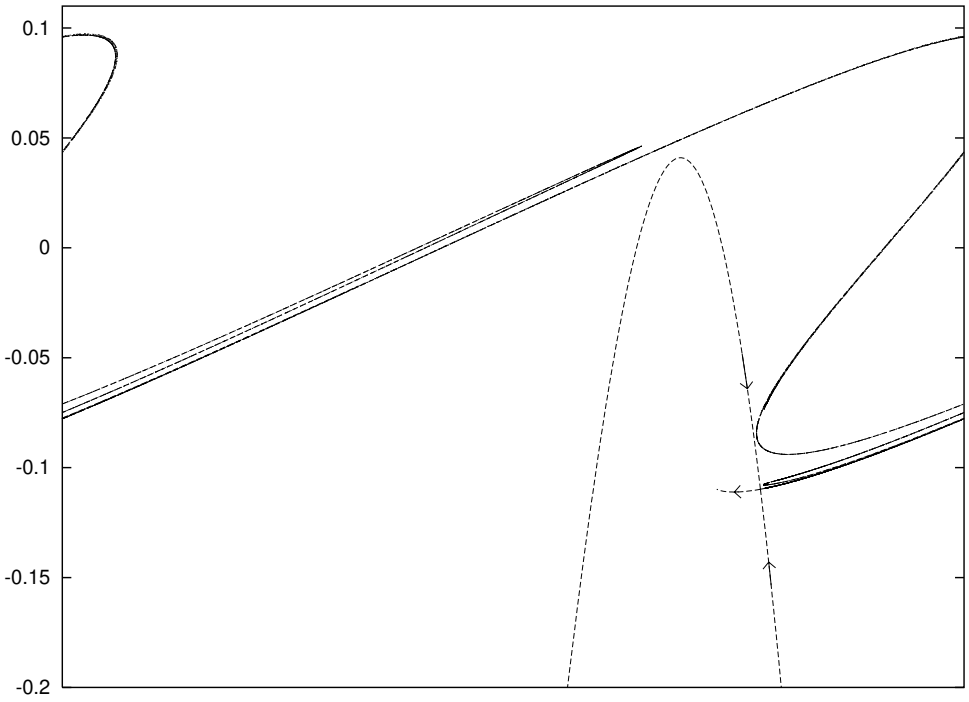

Figure 60. Coexistence of a 'large' strange attractor and an attracting fixed point for $\beta = 0.1$, $\alpha = 2.34$ and $\omega = 2.57$.

circle seems to exist between the two chaotic zones (in the narrow white area in between, not included in the figure). The snake curve is invariant under the map, but as noted in appendix C (see, e.g. figure 79) these invariant circles are far from Lipschitz graphs. For an analysis of the generic existence of non-Lipschitz invariant curves for perturbations of integrable non-twist maps we refer to [53].

In case 2, where the map is weakly dissipative ($\beta = -0.999$), the invariant circle almost coincides with the previous one and the elliptic orbit has been transformed in an attracting periodic orbit. In cases 3 and 4 the invariant circle has been destroyed and instead there is a large strange attractor. In case 4 there is also a period 24 attracting periodic orbit. The numbers presented on top of every picture are, respectively, the values of ω, α and β. All values are inside the Arnold tongue of period 4.

If we take $\beta = 1$ infinitely many elliptic periodic orbits exist. By taking $\beta = 1 - \Delta\beta$, $\Delta\beta > 0$ and sufficiently small, as many as desired (but a finitely many!) of these periodic orbits should persist as sinks. One open problem is whether for the present family it is possible to have coexistence of as many strange attractors as desired. If $\Delta\beta$ is sufficiently small, a large number of the infinitely many periodic hyperbolic points present for $\beta = 1$, will persist as saddles. Another open problem is whether, under the perturbation, these will give rise to strange attractors (eventually, to small attractors) or whether their unstable manifolds will be captured by nearby periodic attractors (sinks).

In figures 60–62 we discovered periodic attractors coexisting with an invariant circle or with a strange attractor. An open question is whether a strange attractor and an invariant circle can coexist.

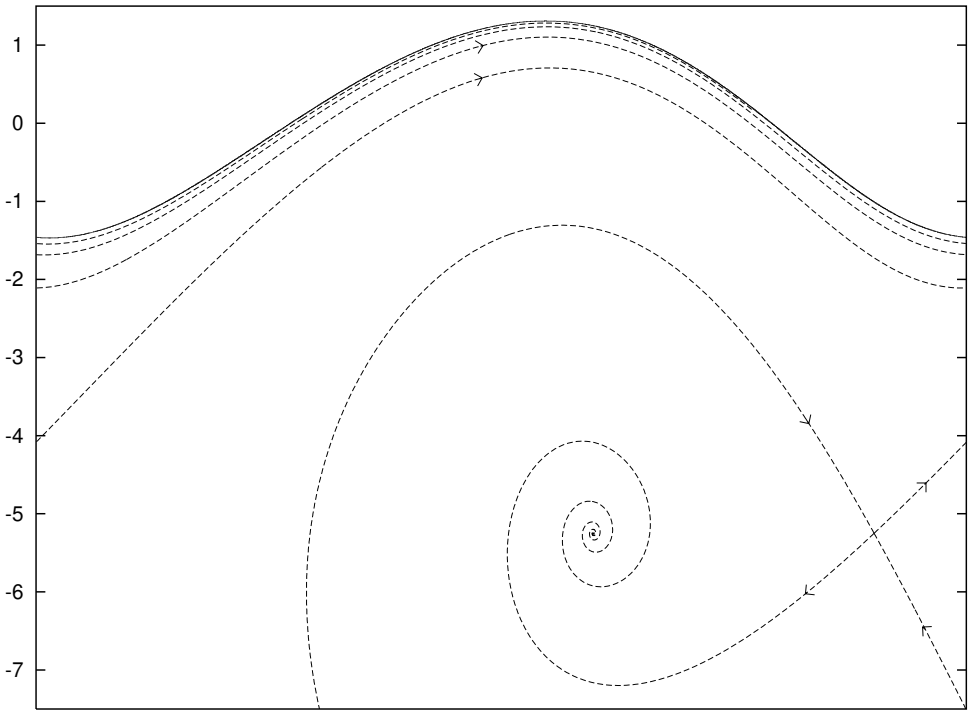

Figure 61. Coexistence of an invariant circle and an attracting fixed point for $\beta = 0.9$, $\alpha = 0.12$ and $\omega = 0.7$.

5.4. Additional facts

We end this section with some additional material found in the numerical exploration of the fattened Arnold family. This exposition certainly again stresses the dynamical richness of this map.

5.4.1. A sample of attractors. We begin with a sample of the attractors as they occur in our example. Figures 63–65 display several types of attractors as observed, most of which are strange attractors (SA). In each case four numerical values are displayed. The first three are $\beta, \omega/(2\pi)$ and α, so indicating how we move through the parameter space. The last number is the vertical semiamplitude of the window. The horizontal scale is always $[0, 2\pi]$; the horizontal axis is also displayed for reference.

Case 1 shows a 6-pieces SA (much like this could appear in the Hénon family) which globalizes in case 2. Cases 3 and 4 show the fusion of a 2-pieces SA into one single piece. Case 5 shows a large SA shortly after some heteroclinic tangency has globalized it. By a stronger density of points, one may still detect the shape of the previous SA. Case 6 shows a SA which can be considered as a typical 'folded' curve, produced after the last homoclinic tangency of a saddle. Case 7 is similar to case 5, but for a larger value of β and a much larger vertical window. Some concentrations of points also give evidence of a 'previous', smaller, SA.

The remaining cases correspond to negative values of β. From case 8 to 9 one sees a globalization produced by heteroclinic tangency, case 8 originating by repeated period doubling of an attracting fixed point. It looks like a parabola. Shortly after, the lower

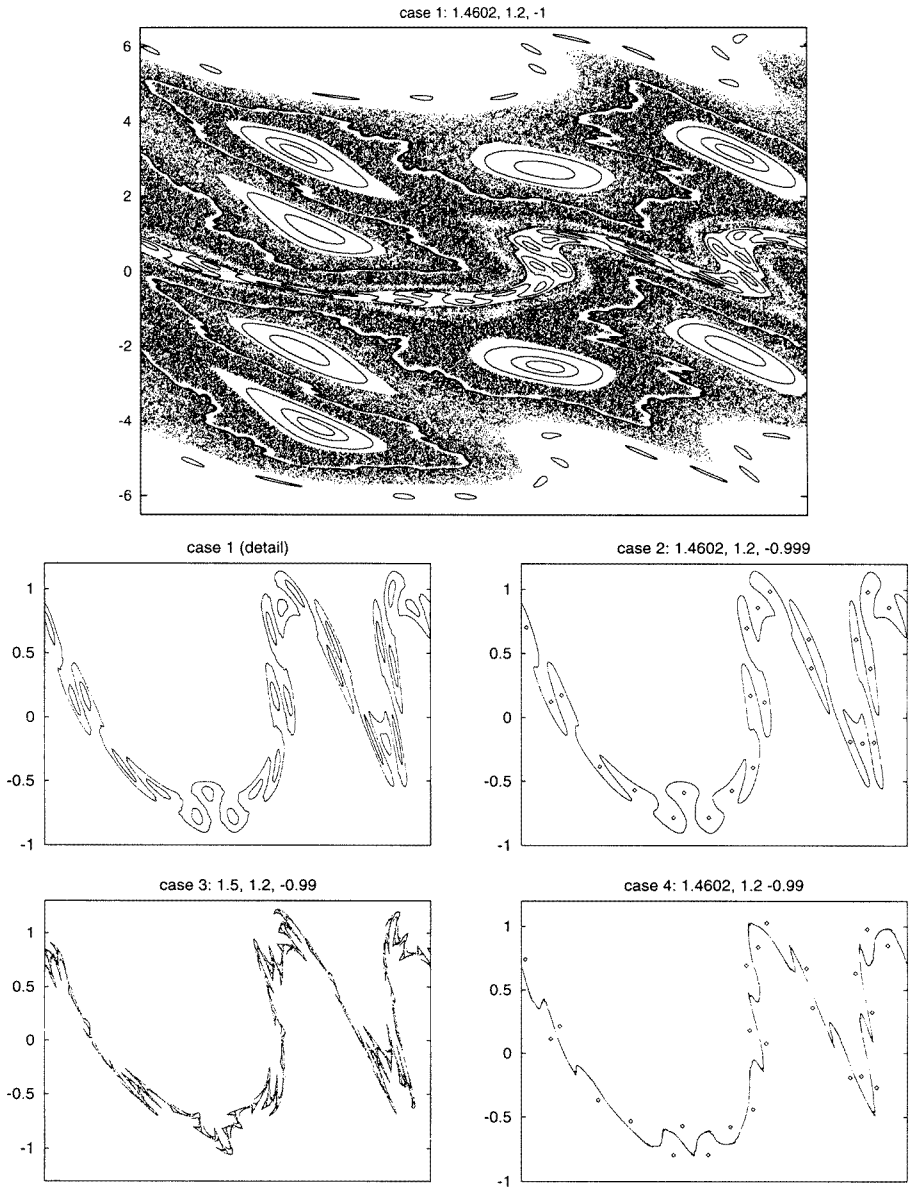

Figure 62. Several orbits (attractors in case 2–4). See explanations in the text.

branch of the parabola becomes as large as the upper one: it has an heteroclinic tangency with the stable manifold of the saddle point created at the same time as the sink. Case 9 frequently suffers destruction to (periodic) sinks, which again become an SA. A figure like case 9 (but slightly larger) reappears when we increase α, keeping the other parameters fixed. Observe that case 9 is quite similar to figure 5, section 1.

Inspired by the logistic family (and also by the Hénon case), we believe that for fixed ω and β, the set of α-values for which a sink exists, is dense. However, in certain regions, this set can have very small relative measure.

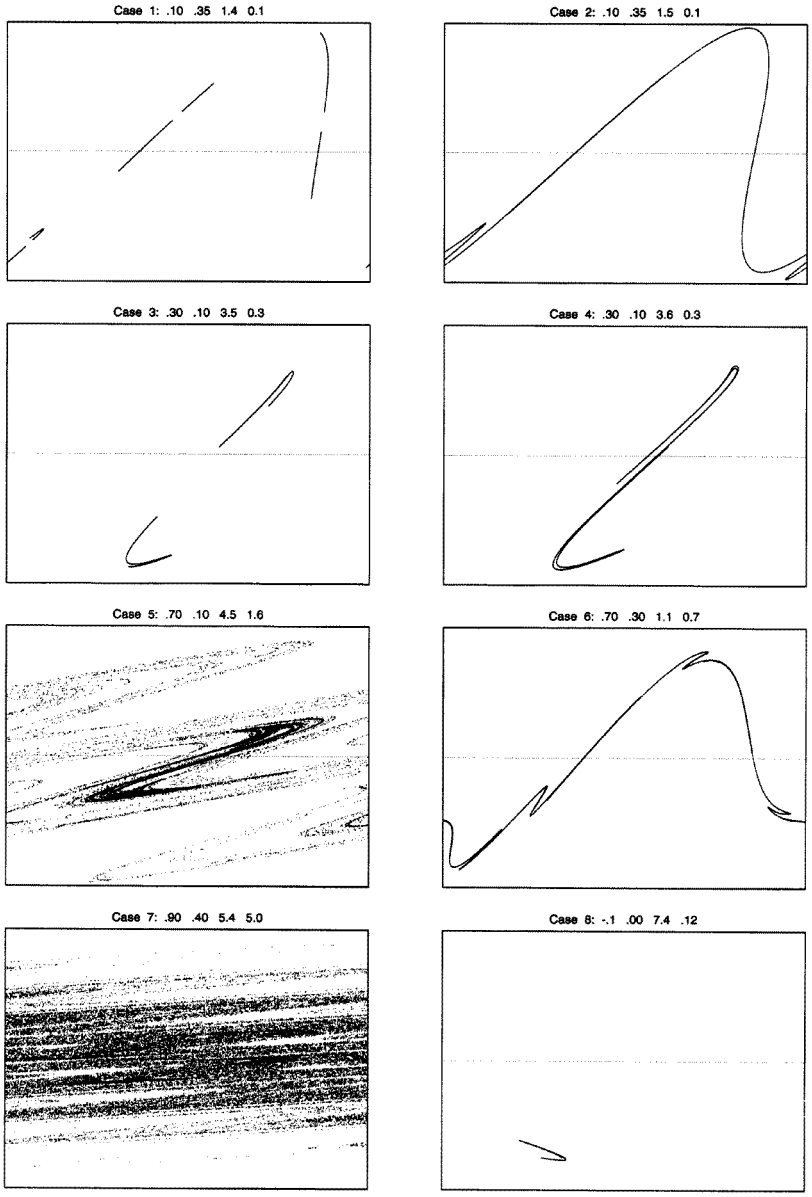

Figure 63. Some attractors. See explanations in the text.

Cases 10–13 show the fate of an invariant circle when it is folded. It may give rise to a large SA, as in cases 12 and 13, or be broken into pieces as in case 11. Case 13 shows an 'onion'-like structure, reminiscent of figure 85 (see appendix D). This kind of structure systematically appears also in attractors of three-dimensional (3D) diffeomorphisms (see [32]). Cases 14 and 15 display a globalization of a 3-pieces SA. Case 16 (symmetric since $\omega = 0$) shows just one SA, but most of the iterates are still located near what, previously, was a 4-pieces SA.

For values of β closer to -1, very wild patterns appear. Case 17 shows a wild invariant

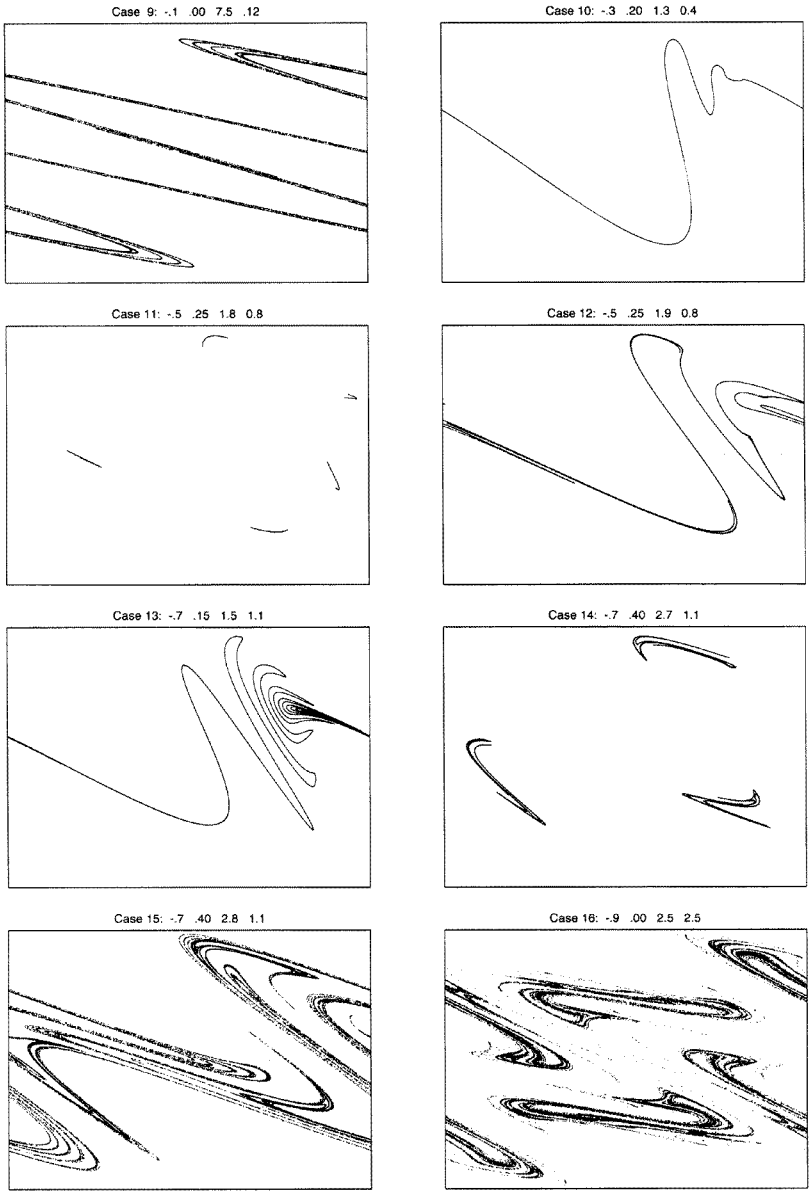

Figure 64. Continuation of the previous figure.

curve, becoming an SA in case 18, starting to display an onion-like character, to be thickened in case 19. In case 20 we see a multipieces SA (58 pieces!). A small variation of α yields case 21, where a stronger density is seen close to a 'curve' obtained by joining the previous pieces. Case 22 is similar to 17 but even wilder. However, in this case, we have preferred to show an SA, coming from an invariant curve which looks quite similar. Case 23 is again a very thick onion-like structure (maybe even closer to an artichoke!). Finally, case 24 displays a connected chain of five onion-like structures. Some of the pictures also have a nice artistic component!

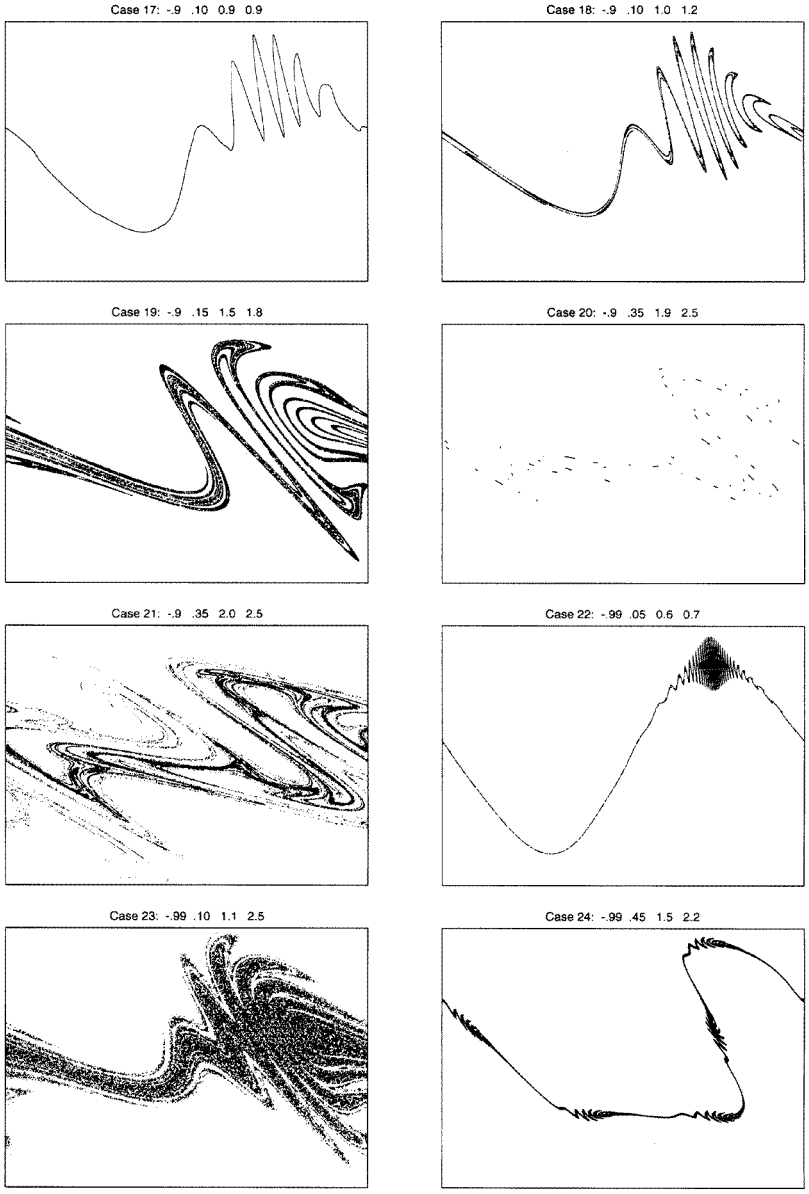

Figure 65. Continuation of the previous figures.

5.4.2. Basins of attraction. We briefly discuss and illustrate some principles regarding basins of attraction and their numerical detection. By hetero- and homoclinic bifurcation these basins can change dramatically.

Keeping β, ω and α fixed we start our iterations in various initial points. Figure 66 shows the (x, y)-plane with several basins of attraction of periodic attractors. For this choice of parameter values, the periods are 1, 2, 3, 4, 5, 7, 8, 11, 13, 14 and 24. Each grey tone corresponds to exactly one basin of attraction.

The principle for production of the different basins is as follows. Assume that, by some

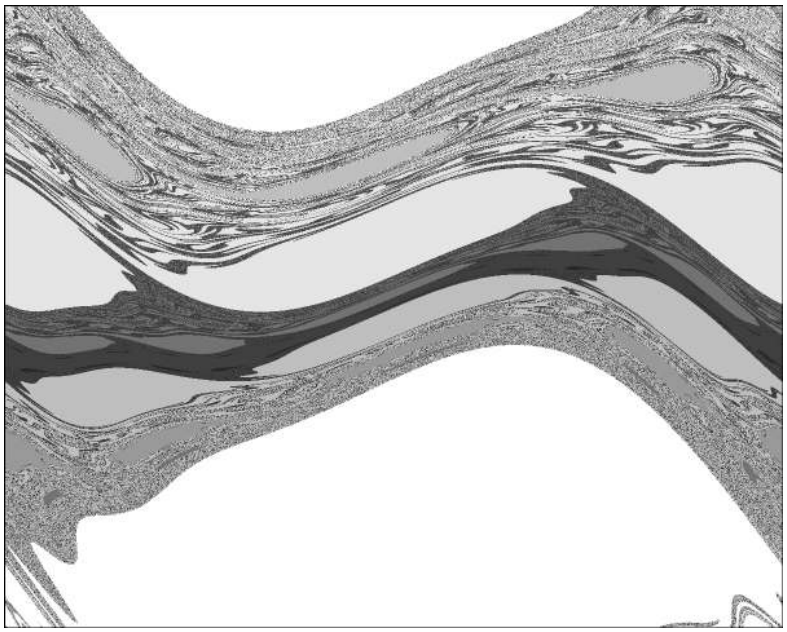

Figure 66. Basins of attraction of the fattened Arnold family for $\alpha = 1$, $\beta = 0.99$ and $\omega = 0.38 \times 2\pi$. The values of (x, y) are in the rectangle $[0, 2\pi] \times [-3, 3]$.

fold bifurcation, a node and a saddle are created. The node then becomes a local attractor which may bifurcate further (e.g. by a cascade of flips giving a strange attractor). The basin of this local attractor is bounded by the stable manifold of the companion saddle (at least close enough to the bifurcation). One branch of the unstable manifold of this saddle is attracted by the local attractor, while the other may go to another attractor. If this happens to be the same, we should look for other unstable manifolds as boundaries of the basin. When several sinks and their companion saddles are interacting, different basins can appear, as shown in figure 66.

By moving parameters, all invariant manifolds change and may give rise to hetero- and homoclinic bifurcations. This causes changes of basins, destruction or fusion of attractors, etc. The pictures can look extremely different, but the mechanims are quite simple.

5.4.3. Lyapunov exponents. Important for the detection of (quasi)periodicity and chaos are the Lyapunov exponents and it is interesting to see how they behave in the fattened Arnold family.

Here we report on a sample of computations, where as an 'arbitrary' initial point we took $(x, y) = (0.123\,456\,789, 0.987\,654\,321)$. The maximal Lyapunov exponent was obtained by iteration of the differential (derivative) map. The computation is typically stopped when, after obtaining some estimate, for 10^5 additional iterates the variation of the estimate is less than 10^{-3}. Initially some transient regime (of 10^5 iterates, unless we ended on a periodic orbit) was used.

Figures 67 and 68 display some results, for $\beta = 0.5$, $\omega \in [0, \pi]$ and $\alpha \in [0, 4]$. The first figure shows the parameter values (ω, α) for which the maximal Lyapunov exponent seems to be zero. Numerically these values obtained range in $[-10^{-5}, 10^{-5}]$ and, therefore, it is reasonable to assume that they correspond to a quasiperiodic circle-attractor. In figure 68

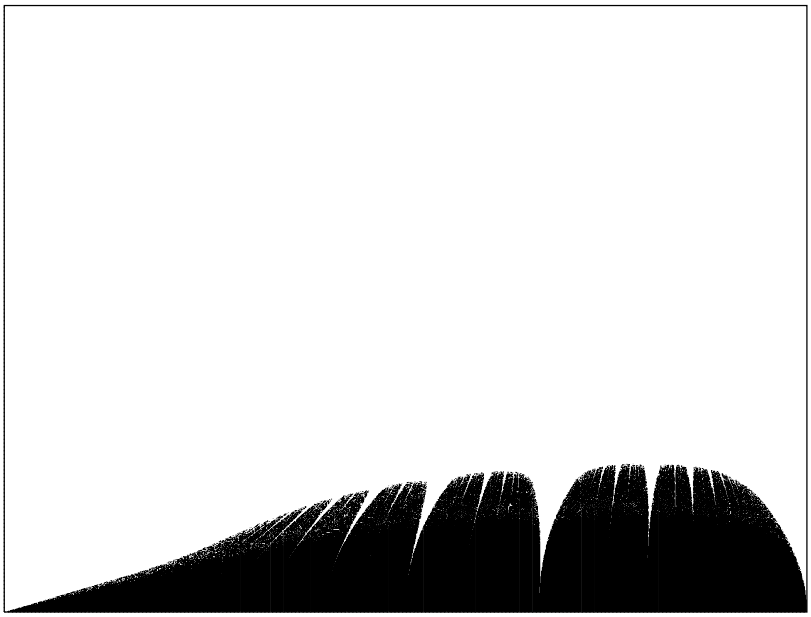

Figure 67. Values of (ω, α) for $\beta = 0.5$, for which the maximal Lyapunov exponent seems to be zero. They correspond to quasiperiodic attractors. Window $[0, \pi] \times [0, 4]$.

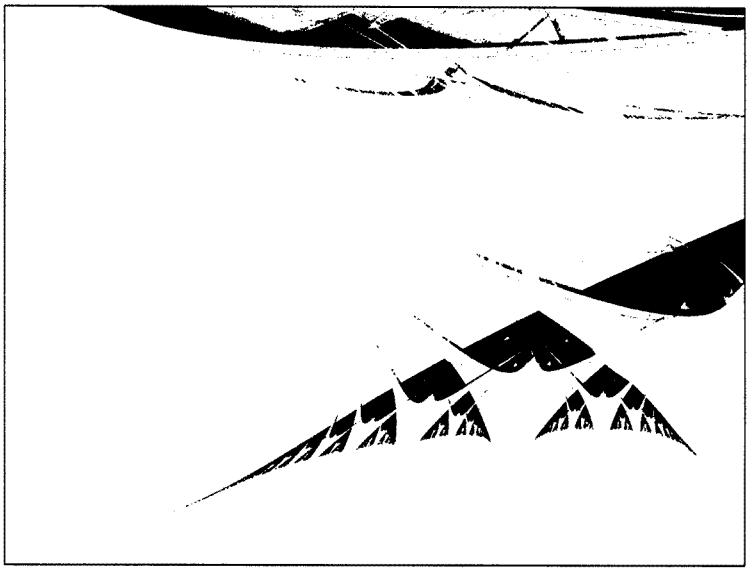

Figure 68. Values of (ω, α) for $\beta = 0.5$, for which the maximal Lyapunov exponent seems to be positive. They correspond to strange attractors. Window $[0, \pi] \times [0, 4]$.

we display the values of (ω, α) for which the maximal Lyapunov exponent seems to be positive, using the bound 10^{-3}. They should correspond to strange attractors. Also compare a global figure, like figure 1, as it occurs for a smaller value of β and for a larger range of α.

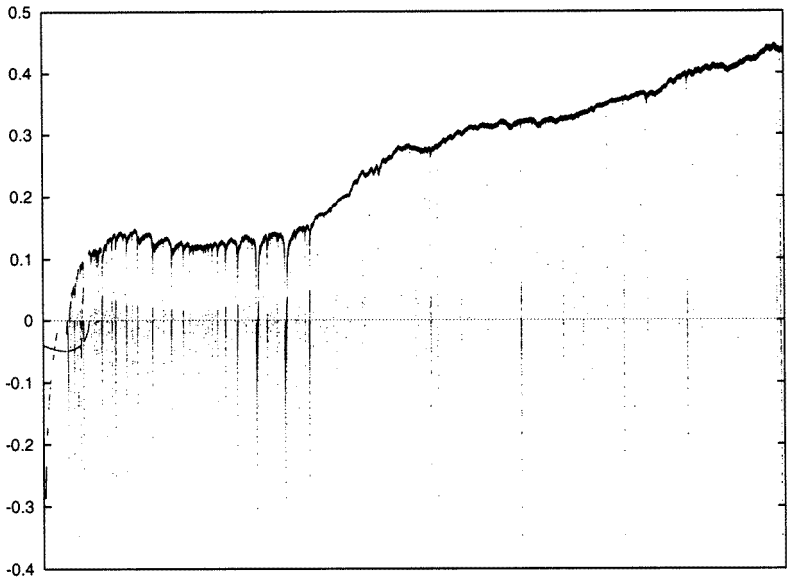

Figure 69. The maximal Lyapunov exponent for $\beta = 0.5$, $\alpha = 4$ and $\omega \in [\pi/8, \pi/4]$, showing windows which frequently seem to interrupt the parameter domain of strange attractors.

In figure 68 it seems that whole segments exist with positive maximal Lyapunov exponent. To check this phenomenon we selected the segment $[\frac{1}{16}, \frac{1}{8}]$ as a range of $\omega/(2\pi)$. In this interval 160 000 equispaced values of $\omega/(2\pi)$ were taken and the Lyapunov exponent was recomputed with this small step size. The result appears in figure 69, where the Lyapunov exponent is plotted against ω. Indeed, there are still ranges where the exponent is positive for almost all values in the lattice, but they are also interrupted by parameter values with negative exponent, corresponding to periodic attractors (sinks).

Points appearing neither in the first figure nor in the second, correspond to values of (ω, α) for which our initial point evolves to a periodic attractor.

5.5. A summarizing 'movie'...

Many readers often find themselves looking at a computer screen displaying dynamics, particularly concerning a family of 2D maps. As said in the introduction (also see appendix A), the present, fattened Arnold family, is not 'just another dynamical system', but extremely representative for the case of 2D maps. We claim that, in view of this paper, the corresponding phenomenology should contain no further secrets. Indeed, the reader is invited to sit in front of his computer screen and join us in the following experiment. If necessary the appropriate software can be obtained from the authors.

We follow the fate of attractor(s) for different values of (β, ω) and α ranging in a suitable interval, so moving along a number of representative paths. The attractor(s) are obtained as follows by iteration of the map. If for given parameter values a saddle point occurs, we start the iterations at two different initial points located in the corresponding unstable manifold. In all other cases we take our favourite 'arbitrary' initial point $(x, y) = (0.123\,456\,789, 0.987\,654\,321)$. We first perform a transient of 10^5 iterates, and then observe the attractor(s) obtained by 10^4 consecutive iterates. The values of α for which a bifurcation is produced are only given approximately.

(1) $\beta = 0.2$, $\omega = 0.4 \times 2\pi$.

(a) $\alpha \in [0, 0.9]$. In these cases the attractor is an invariant circle (IC) with either rational or irrational rotation number. If α is small we can only observe the IC with irrational rotation number. If the rotation number is rational the minimal attractor is periodic and it occurs inside an Arnold tongue. This periodic attractor starts at a fold (saddle-node) bifurcation. Later the node can become a focus if the width of the tongue is large enough, but this has not been observed in the present exploration. The saddle created at the fold bifurcation persists as a saddle until, when leaving the Arnold tongue, it again joins the node in another fold bifurcation.

(b) $\alpha \in [1, 1.23]$. When $\alpha \approx 1$ we enter a 5-periodic Arnold tongue. The 5-periodic node turns into a focus, later a node with negative eigenvalues and then a saddle with reflection. Increasing α further leads to a typical cascade of flip (period doubling) bifurcations. The IC is preserved until the first flip bifurcation.

(c) $\alpha \in [1.23, 1.25]$. After the cascade of flips there is an inverse cascade of fusions of SA. In this cascade $2^n \times 5$ pieces merge to $2^{n-1} \times 5$ pieces, finally arriving at a 5-pieces SA. This attractor is the closure of the unstable invariant manifold of the saddle with reflection as mentioned in item (b).

(d) $\alpha \in [1.26, 1.4]$. For $\alpha = 1.26$ a heteroclinic tangency occurs of the unstable manifold of the 5-periodic saddles mentioned under (b) and the stable manifold of the 5-periodic saddles which appeared under (a). This produces the birth of a large SA, the invariant measure of which, is concentrated mainly near the 'old' 5-pieces SA. Values of α inside the interval $[1.26, 1.4]$ exist, for which periodic attractors or SA, consisting of several pieces, occur. This phenomenon is due to heteroclinic intersections associated to other periodic points (cf [50] in the case of the Hénon map).

(e) $\alpha \in [1.41, 1.65]$. The same phenomenon as described in the two previous items occurs for other periods.

(f) $\alpha \in [1.66, 2.18]$. We again see the birth of a periodic attractor of period 2 undergoing a cascade of flips, followed by an inverse cascade of SA. However, there is a difference in this case. For $\alpha = 2.010\,61\ldots$ we enter the Arnold tongue of period 1. Then we observe a 2-pieces SA and, after the fold bifurcation, a fixed point attractor. Moreover, the branch of the unstable manifold of the companion saddle (see (a)) that does not tend to the node is in the basin of attraction of the SA. In this case, the invariant manifolds of this point behave as in figure 17(*b*) (after the last homoclinic tangency). Again, the existence of heteroclinic intersections produces a large SA that, in this case, coexists with an attracting fixed point. The large SA is destroyed for $\alpha = 2.185$ by an outer homoclinic intersection of the fixed point.

(g) $\alpha \geqslant 2.186$. The same phenomena occur for fixed and other periodic points: existence of cascade of bifurcations, inverse cascades of a SA and creation or destruction of a large SA.

(2) $\beta = 0.9$, $\omega = 0.25 \times 2\pi$.

(a) $\alpha \in [0, 0.156]$. One sees an IC of rational or irrational rotation number.

(b) $\alpha \in [0.157, 0.86]$. The parameter α enters the Arnold tongue of period 1 and an attracting fixed point coexists with an IC. The unstable manifold of the saddle which appears at the fold bifurcation has a transversal intersection with the strong stable foliation of the saddle, as in figure 17 (*d*).

(c) $\alpha \in [0.87, 0.93]$. A periodic attractor of period 13 shows up that undergoes a cascade of period-doubling bifurcations followed by an inverse cascade of SA. Finally there appears a large SA. For these values of α the unstable manifold mentioned in the previous item has quadratic tangencies with the strong stable foliation. We note that apart from these

attractors, a 4-periodic attractor exists.

(d) $\alpha \geqslant 0.94$. There appear more periodic attractors and SA, as in the case $\beta = 0.2$.

(3) $\beta = -0.2$, $\omega = 0.05 \times 2\pi$.

(a) $\alpha \in [0, 0.377]$. A quasiperiodic attractor exists for most of the values checked, which is in accordance with the very small size of the Arnold tongues in this zone of the parameter space.

(b) $\alpha \in [0.378, 3.594]$. When $\alpha = 0.378$ the parameters enter the 1-periodic Arnold tongue. Then, as α increases, the IC loses differentiability. For $\alpha = 1.65$ there is a flip bifurcation and the IC is destroyed. Then the typical flip cascade occurs and finally a 1-piece SA appears. For larger values of α this SA is destroyed by other attractors, as usual, or it coexists with other periodic or strange attractors. For example, for $\alpha = 3.52$ there simultaneously are a 1-piece and a 2-pieces SA.

(c) $\alpha \geqslant 3.594$. For this value of α the first homoclinic bifurcation occurs for the saddle that first appears at the fold. Then the 1-piece SA becomes a large SA. After this we find strange or periodic attractors.

(4) $\beta = -0.9$, $\omega = 0.05 \times 2\pi$.

(a) $\alpha \in [0, 0.59]$. There is a globally attracting IC.

(b) $\alpha \in [0.6, 0.6925]$. The parameters enter the 1-periodic Arnold tongue. The invariant curve loses differentiability as explained before, until it is only continuous.

(c) $\alpha \in [0.6926, 2.195\,456]$. There is a flip bifurcation at the first value of α after which the IC disappears. For this range of the parameter one finds many 'windows' of different periodic attractors (with quite varying periods) coexisting with the 2-periodic attractor, 4-periodic attractor, etc which appear in the usual cascade of flips. For $\alpha = 2.194$ the cascade finishes and an SA of several pieces appears. For instance, for $\alpha \in [2.1954, 2.195\,455]$ we find a 8-pieces SA. This attractor becomes a large SA via a heteroclinic bifurcation with the stable invariant manifold of the saddle created at the fold bifurcation of period 1. This occurs, approximately, for $\alpha = 2.195\,455$.

(d) $\alpha > 2.195\,455$. For values near 2.195 455, the invariant measure of the SA seems to be concentrated mainly near the 'old' 8-pieces SA. Increasing α again, the distribution on the SA is more 'homogeneous'. (The measure is quite well distributed on the related unstable manifold.) After this, more periodic and (both small and and large) SA show up.

Acknowledgments

The authors are indebted to V Gelfreich, I Hoveijn, Y S Il'yashenko, F Takens and F O O Wagener for their interest in the subject and for several suggestions. They are specially grateful to the (anonymous) referee who kindly provided a proof of proposition B.1. The authors also thank each other's Universities and the Centre de Recerca Matemàtica for hospitality. This work has been supported by the Netherlands Organization for the Advancement of Scientific Research (NWO), a CIRIT grant for computing facilities and by DGICYT grants PB 90-0580 and PB 94-0215. Partial support of the EC grant ERBCHRXCT940460, and catalan grants CIRIT GRQ93-1135 and 1996S0GR-105 is also acknowledged.

Appendix A. Modelling the return map near homoclinic tangency

We give a heuristic derivation of the fattened Arnold family as a return map near homoclinic bifurcation, in an appropriate setting. Let a diffeomorphism F on the plane be given with

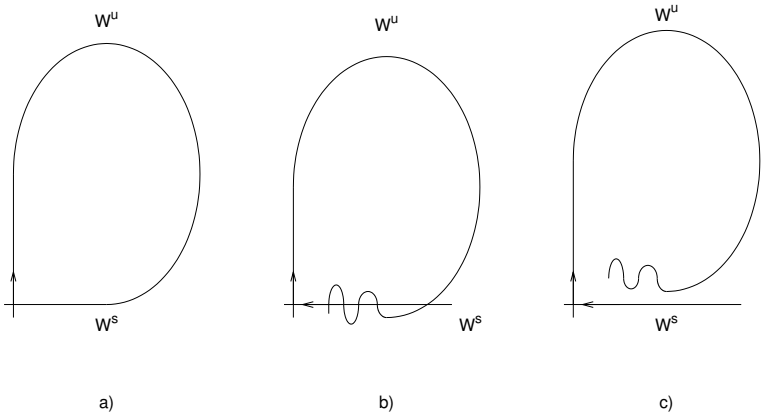

Figure 70. Non-conservative perturbation of a symplectic map: (*a*) The time ϵ map $\varphi^H_{t=\epsilon}$ of a Hamiltonian vector field, (*b*) a conservative perturbation $\varphi^H_{t=\epsilon} + \mathrm{O}(\epsilon^2)$, (*c*) a non-conservative perturbation which 'pulls up' the unstable manifold.

a hyperbolic fixed point such that the corresponding stable and unstable manifolds are near a homoclinic tangency. Furthermore, for simplicity, assume that F is near the identity and relatively near conservative. This means that the map is close to the time ϵ flow (for ϵ small) of a vector field on the plane, and this vector field is nearly Hamiltonian. In summary this means that

$$F = \varphi^H_{t=\epsilon} + \mathrm{O}(\epsilon^2),$$

for a Hamiltonian H. All elements are assumed to be real analytic. We shall consider the following three steps to construct the diffeomorphism.

(1) We start with the time ϵ flow of a Hamiltonian, $\varphi^H_{t=\epsilon}$, with a homoclinic loop.

(2) This 'integrable map' first is perturbed by adding an $\mathrm{O}(\epsilon^2)$ terms *maintaining* the conservative character. This generically gives an exponentially small splitting of the separatrices (see [21]) such that, in a suitable parametrization, the unstable manifold with respect to the stable manifold, is locally given by an expression of the form $\sum_{n\geqslant 1} a_n \sin(nz + \varphi_n)$, where $a_n = \mathrm{O}(\exp(-nc\epsilon^{-d}))$ for some positive constants c and d. Generically the first coefficient is bounded from below by $\exp(-c(1+\delta)\epsilon^{-d})$ with $\delta = \delta(\epsilon)$, $\delta \searrow 0$ as $\epsilon \searrow 0$. The φ_n are suitable phases.

(3) Second we perturb in a non-conservative way, assuming that the main effect of this perturbation is to 'pull up' the unstable manifold with respect to the stable manifold (see figure 70).

To model a return map we split the diffeomorphism as the composition of two maps, one near the saddle, the other being the reinjection (figure 71).

Let u parametrize the stable manifold. Instead of u we shall use $z = 2\pi \log u / \log \lambda_2$. Hence $z \in [0, 2\pi]$ as u moves on a fundamental domain. Near the saddle, for simplicity, we assume that our map is linear. Let $v = (a - b\cos z)\lambda_1^{z/2\pi}$ be the local expression of the unstable manifold W^u. This is compatible with the linear behaviour of the map. The parameter a measures the distance between W^s and an 'averaged' W^u_{av}, while b measures the size of the oscillations of W^u with respect to W^u_{av}, due to the splitting. A point P is determined by the coordinates (z, w) and then $u = \lambda_2^{z/2\pi}$, $v = (w + a - b\cos z)\lambda_1^{z/2\pi}$.

After a suitable number of iterates, P is mapped to $\bar{P}$ with u small and $v \in [\lambda_1^{-1}, 1]$. In view of the reinjection, a region like $\mathcal{R}$ is sent to $\mathcal{R}^*$ and then shifted to $\mathcal{R}'$. A point like

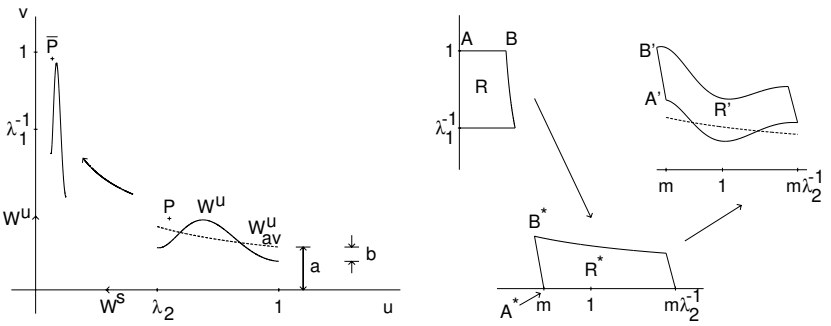

Figure 71. A sketch of the derivation of the return map.

A is moved to A^*, with u coordinate $m \in [\lambda_2, 1)$ and then to A'. Again assuming linearity in the passage from AB to A^*B^*, a vector $(s, 0)$ is mapped to $s(p, q)$. In this set-up the quantities λ_1, λ_2, a, b, m, p, q, completely describe the geometry of the return map.

An additional simplification is obtained by neglecting the effect of p. It affects the final value of z only in a mild way. Then, an elementary computation gives the return map. We assume $b > 0$ and scale w by $w = b\eta$. We obtain, by changing the origin of z:

$$\begin{pmatrix} z \\ \eta \end{pmatrix} \mapsto \begin{pmatrix} \frac{2\pi}{\log \lambda_2} \log m + z + \frac{2\pi}{\log \lambda_1} \log(a + b(\eta + \sin z)) \bmod 2\pi \\ \frac{q}{b} m^{-\log \lambda_1 / \log \lambda_2} (a + b(\eta + \sin z))^{-\log \lambda_2 / \log \lambda_1} \end{pmatrix}. \tag{5}$$

After some rearrangement (5) can be written as

$$\begin{pmatrix} z \\ \eta \end{pmatrix} \mapsto \begin{pmatrix} z + \hat{\omega} + A \log(\hat{a} + \hat{b}(\eta + \sin z)) \\ (\hat{a} + \hat{b}(\eta + \sin z))^{\psi} \end{pmatrix} = \begin{pmatrix} z' \\ \eta' \end{pmatrix}, \tag{6}$$

depending on five parameters A, $\hat{a}$, $\hat{b}$, $\hat{\omega}$ and $\psi = -\log \lambda_2 / \log \lambda_1$.

The above hypotheses imply that $\psi = 1 + \mu$, with μ small. Hence

$$\eta' = (\hat{a} + \hat{b}(\eta + \sin z))^{\mu} (\hat{a} + \hat{b}(\eta + \sin z)).$$

If $\hat{a} \gg \hat{b}$ and η is not too large ($\eta \hat{b} \ll \hat{a}$), the first factor in η' is almost constant:

$$\eta' \approx \hat{a}^{\mu} (\hat{a} + \hat{b}(\eta + \sin z)).$$

As this is linear in η, if $\hat{a}^{\mu} \hat{b} \neq 1$ we can shift the origin of η to cancel the independent term, obtaining in this way a new vertical variable ρ, and (6), with $\beta = \hat{a}^{\mu} \hat{b}$, becomes of the form

$$\begin{pmatrix} z \\ \rho \end{pmatrix} \mapsto \begin{pmatrix} z + \omega + A \log(1 + \bar{b}(\rho + \sin z)) \\ \beta(\rho + \sin z) \end{pmatrix}, \tag{7}$$

a map which depends only on the four parameters ω, A, $\bar{b}$ and β. Finally, we again use the fact that $\bar{b}$ $(= b/a)$ is small to expand the logarithmic term in (7). Keeping the first term in the expansion and introducing $\alpha = A\bar{b}$, we have the simplified final form given by

$$\begin{pmatrix} z \\ \rho \end{pmatrix} \mapsto \begin{pmatrix} z + \omega + \alpha(\rho + \sin z) \\ \beta(\rho + \sin z) \end{pmatrix}. \tag{8}$$

This exactly is the fattened Arnold family of maps we consider in this paper.

Remarks.

(i) We assumed that $a + b\sin z$ gives the typical behaviour of W^u with respect to W^s with the generic assumption $b > 0$. A complete expression would be of the type

$$a + b\sin z + \sum_{j\geqslant 2} \mathrm{O}(b^j)\sin(jz + \varphi_j).$$

Dividing by a leads to the form

$$1 + \frac{b}{a}\sin z + \sum_{j\geqslant 2} a^{j-1}\mathrm{O}\left(\left(\frac{b}{a}\right)^j\right)\sin(jz + \varphi_j).$$

Hence, the jth order harmonic has a coefficient not only small, if b/a is small, but even small compared with $(b/a)^j$ if a is small. That is, the coefficient of $\sin(jz + \varphi_j)$ is small compared with the jth power of the one of $\sin z$.

(ii) In contrast, going from (7) to (8), and assuming $\rho = 0$ to make this consideration,

$$\log(1 + \bar{b}\sin z) = \bar{b}\sin z - \tfrac{1}{2}\bar{b}^2\sin^2 z + \tfrac{1}{3}\bar{b}^3\sin^3 z - \cdots,$$

and the coefficient of the jth harmonic has a size comparable with the jth power of the one of $\sin z$. This difference with the behaviour of the first item will have effects to be considered in appendix B.

(iii) However, if we consider A large in (7) (which holds true if the map is close to the identity, since then $A = 2\pi/\log\lambda_1$ and $\lambda_1 > 1$ is close to 1) then the first harmonic has coefficient $\alpha = A\bar{b}$ and the jth one has $\mathrm{O}(A\bar{b}^j) = \mathrm{O}(\alpha^j/A^{j-1})$, again small with respect to α^j.

Figure 72 displays the bifurcation diagram of (7) for $A = 5$, $\beta = 0.3$, as a function of ω (the horizontal coordinate ranging from 0 to 2π) and $\bar{b}$ (the vertical coordinate ranging from 0 to $\frac{5}{4}$). The initial conditions are taken 'arbitrarily' as $(z, \rho) = (0.123\,456\,789, 0)$ and the transient is 10^4 iterates. Periods up to 34 have been recorded. The black part corresponds to some iterate with negative argument in the logarithmic term in (7). The white region in the lower part of the tongues, corresponds to quasiperiodic invariant circles. The upper white region to strange attractors. Different grey tones correspond to attractors of different periods.

The main idea of this approach is as follows. To study the return map near homoclinic tangency (see [36, 38, 45]) captures just a small part of the dynamics. This approach, certainly restricted with some limitations concerning the nonlinearities, tries to capture the full dynamics on a fundamental domain and furthermore to make clear that, modulo some deformations, there are relatively few parameters to describe the typical behaviour of a large class of systems close to homoclinic tangency.

We note that if the initial diffeomorphism (as in figure 70(c)) has a negative compressing eigenvalue, $-1 < \lambda < 0$, the computations can be carried out in a similar way. After suitable identifications the only difference in equation (8) is that now $\beta < 0$. This justifies why we are also interested in the case of negative β.

Appendix B. Effective computation of the dominant coefficient in the Arnold tongue

In this section we reconsider the resonant normal form coefficient $A_{p/q}$ of the fattened Arnold family (cf section 2.4). Indeed, the dynamical properties heavily depend on conjecture 2.8, saying that $A_{p/q}(0) \neq 0$. Here we shall give strong evidence in favour of this.

Figure 72. Bifurcation diagram for the map (8).

To compute $A_{p/q}(0)$ (or for shortness, $A_{p/q}$) we can parametrize the invariant circle by

$$x = \xi + \sum_{j\geqslant 1} \alpha^j u_j(\xi), \qquad y = \sum_{m\geqslant 0} \alpha^m v_m(\xi),$$

where $u_j(\xi) = \sum_{|k|\leqslant j, k-j=\dot{2}, k\neq 0} u_{j,k} \mathrm{e}^{\mathrm{i}k\xi}$ and $v_m(\xi) = \sum_{|k|\leqslant m+1, k-m=\dot{2}+1} v_{m,k} \mathrm{e}^{\mathrm{i}k\xi}$, in such a way that the map restricted to the invariant curve is given by

$$\xi \mapsto \hat{h}(\xi) = \xi + \omega + c_1\alpha^2 + \cdots + \alpha^q (B_{p/q}\mathrm{e}^{\mathrm{i}q\xi} + B_{-p/q}\mathrm{e}^{-\mathrm{i}q\xi}) + \mathrm{O}(\alpha^{q+1}),$$

with $B_{-p/q} = \overline{B_{p/q}}$. Then $A_{p/q} = 2|B_{p/q}|$.

To ask for invariance we write

$$\hat{h}(\xi) + \sum_{j\geqslant 1} \alpha^j u_j(\hat{h}(\xi)) = \xi + \sum_{j\geqslant 1} \alpha^j u_j(\xi) + \omega$$
$$+\alpha\left(\sum_{m\geqslant 0} \alpha^m v_m(\xi) + \sin\left(\xi + \sum_{j\geqslant 1} \alpha^j u_j(\xi)\right)\right),$$

$$\sum_{m\geqslant 0}\alpha^m v_m(\hat{h}(\xi)) = \beta\Big(\sum_{m\geqslant 0}\alpha^m v_m(\xi) + \sin\Big(\xi + \sum_{j\geqslant 1}\alpha^j u_j(\xi)\Big)\Big).$$

By equating the coefficients of α^{j-1} in the second relation and of α^j in the first one, for $j = 1, 2\ldots$, we obtain, recurrently, v_0, u_1, v_1, c_1, u_2, v_2, u_3, v_3, c_2, $u_4, \ldots$. Due to the special structure of the v_m and u_j functions, to obtain $B_{p/q}$ we proceed as follows.

Let $\omega = 2\pi p/q$, $(p,q) = 1$, $q > 1$, $0 < p < q$, $f_j = (\mathrm{e}^{\mathrm{i}j\omega} - \beta)(1 - \mathrm{e}^{-\mathrm{i}j\omega}) = (1+\beta)(\cos(2\pi pj/q) - 1) + \mathrm{i}(1-\beta)\sin(2\pi pj/q)$, $z_j = 2\mathrm{i}u_{j,j}f_j$. Then, determine $z_1, \ldots, z_q$ by equating powers of ρ in the relation

$$\sum_{j=1}^{q} z_j\rho^{j-1} = \exp\Big(\sum_{j=1}^{q-1}\frac{z_j}{2f_j}\rho^j\Big) + \mathrm{O}(\rho^q),$$

that is,

$$z_1 = 1, \qquad z_j = \frac{1}{j-1}\sum_{k=1}^{j-1}(j-k)\frac{z_k z_{j-k}}{2f_{j-k}}, \qquad \text{for } j = 2, \ldots, q.$$

We obtain in this way

$$z_1 = 1,\ z_2 = \frac{1}{2f_1},\ z_3 = \frac{1}{4f_1f_2} + \frac{1}{8f_1^2},\ z_4 = \frac{1}{8f_1f_2f_3} + \frac{1}{16f_1^2f_3} + \frac{1}{8f_1^2f_2} + \frac{1}{48f_1^3}, \ldots.$$

The value of $A_{p/q}$ coincides with $|z_q|/(1-\beta)$, computed with $\omega = 2\pi p/q$. For instance,

$$A_{1/2} = \frac{1}{4(1-\beta^2)}, \qquad A_{1/3} = \frac{1}{24(1-\beta)}\frac{(7+13\beta+7\beta^2)^{1/2}}{(1+\beta+\beta^2)^{3/2}},$$
$$A_{1/4} = \frac{1}{96(1-\beta)}\frac{(41+18\beta+41\beta^2)^{1/2}}{(1+\beta^2)^2}.$$

These coefficients can be considered, in particular, for Arnold's circle map, when $\beta = 0$. A comparison with the formulae given in [1, p 274] shows the agreement. In [25, p 304] there is an obvious π factor missing. This has been propagated to several textbooks.

It is immediate that z_q is of the form $\sum_l \gamma_l / \prod_{i=1}^{q-1} f_{(j_i,l)}$ and $(j_i, l) \in \{1, \ldots, q-1\}$, the sum being finite and $\gamma_l \in \mathbb{Q}$. It is also easy to check, by induction on j, that z_q can be expressed as the quotient of two polynomials, $z_q = P(\beta)/Q(\beta)$, where P, $Q \in \mathbb{Q}(e_p)$, e_p being a pth primitive root of the unity. More concretely, for $Q(\beta)$ one has $Q(\beta) = \prod_{j=1}^{q-1} f_j^{[(q-1)/j]}$, where [ ] denotes the integer part. For a fixed p/q one has to see $A_{p/q} \neq 0$ as a function of β $\forall\,\beta \in (-1, 1)$. For $\beta = 1$ we have $f_j < 0$, and, hence, $z_{p/q} \neq 0$, and, therefore, $A_{p/q}(\beta)$ becomes unbounded when $\beta \nearrow 1$. Hence, given p/q, conjecture 2.8 is true for $\beta \in (\beta^*, 1)$, where β^* depends on p and q. A direct check suggests that $A_{p/q} \neq 0$ for all $\beta \in (-1, 1)$ and all p/q such that $(p,q) = 1$, $0 < p < q$, $q \leqslant 250$. For some selected β and p the checks have been done up to $q = 50\,000$.

The numerical experiments seem to suggest that

$$\frac{\log(A_{p/q})}{q\log q} = 1 - \frac{C(p,q,\beta)}{\log q},$$

where for fixed p and β, $C(p,q,\beta)$ seems to have a finite limit for $q \to \infty$. Figure 73 displays $C(p,q,\beta)$ versus p/q for several values of β and $0 < p < q/2$, $(p,q) = 1$, $q \leqslant 250$. However, if we allow p and q to vary, $C(p,q,\beta)$ seems to increase, at most, as $\log q$.

Table 2 gives, for $\beta = \pm 0.3$, the values of $A_{p/q}$ for several values of p/q and the values $\alpha^*_{p/q}$ such that up to this value the width (in ω) of the corresponding tongue, differs from

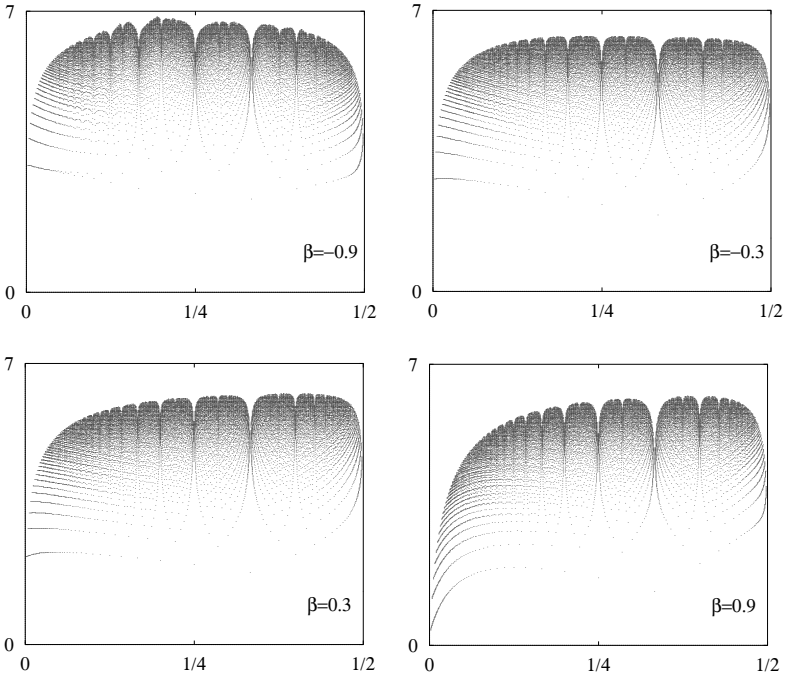

Figure 73. Behaviour of $C_{p/q}$. See the text for additional explanation.

Table 2. Values of $A_{p/q}$.

	$\beta = 0.3$		$\beta = -0.3$	
p/q	$A_{p/q}$	$\alpha_{10\%}$	$A_{p/q}$	$\alpha_{10\%}$
1/2	0.274 7253E+00	> 1	0.274 7253E+00	0.864
1/3	0.123 3341E+00	0.931	0.881 5748E−01	0.929
1/4	0.886 4480E−01	0.564	0.422 7401E−01	0.493
1/5	0.876 5090E−01	0.374	0.234 8492E−01	0.341
2/5	0.399 6585E−01	0.985	0.297 2281E−01	> 1
1/6	0.110 2128E+00	0.269	0.165 7611E−01	0.267
1/7	0.168 1969E+00	0.204	0.143 6092E−01	0.221
2/7	0.277 9286E−01	0.784	0.948 2976E−02	0.493
3/7	0.211 6816E−01	0.866	0.154 8412E−01	0.967
1/8	0.302 1543E+00	0.161	0.149 2875E−01	0.187
3/8	0.153 6294E−01	0.985	0.819 7756E−02	> 1
1/9	0.625 2427E+00	0.131	0.180 2122E−01	0.162
2/9	0.339 1009E−01	0.462	0.415 5330E−02	0.284
4/9	0.152 3261E−01	0.722	0.108 7782E−01	0.836
1/10	0.146 6228E+01	0.109	0.247 2099E−01	0.142
3/10	0.142 9592E−01	0.839	0.338 4015E−02	0.467

the theoretical value, $2A_{p/q}\alpha^q$, by less than 10%. Figure 74 displays the corresponding tongues up to $\alpha = 1$. We also note that for $\beta = -1$, if q is even and $j = q/2$ then $f_j = 0$. Hence, in principle, if $\beta \searrow -1$ and q is even, we shall have $|A_{p/q}| \nearrow \infty$. The only exception seems to occur when $q = 4$ ($p = 1$ or 3), because the terms $1/(8 f_1 f_2 f_3)$

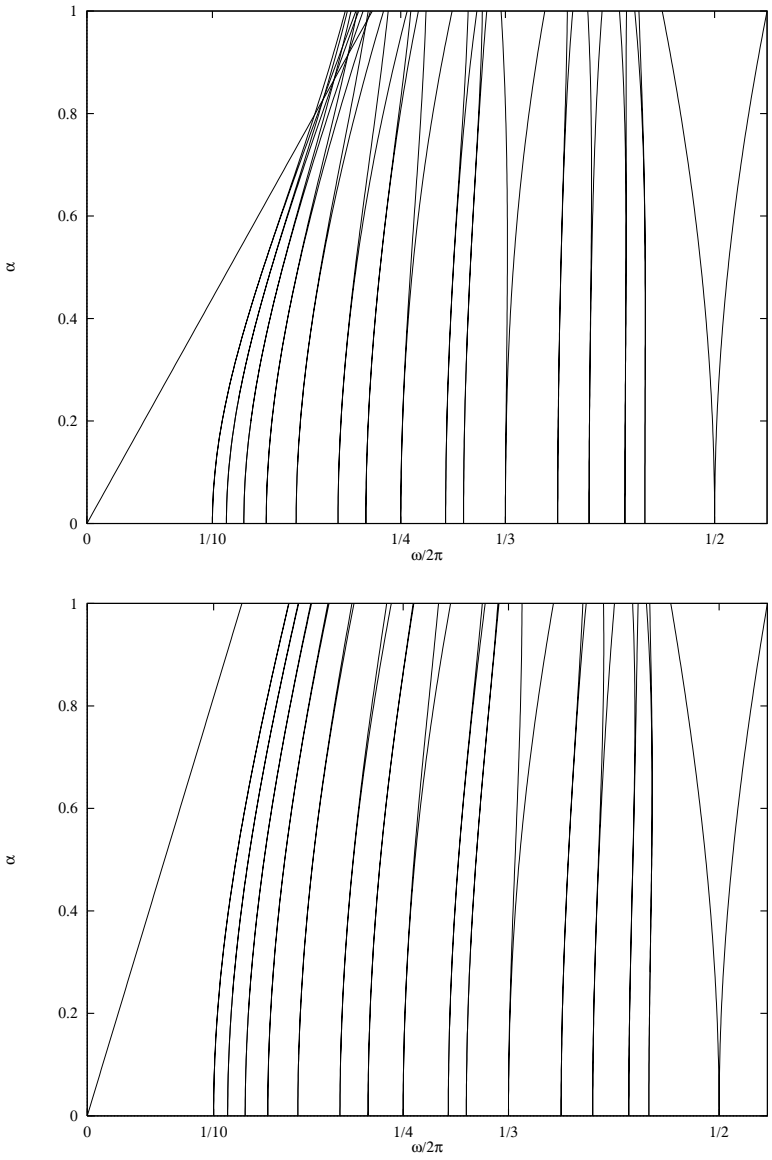

Figure 74. First Arnold tongues for the cases $\beta = 0.3$ (top) and $\beta = -0.3$ (bottom).

and $1/(8f_1^2 f_2)$ almost cancel and $\lim_{\beta\to -1} A_{1/4}$ exists ($= \frac{1}{96}$). For period two, $p/q = \frac{1}{2}$, it is easy to see that the saddle-node bifurcations (or, better, elliptic-hyperbolic) occur for $\omega = \pi \pm \frac{1}{2}\alpha$, displaying a linear, instead of a quadratic, character in α. When $\alpha \searrow 0$ then the y coordinates of the 2-periodic points become unbounded.

To have $A_{p/q} > 0$ for all $\beta \in (-1, 1)$ can seem also natural because of the following consideration. As said before, to have $A_{p/q} = 0$ one must have $P(\beta) = 0$ (using the representation $z_q = P(\beta)/Q(\beta)$). For $\beta \in \mathbb{R}$ we can write $P(\beta) = P_1(\beta) + \mathrm{i}P_2(\beta)$, P_1 and P_2 having real coefficients. Then $A_{p/q} = 0$ requires $P_1(\beta) = P_2(\beta) = 0$, two conditions to be satisfied.

In the case $\beta = 0$, the conjecture can be proved. We have the following.

Proposition B.1. *Let $\beta = 0$, $\omega = 2\pi p/q$, $(p, q) = 1$, $q > 1$, $0 < p < q$. Then $A_{p/q} > 0$.*

Proof. First we note that in this case $f_j = \lambda^j - 1$, where $\lambda = \exp(2\pi \mathrm{i} p/q)$. Let z_j be defined as above, introduce auxiliar variables $u_k = 2^{k-1} z_k$, and let $t = \rho/2$. The previous relation between the z_j is expressed as $\sum_{k=1}^{q} u_k t^{k-1} = \exp(\sum_{j=1}^{q-1} u_j t^j / f_j) + \mathrm{O}(t^q)$. Expanding the exponential we get $u_k = \sum \frac{(u_1/f_1)^{r_1} \ldots (u_m/f_m)^{r_m}}{r_1! \ldots r_m!}$, where the sum is over all finite sequences $r_1, \ldots, r_m$ of non-negative integers with $\sum_{j=1}^{m} j r_j = k - 1$. This can be used to compute recurrently u_k, $k = 1, \ldots, q$, with $u_1 = 1$. It follows

$$u_q = \frac{P(\lambda)}{(q-1)!(\lambda^{q-1} - 1) \ldots (\lambda - 1)},$$

where P is a polynomial with integer coefficients. This implies that, in this case the expression of u_q is simpler than the one given before for z_q as quotient of two polynomials. This fact can be easily seen by introducing $v_j = f_1 \ldots f_{j-1} u_j$. Then, the quadratic recurrence reads as $v_j = \frac{1}{j-1} \sum_{s=1}^{j-1} (j - s) v_s v_{j-s} M(\lambda)$, where $M(\lambda) = \frac{f_1 \ldots f_{j-1}}{f_1 \ldots f_{s-1} f_1 \ldots f_{j-s-1} f_{j-s}}$ is a polynomial with integer coefficients. Moreover, noting that for any sequence $r_1 \ldots$ with $\sum j r_j = q - 1$ other than $q - 1, 0, \ldots$ we have that the product $r_1! \ldots$ divides $(q-2)!$, we can write

$$P(X) = (X + 1)(X^2 + X + 1) \ldots (X^{q-2} + \cdots + 1) + (q - 1) Q(X),$$

where $Q(X)$ is a polynomial with integer coefficients.

We have to show $P(\lambda) \neq 0$. Suppose, in contrast $P(\lambda) = 0$. Then P is divisible over the integers by the cyclotomic polynomial $\Phi_q = X^{q-1} + \cdots + 1$. Let r be a prime factor of $q - 1$. Then Φ_q divides $(X^2 - 1)(X^3 - 1) \ldots (X^{q-1} - 1)$ over the field $\mathbb{Z}_r$. But then some root σ of Φ_q in a splitting field over $\mathbb{Z}_r$ must satisfy $\sigma^j = 1$ for some $2 \leqslant j < q$, which is impossible by the theory of cyclotomic extensions, since r is prime to q. □

Now we go back to a map like (7)

$$\begin{pmatrix} x \\ y \end{pmatrix} \mapsto \begin{pmatrix} x' \\ y' \end{pmatrix} = \begin{pmatrix} x + \omega + \gamma \log(1 + \alpha(y + \sin x)) \\ \beta(y + \sin x) \end{pmatrix}.$$

Let us introduce a new variable, w, given by $w = \alpha(y + \sin x)$. Then the map (7) reads

$$\begin{pmatrix} x \\ y \end{pmatrix} \mapsto \begin{pmatrix} x' \\ y' \end{pmatrix} = \begin{pmatrix} x + \omega + \gamma \log(1 + w) \\ \beta(y + \sin x) \end{pmatrix}.$$

As we did before for the case of the fattened Arnold family, we look for an invariant curve of the form

$$x = \xi + \sum_{j \geqslant 1} \alpha^j u_j(\xi), \qquad w = \xi + \sum_{m \geqslant 1} \alpha^m w_m(\xi),$$

where u_j, w_m are trigonometric polynomials (depending on ω, β, γ) whose highest-order harmonic is j (or m). The parameter ξ of the invariant curve goes, under the map, to

$$\xi \mapsto \hat{h}(\xi) = \xi + \omega + c_1 \alpha^2 + \cdots + c_{[q/2]} \alpha^q + \alpha^q (B_{p/q} \mathrm{e}^{\mathrm{i} q \xi} + \cdots) + \mathrm{O}(\alpha^{q+1}).$$

Let $\omega = 2\pi p/q + \delta$. As before, asking for invariance, one can compute the coefficients w_1, u_1, w_2, u_2, etc recurrently. To obtain $B_{p/q}$, let a_j be the coefficient of $\alpha^j \mathrm{e}^{\mathrm{i} j \xi}$ in u_j, and b_j

the one in w_j. Let $b_j = \mathrm{i}c_j$. Then the coefficients a_j, c_j and, finally, $B_{p/q}$, are obtained by equating powers of ψ in the formulae

$$B_{p/q}\psi^q + \sum_{j\geqslant 1} a_j\psi^j \mathrm{e}^{\mathrm{i}j\omega} = \sum_{j\geqslant 1} a_j\psi^j + \gamma \log\left(1 + \mathrm{i}\sum_{j\geqslant 1} c_j\psi^j\right),$$

$$\mathrm{i}\sum_{j\geqslant 1} c_j\psi^j \mathrm{e}^{\mathrm{i}j\omega} = \mathrm{i}\beta\sum_{j\geqslant 1} c_j\psi^j + \frac{1}{2\mathrm{i}}\mathrm{e}^{\mathrm{i}\omega}\psi\exp\left(\mathrm{i}\sum_{k\geqslant 1} a_k\psi^k\right),$$

where one has to use $\omega = 2\pi p/q$. Let

$$\exp\left(\mathrm{i}\sum_{k\geqslant 1} a_k\psi^k\right) = \sum_{j\geqslant 0} M_j\psi^j, \qquad \log\left(1 + \mathrm{i}\sum_{j\geqslant 1} c_j\psi^j\right) = \sum_{j\geqslant 1} N_j\psi^j.$$

One derives immediately the recurrence

$$M_0 = 1, \qquad c_j = \frac{1/2}{\beta\mathrm{e}^{-\mathrm{i}j\omega} - 1}M_{j-1}, \qquad N_j = \mathrm{i}c_j - \frac{\mathrm{i}}{j}\sum_{k=1}^{j-1}(j-k)c_kN_{j-k},$$

$$a_j = \frac{\gamma}{\mathrm{e}^{\mathrm{i}j\omega} - 1}N_j, \qquad M_j = \frac{\mathrm{i}}{j}\sum_{k=1}^{j} ka_kM_{j-k}, \qquad j \geqslant 1,$$

and then $B_{p/q} = \gamma N_q$, and the desired coefficient $A_{p/q} = A(p, q, \beta, \gamma) = 2|B_{p/q}|$. We note that now the symmetry is broken and one has to consider all the values $0 \leqslant p/q < 1$. First we have set $\gamma = 1$. The minimum value of $2A_{p/q}$ as a function of β, for $\beta \in [-1, 1]$ has been computed for $q \leqslant 125$. The value of $C(p, q, \beta_{\min}(p, q), \gamma = 1)$ is displayed in figure 75, where $C(p, q, \beta, \gamma)$ is defined in an analogous way to the previous $C(p, q, \beta)$, as a function of p/q. Figure 76 displays $\beta_{\min}(p, q)$ as a function of p/q, showing nice features and interesting scaling properties. Again for $\gamma = 1$ it seems that $A(p, q, \beta, 1)$ is non-zero for all $0 < p/q < 1$, $|\beta| < 1$. Allowing now γ to change, it is easy to see that $B_{p/q} = P(\beta, \gamma)/Q(\beta)$, Q being the same polynomial we had for z_q before. As an example we display $A_{1/2}$, $A_{1/3}$:

$$A_{1/2} = \frac{\gamma((1-\beta)^2 + \gamma^2(1+\beta)^2)^{1/2}}{4(1-\beta)(1+\beta)^2},$$

$$A_{1/3} = \frac{\gamma}{48(1-\beta)(1+\beta+\beta^2)^2}$$
$$\times\{[\gamma^2(-\beta^2+5\beta+5) + \sqrt{3}\gamma(-5\beta^2+\beta+1) + 2\beta^2 + 2\beta - 4]^2$$
$$+[\sqrt{3}\gamma^2(3\beta^2+5\beta+1) + \gamma(-3\beta^2+3\beta-9) + 2\sqrt{3}(-\beta^2+\beta)]^2\},$$

the value of $A_{2/3}$ being obtained by replacing $\sqrt{3}$ by $-\sqrt{3}$. The only zeros of $A_{1/3}$ occur for the values of (β, γ): $(1, 0)$, $(1, \frac{1}{\sqrt{3}})$, $(-1, \frac{1}{2}(-\sqrt{75} + \sqrt{59}))$, $(-1, \frac{1}{2}(-\sqrt{75} - \sqrt{59}))$. Those of $A_{2/3}$ are obtained by changing the sign of γ. But none of them occur in the domain of interest: $|\beta| < 1$, $\gamma > 0$. When we increase q it is easy to obtain many zeros of $A_{p/q}$ for suitable values of (β, γ). Now we have two parameters at our disposal! For instance, for $p/q = \frac{1}{5}$, $\beta \approx 0.401\,406\,37$, $\gamma \approx 0.812\,890\,41$ a zero is found. We have numerically checked the behaviour of the width of the corresponding Arnold tongue. It is of the form width$\approx 0.0101\alpha^7$ for α small. The term in $\alpha^5\sin(5\xi)$ is zero, and the next term with $\sin(5\xi)$ is of order α^7. No terms in $\alpha^6\sin(5\xi)$ appear due to the symmetries of sin. Hence, when a degeneracy occurs, the tongue seems to be 'as generic as possible'.

Table 3 displays some zeros of $A(p, q, \beta, \gamma)$ for different values of p/q (up to $q = 10$). In agreement with the comments at the end of appendix A and with conjecture 2.8, it seems that the zeros are confined to moderate values of γ.

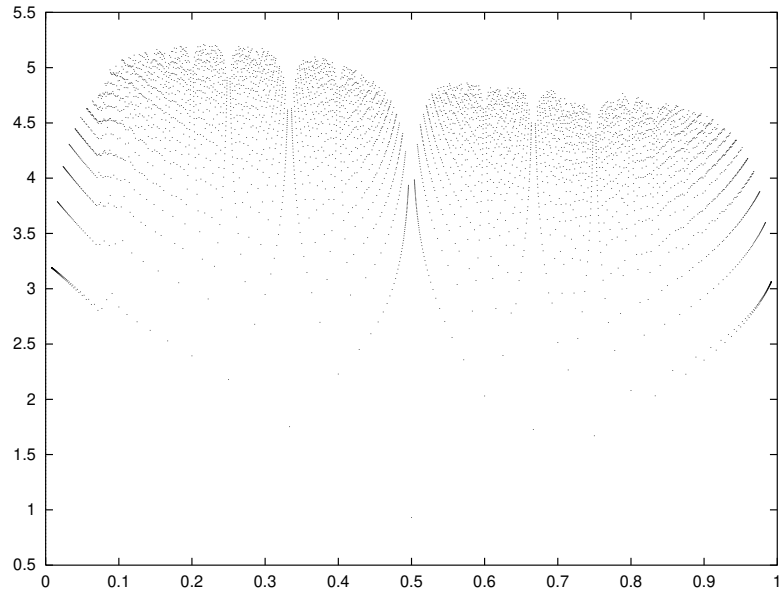

Figure 75. Value of C, for $\gamma = 1$, at the value of β which makes C minimum. See text for additional explanation.

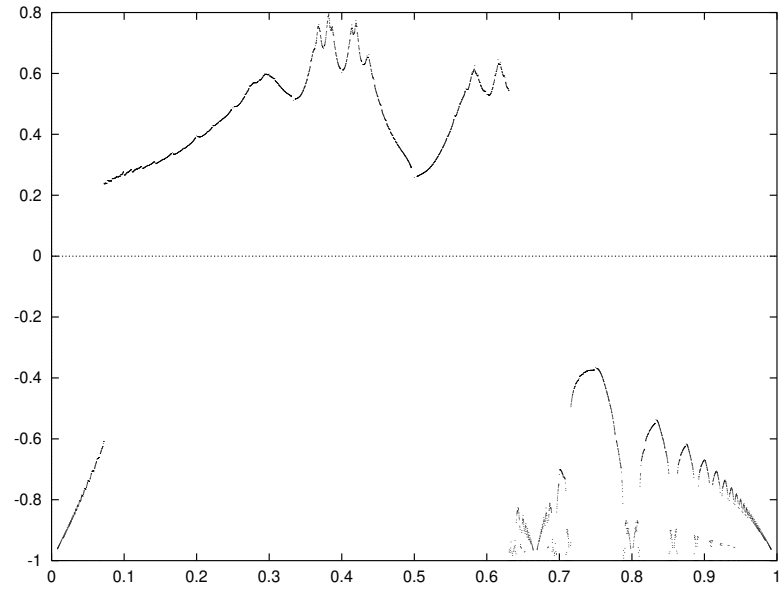

Figure 76. Value of β where the minimum of C is attained. See text for additional explanation.

Appendix C. Conservative cases

For values of $|\beta|$ close to 1 the fattened Arnold family can be considered as a perturbation of an area-preserving map, either orientation preserving or reversing. Certainly these maps are far from trivial, so a general perturbation scheme can not be carried out, from the

Table 3. Zeros of $A_{p/q}(\beta, \gamma)$ in $\beta \in (-1, 1)$, $\gamma > 0$.

p	q	β	γ	p	q	β	γ
1	4	0.520 917 1523E+0	0.720 552 3590E+0	1	9	−0.926 758 3111E+0	0.226 197 8268E+0
1	5	0.401 406 3687E+0	0.812 890 4108E+0	1	9	−0.448 427 3572E+0	0.470 694 3503E+0
3	5	−0.825 016 2406E+0	0.676 513 8685E+0	1	9	0.829 992 3829E+0	0.583 430 6941E+0
3	5	−0.827 598 5143E+0	0.969 831 3264E+1	1	9	0.581 664 5686E+0	0.721 250 5267E+0
1	6	−0.747 960 1390E+0	0.483 670 4164E+0	1	9	0.278 927 1515E+0	0.963 676 8552E+0
1	6	0.779 544 5817E+0	0.652 758 9239E+0	2	9	0.473 543 6843E+0	0.737 310 7065E+0
1	6	0.346 026 2395E+0	0.871 468 9495E+0	2	9	0.416 104 6436E+0	0.810 041 0664E+0
1	7	−0.602 018 2089E+0	0.534 942 0497E+0	5	9	0.627 950 6846E+0	0.455 619 0918E+0
1	7	0.678 882 3733E+0	0.680 281 2598E+0	5	9	−0.699 261 7653E+0	0.843 644 2044E+0
1	7	0.314 159 2592E+0	0.911 810 8079E+0	5	9	−0.742 530 9959E+0	0.105 828 1840E+2
2	7	0.880 399 6530E+0	0.556 815 1047E+0	5	9	−0.940 207 3440E+0	0.142 994 9638E+2
2	7	0.552 729 4751E+0	0.697 939 6894E+0	7	9	−0.918 399 1187E+0	0.411 697 9675E+0
4	7	0.724 064 3397E+0	0.426 696 2975E+0	7	9	−0.896 158 9007E+0	0.322 034 1449E+2
4	7	−0.737 188 1058E+0	0.788 297 7662E+0	1	10	−0.812 332 8485E+0	0.239 091 4636E+0
4	7	−0.772 304 2786E+0	0.103 388 5290E+2	1	10	−0.875 061 5100E+0	0.362 051 8098E+0
1	8	−0.509 283 1366E+0	0.502 864 0631E+0	1	10	−0.408 750 8972E+0	0.439 762 6348E+0
1	8	0.894 353 8222E+0	0.578 359 2289E+0	1	10	0.946 846 4224E+0	0.511 305 2658E+0
1	8	0.620 187 4945E+0	0.703 090 3335E+0	1	10	0.784 866 2948E+0	0.592 188 6540E+0
1	8	0.293 459 3517E+0	0.941 253 2552E+0	1	10	0.554 427 2103E+0	0.735 821 3085E+0
3	8	0.765 802 7497E+0	0.393 073 5769E+0	1	10	0.268 159 6467E+0	0.981 319 6328E+0
3	8	0.837 510 0805E+0	0.540 142 9290E+0	3	10	0.782 917 0714E+0	0.586 548 3069E+0
5	8	−0.923 110 9964E+0	0.642 662 7020E+0	3	10	0.567 973 0396E+0	0.691 520 0797E+0
5	8	−0.788 150 7906E+0	0.199 377 6346E+2	7	10	−0.934 968 7039E+0	0.266 550 4923E+0
				7	10	0.831 784 4842E+0	0.304 359 1977E+0

conservative case, except in the case of small α. We refer to the conservative cases in section 5.3.4, to make evident that $|\beta|$ close to 1 is a good candidate for having several simultaneous attractors, and also in appendix D, to study the limiting behaviour of homoclinic tangencies in the saddle node case for $\beta \to \pm 1$.

However, it is interesting to display some facts for the conservative cases. To distinguish them hereafter, we shall reserve the name 'conservative' only for the case $\beta = 1$, referring to the $\beta = -1$ as 'anticonservative'.

In all cases for $\alpha = 0$ the maps become integrable, with the phase space foliated by invariant curves (easy to make explicit) if $\omega \neq 2k\pi$, for some $k \in \mathbb{Z}$, or with all the orbits unbounded (except for the fixed points), otherwise. Hereafter we take $\alpha \neq 0$.

In the conservative case the change of variables $(X, Y) = (x, \omega + \alpha y)$ allows us to rewrite the fattened Arnold family as

$$(X, Y) \mapsto (X + Y + \alpha \sin(X), Y + \alpha \sin(X)),$$

the standard map in the 2-torus, independent of the value of ω. This is fairly well known and we shall not pursue this way.

In the anticonservative case different values of ω lead to different families of maps. The change of variables $(X, Y) = (x, \alpha y)$ leads to

$$(X, Y) \mapsto (X + \omega + Y + \alpha \sin(X), -(Y + \alpha \sin(X))), \tag{9}$$

also a map in $\mathbb{T}^2$. If we introduce the new variables $(\xi, \eta) = (X, X + Y + \omega)$ the map can also be written as

$$AC_{(\omega,\alpha)}(\xi, \eta) = (\eta + \alpha \sin(\xi), \xi + 2\omega),$$

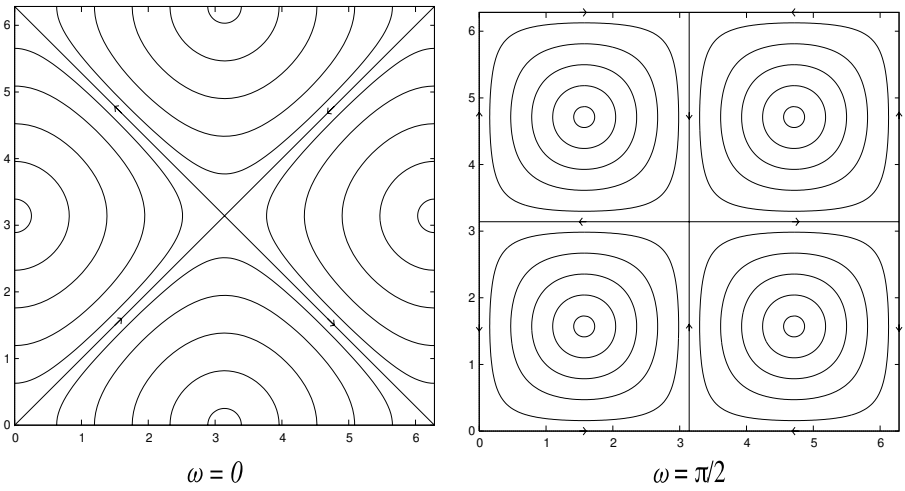

Figure 77. Limit flows, for $\alpha \to 0$, of the second and fourth power, respectively, of the anticonservative map for $\omega = 0$ and $\omega = \pi/2$.

which makes clear that it is π-periodic in ω. This fact, combined with the symmetries displayed at the end of section 1.2, implies that only the range $\omega \in [0, \pi/2]$ has to be studied. Let us consider first the extrema of that interval looking for the square (double iterate) ${AC_{(\omega,\alpha)}}^2$ which is a conservative family of maps depending on α.

If $\omega = 0$ one has

$$ {AC_{(0,\alpha)}}^2(\xi, \eta) = (\xi + \alpha \sin(\eta + \alpha \sin(\xi)), \eta + \alpha \sin(\xi)), $$

denoted as 'twist map' (TM) and introduced in [62]. Further information on this family of maps can be found in [40] and in [52]. For values of α small enough the map can be approximated by the time α flow of the Hamiltonian $H(\xi, \eta) = \cos(\xi) - \cos(\eta)$. An illustration of this flow in $\mathbb{T}^2$ is given in figure 77. For the TM the heteroclinic connections split for all $\alpha \neq 0$. The special structure of these connections implies that all invariant curves are homotopically trivial. Hence, some 'diffusion' can take place for all non-zero values of α. That is, if we do not consider in the original map $AC_{(0,\alpha)}$ the values of Y modulus 2π, there are unbounded orbits.

For $\omega = \pi/2$ it is better to consider the fourth power of the original map. Several cancellations occur and the map, for small values of α, can be approximated by the time α^2 flow of the Hamiltonian $H(\xi, \eta) = \sin(\xi)\sin(\eta)$. An illustration of this flow is also given in figure 77. Again it seems that for all non-zero values of α the heteroclinic connections split and diffusion is present. A study of this map, mainly concerning hyperbolic and statistical properties, can be found in [24].

For values of ω not too close to 0 or 2π the phase portrait looks familiar: there are periodic islands and also invariant curves of rotational type (in the (X, Y) variables they perform one revolution in the X direction) under the square of the map. Under the initial map the rotational invariant curves can be 2-'periodic' or 1-'periodic'. That is, the image under the map (not the square) can give a different ('twin') curve or the same initial curve. But for moderate values of α there is no diffusion. Increasing α a sufficiently large amount, strongly depending on ω, diffusion is found again, after all the rotational invariant curves have been destroyed. A big difference with the standard map case and other well known cases is that, after losing all the invariant curves for

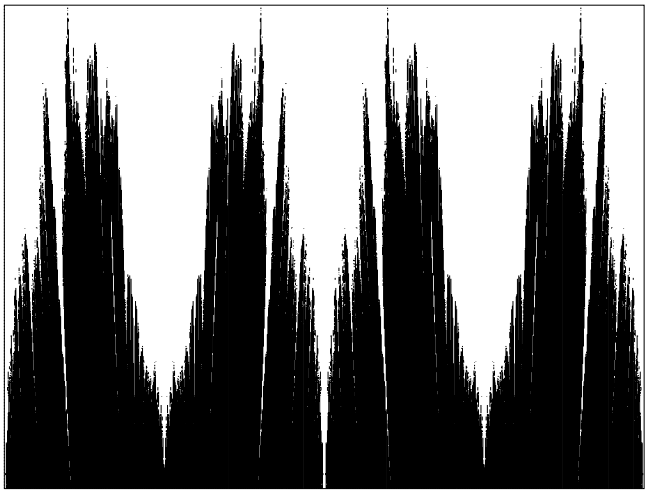

Figure 78. An approximation of the set of values of (ω, α) for which a rotational invariant curve exists and, hence, no diffusion occurs. The window is $[0, 2\pi] \times [1, 2]$.

some value $\alpha = \alpha_1$, some invariant curves can reappear for $\alpha = \alpha_2 > \alpha_1$. In fact the set of values of (ω, α) for which it seems there exists an invariant curve is rather wild. It seems that there are values of the parameters (ω, α) for which no invariant curve exists, completely surrounded by values for which these curves exist. A rough picture is shown in figure 78, obtained by a combination of brute force iteration of (9), visual inspection and some refined methods to approximate the 'last' invariant curve (see [55] for a description of these methods). For completeness it is displayed for ω in $[0, 2\pi]$.

This irregular behaviour is easy to understand, because a main reason for destruction of invariant curves is the appearance of relatively large chaotic zones if an invariant 1-'periodic' curve approaches a rational rotation number (cf appendix D in the case of period 1). This is a 'dangerous' situation, because this resonance, having a big bump in the central part, can destroy a bunch of invariant curves. Resonances at other places are not so dangerous. By moving parameters (e.g. increasing α) the resonance can migrate to another place and invariant curves can reappear.

When the values of ω approach to 0 or $\pi/2$ the values of α for which diffusion starts to appear, seem to decrease to zero. It is suspected that in the boundary of the set of couples for which a rotational invariant curve still exists, the behaviour of ω (or $\omega - \pi/2$) is exponentially small with respect to α.

Another characteristic fact of the map (9) is that it no longer has the 'monotone twist' character of the standard map. This is the source of invariant curves like the one shown in figure 79, which are far away from Lipschitz graphs. The curve is shown together with three successive magnifications. After the second magnification irregular behaviour is seen with vertical oscillations of the order of 10^{-10} when 2×10^9 iterations are carried out, due to rounding errors. Using higher-precision arithmetics it is possible to see that, for the initial condition, (0, 2.099 884 725 07), used in figure 79, there are in fact two nearby curves, one being the image of the other under the map. To this end it is convenient to take 10^{10} iterates and use the window $[1.484\,056\,17, 1.484\,056\,25] \times [3.946\,100\,521\,18, 3.946\,100\,521\,22]$, near the minimum of the figure displayed after the second magnification. These two curves

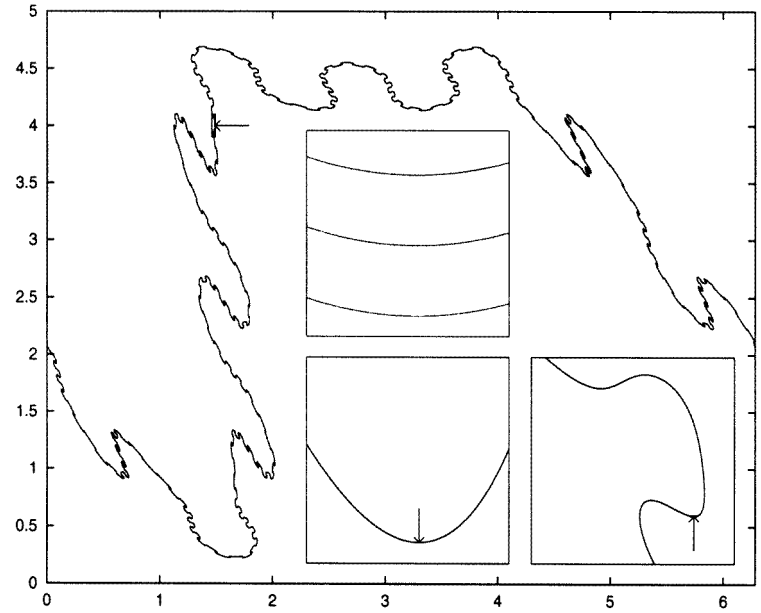

Figure 79. An invariant curve for $\omega = 0.07 \times 2\pi, \alpha = 1.39$ under the map (4). As an initial condition we took the point $(0, 2.099\,884\,725\,07)$. In the lower right corner appears a magnification of the small rectangle marked in the full figure, corresponding to the window $[1.46, 1.49] \times [3.9, 4.1]$. In the frame which appears on the mid lower part, there is a magnification of the very small rectangle marked in the previous one. The corresponding window is $[1.4835, 1.4845] \times [3.946, 3.947]$. Above this frame there is another one with a extremely small window (see text).

are shown in the third magnification as upper and lower curves. The vertical distance between them is close to 2.74×10^{-11}. The best determination of the initial condition, to have a single invariant curve, that we have found, is $(0, 2.099\,884\,725\,066\,170\,395)$. The corresponding curve is the middle one in the third magnification.

In many cases the last invariant curve seems to be of the type shown. This implies that after the last curve is destroyed the diffusion is quite fast. In the standard map case it is hard to see any diffusion if the value of the parameter is increased by 0.01 from the critical one. In some sense, it seems 'difficult' to cross the Aubry–Mather sets, despite the fact that they no longer separate the phase space. For the map (9), after the destruction of the last invariant curve, the diffusion is very fast.

Certainly these families of anticonservative maps deserve a thorough study!

Appendix D. Perturbations of conservative cases

The conservative case and orientation-preserving case, $\beta = 1$, is just a standard map under a suitable change in y (see appendix C). KAM theory can be applied to show the persistence of invariant circles, filling most of the space for α small. There also exist infinitely many resonant zones in which very small islands exist. Furthermore, the homoclinic tangles fill zones which are exponentially small in α.

When β goes away from 1 at most one invariant curve can persist, but the number of attracting periodic orbits, obtained by perturbation of the previous elliptic periodic points,

can be as large as desired. This may require very small variations of β.

Further variation of β may make former elliptic points pass through a flip bifurcation. Their invariant manifolds can have homoclinic intersections and give rise to periodic strange (small) attractors. It is not clear to the authors if the number of coexisting strange attractors can be arbitrary large in this family, but we conjecture that this is true. Compare the discussion in sections 3.2 and 5.3.4 and appendix C.

We now turn to the behaviour of saddle-node homoclinic tangencies for $|\beta| \nearrow 1$. To be precise, we analyse, for our family of maps, the behaviour of the couples (ω, β) for which a homoclinic tangency to a saddle node is produced, for values of $|\beta|$ close to 1, but less.

We start near $\beta = 1$. Let $\beta = 1-\epsilon$. We recall that the fold is produced for $\alpha = (1-\beta)\omega$ and then the fold is at $(-\pi/2, -\beta/(1-\beta))$. The changes $\xi = x+\pi/2$, $\eta = 1+\epsilon(y+\sin x)$ lead to the map

$$\begin{pmatrix} \xi \\ \eta \end{pmatrix} \mapsto \begin{pmatrix} \bar{\xi} \\ \bar{\eta} \end{pmatrix} = \begin{pmatrix} \xi + \omega\eta \\ \eta + \epsilon(-\eta + 2\sin^2(\bar{\xi}/2)) \end{pmatrix}.$$

Let us look for values of $\omega = a\epsilon$, a being a finite constant. Then the map can be approximated by a limit flow such that, the difference between the map and the time-ϵ flow is exponentially small. The proof of this is similar to the one used for Bogdanov–Takens diffeomorphisms in [11]. The vector field of the limit flow is $X = X_0 + \epsilon X_1 + \cdots$, with

$$X_0 = \begin{pmatrix} a\eta \\ -\eta + 2\sin^2(\xi/2) \end{pmatrix}.$$

Now we look for the suitable value of a to have a homoclinic connection. The fixed point $(0, 0)$ is a saddle node and we look for a such that the unstable branch of the saddle node coincides with one of the branches of the stable manifold. Due to the form of the vector field, this must be the upper branch. Rough bounds on a can be easily obtained. Due to the form of X_0, by increasing a, the vector field rotates (and change modulus) anticlockwise. This also shows the uniqueness of a. The stable manifold has a limit slope $-1/a$. Let us consider the line through $(0, 0)$ with slope $-4/\pi$. The segment of this line between $\xi = -\pi/2$ and $\xi = 0$ is crossed by the vector field going downwards if $a < \pi/8$.

On the other hand, along the homoclinic conection (between, say $(-2\pi, 0)$ and $(0, 0)$) one should have

$$2\pi = \int_{-\infty}^{\infty} (\dot{\xi} + a\dot{\eta})dt = 2a\int_{-\infty}^{\infty} \sin^2\frac{\xi}{2}dt = 2a\int_{-2\pi}^{0} \sin^2\frac{\xi}{2}\frac{d\xi}{a\eta} > \frac{2\pi}{\eta_{\max}},$$

where $\eta_{\max}$ is the maximum value of η along the connection. Hence, one should have $\eta_{\max} > 1$. As the vector field is horizontal on $\eta = 2\sin^2(\xi/2)$, the unstable branch is bounded by $\eta = 1$ if $\xi \in (-2\pi, -3\pi/2)$. Moreover, on the line $\eta = -\xi/a$ the vector field points to the upper part and the curve entering $(0, 0)$ through the (strong) stable manifold should remain below this line. Hence, if $a > 3\pi/2$ we shall have $\eta_{\max} < 1$.

Therefore we have proved the following.

Proposition D.1. *The line on the (ω, β) plane of internal homoclinic tangencies for β tending to 1 is of the form $\omega = a(1-\beta) + \mathrm{O}((1-\beta)^2)$ with $a \in (\pi/8, 3\pi/2)$.*

Remarks.

(i) The same is true for the outer tangencies and for the cubic tangencies to the strong stable foliation, the differences between all those lines being exponentially small in $1-\beta$.

(ii) A direct numerical computation shows $a \simeq 0.702\,563\,658\,236$. The behaviour is shown in figure 80.

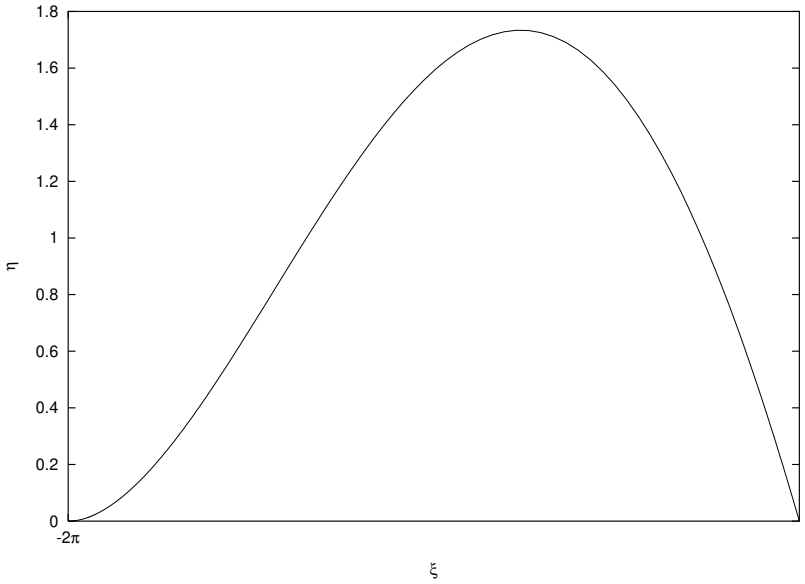

Figure 80. Limit behaviour of the homoclinic connection near $\beta = 1$.

Now we pass to the case $\beta \searrow -1$. This is more involved because, to have a limit flow as a good approximation, one has to work with the square of the map. We put $\beta = -1+\mu$, μ small, and then $\alpha = \omega(2-\mu)$.

Let $u = x + \pi/2$, $v = 2(y - \frac{1-\mu}{2-\mu} + \sin^2(u/2))$. The map is expressed as

$$\begin{pmatrix} u \\ v \end{pmatrix} \overset{T}{\mapsto} \begin{pmatrix} \bar{u} \\ \bar{v} \end{pmatrix} = \begin{pmatrix} u + \omega(1 - \frac{\mu}{2})(v + 2s^2) \\ -(1-\mu)(v + 2s^2) + 2\bar{s}^2 \end{pmatrix},$$

where $s = \sin(u/2)$, $\bar{s} = \sin(\bar{u}/2)$. We shall denote also $\bar{\bar{s}} = \sin(\bar{\bar{u}}/2)$. For T^2 we obtain

$$\begin{pmatrix} u \\ v \end{pmatrix} \overset{T^2}{\mapsto} \begin{pmatrix} \bar{\bar{u}} \\ \bar{\bar{v}} \end{pmatrix} = \begin{pmatrix} u + \omega(1-\mu/2)(\mu(v + 2s^2) + 4\bar{s}^2) \\ (1-\mu)^2(v + 2s^2) - (1-\mu)4\bar{s}^2 + 2\bar{\bar{s}}^2 \end{pmatrix}.$$

The map T has a saddle node at $(0, 0)$ with stable eigenvalue $-(1-\mu)$ and related eigenvector $(\omega, -2)$.

First we consider the conservative case, $\mu = 0$. Then T^2 reduces to

$$T_c^2 : (u, v) \mapsto (u + 4\omega\bar{s}^2, v + 2(s^2 - 2\bar{s}^2 + \bar{\bar{s}}^2)).$$

The origin has a centre manifold which contains an unstable and a stable branch (for $u > 0$, $u < 0$, respectively, locally). No other manifold enters or leaves the origin.

Assuming $\omega \ll 1$ the map T_c^2 is a perturbation of the identity. It is possible to construct a Hamiltonian such that T_c^2 is the time-1 flow of the Hamiltonian plus a remainder bounded by $\exp(-c/\omega)$ for a suitable $c > 0$ (cf Neishtadt [37, 11]). The Hamiltonian up to order 3 in ω is

$$H = \omega 4s^2 v + \omega^2(2csv^2 - 8cs^5) + \omega^3\left(\frac{v^3}{3}(1 - 2s^2) + v\left(-12s^4 + \frac{40}{3}s^6\right)\right),$$

where, as before, $s = \sin(u/2)$ and $c = \cos(u/2)$. It is necessary to use, at least, approximations to order ω^3, lower order (in ω) Hamiltonians being degenerate.

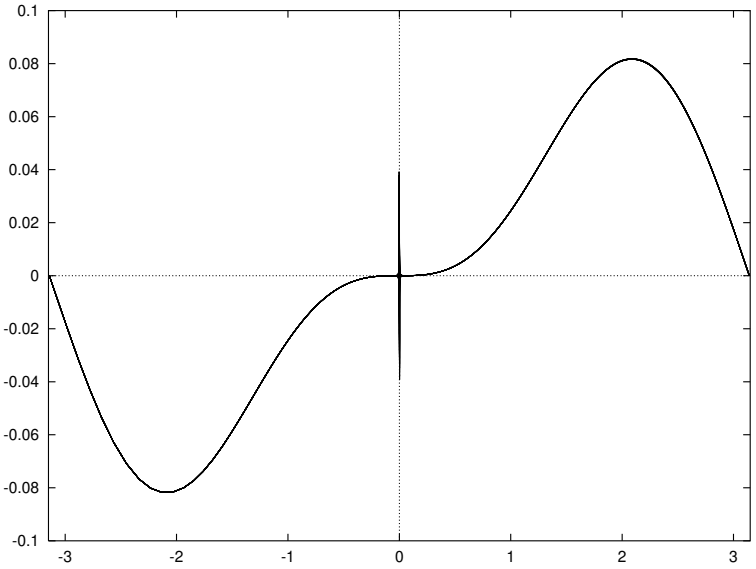

Figure 81. Level lines of the Hamiltonian which approximates T_c^2.

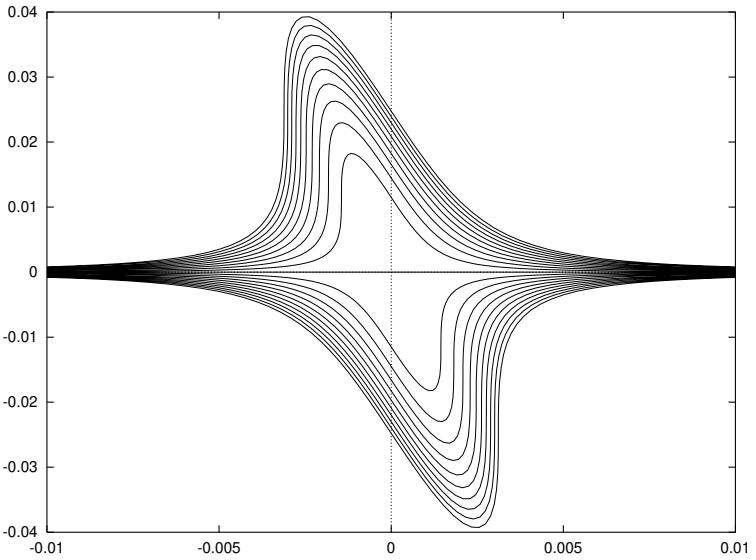

Figure 82. Magnification of the previous figure near the origin.

In fact higher-order terms (in ω^k, $k \geqslant 4$) pruduce minor qualitative and quantitative modifications to the dynamics. Also the term in $\omega^3 v$ can be skipped to analyse the behaviour of H.

The centre manifold through $(0, 0)$ for H has the expression $v = 2\omega c s^3 + \mathrm{O}(\omega^3)$. It is a separatrix of the Hamiltonian. Along the separatrix one has $\dot{u} = 4\omega s^2(1 + \mathrm{O}(\omega^2 s^2))$. Hence, the dominant temporal behaviour of the separatrix is $u = 2\,\mathrm{arccot}(-2\omega t)$, having singularities at $t = \pm \mathrm{i}/(2\omega)$.

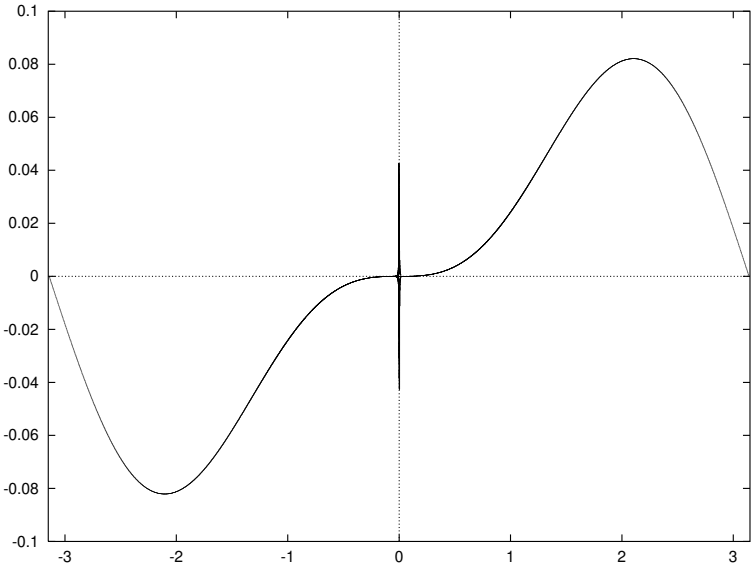

Figure 83. The stable and unstable manifolds of the fixed point under T_c^2 in the (u, v) variables.

Figure 81 contains a plot of the level lines of H for $\omega = 0.02 \times 2\pi$ and values of the energy, h, between -10^{-8} and 10^{-8} with step 10^{-9}. All the lines are rather close to $v = 2\omega cs^3$ except in a neighbourhood of the origin, displayed in figure 82. Near the origin the dominant terms are

$$H = \omega u^2 v + \omega^2(uv^2 - u^5/4) + \omega^3 v^3/3.$$

A Newton polygon analysis shows that there is only one component of $H = 0$. The flow is vertical ($\dot{u} = 0$) only at $u + \omega v = 0$, and horizontal ($\dot{v} = 0$) near $2u + \omega v = 0$. The local maximum of $H = h$ is attained at $u = -(\frac{3h}{2})^{1/3} + \mathrm{o}(h)$ and then $v \simeq \frac{2}{\omega}(\frac{3}{2}h)^{1/3}$. Furthermore, the period on the level lines $H = h \neq 0$ is of the form ctant$/(\omega h^{1/3})$, for h and ω small.

We return to the conservative diffeomorphism T_c^2. Using arguments similar to those given in [21, 22] it is possible to show that the splitting of separatrices, that is the distance between the stable and unstable manifolds of the origin for a fixed u, has an upper bound of the form $N(\delta)\exp(-(\pi - \delta)/\omega)$ for any $\delta > 0$, uniformly in ω for $0 < |\omega| < \omega_0$. The existence of homoclinic points is ensured by different considerations. The simplest one is that, locally near the origin, T_c changes the sign of v. Hence, W^u cannot remain at one side of W^s. Another consideration is to look at T_c^2 as a perturbation of the time-one flow of H. As this last one is a twist map (singular at the level $h = 0$) invariant curves exist for ω small enough (and h not too small). Then area-preserving arguments show the existence of homoclinic points. Generically (see again [21]) the oscillation of W^u with respect to W^s is modelled by a sinusoidal function (higher-order harmonics being much less important).

Figure 83 displays a plot of W^u and W^s for T_c^2. For the centre manifold a local expression as a graph (see [51]) $v = g(u) = \sum_{k\geqslant 3, k=2\dot{+}1} a_k u^k$ is used up to order 29. It is easy to derive a recurrence for the a_k coefficients. This approximation gives small errors for $|u| < 0.620\,18$. A fundamental domain $u \in [0.597\,63, 0.620\,18]$ has been chosen and the points have been iterated for 24 001 times. Figure 84 shows W^u, W^s on a magnification, obtained by taking 1000 points in the fundamental domain and iterating 5000 times. Finally,

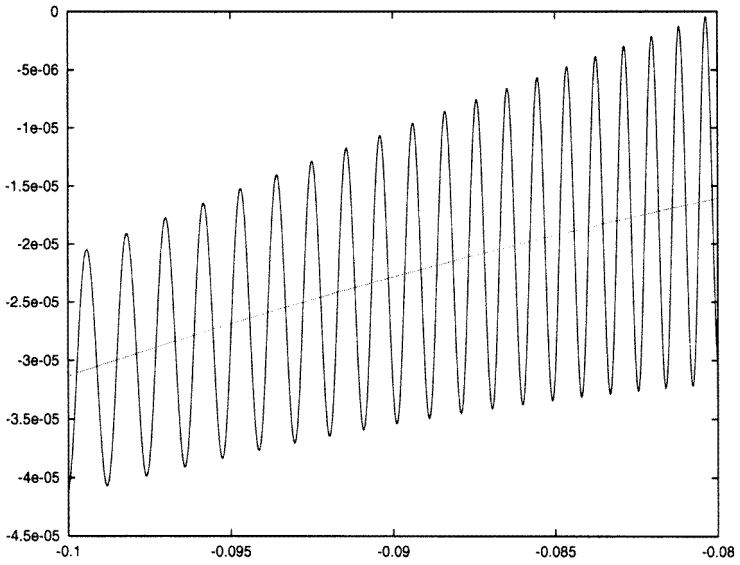

Figure 84. Magnification of the previous figure to the left of the fixed point, showing the oscillations of the unstable manifold.

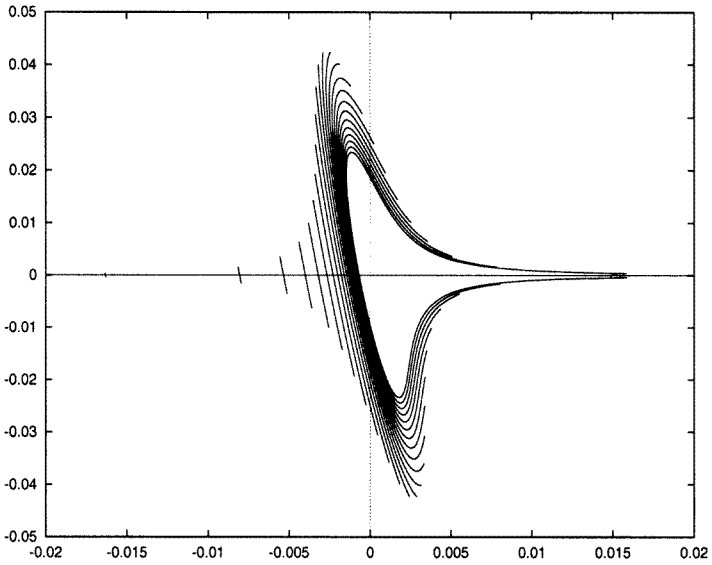

Figure 85. Magnification of the invariant manifolds near the origin. See the text for additional explanation.

figure 85 shows W^u, W^s near the origin. It has been obtained with 5000 points on a fundamental domain and 24 001 iterates, but only the iterates $\equiv 0, 1 \pmod{1000}$ have been displayed. Hence, it contains just one 'wave' every 500 'waves'.

The splitting can be measured as the maximum difference between W^u and W^s in one wave. This depends on the value of the domain of u where this is explored. See later for the relation between the amplitudes of the waves at different u ranges. We know this amplitude is exponentially small in ω. Guided by the results of Lazutkin [31] for similar

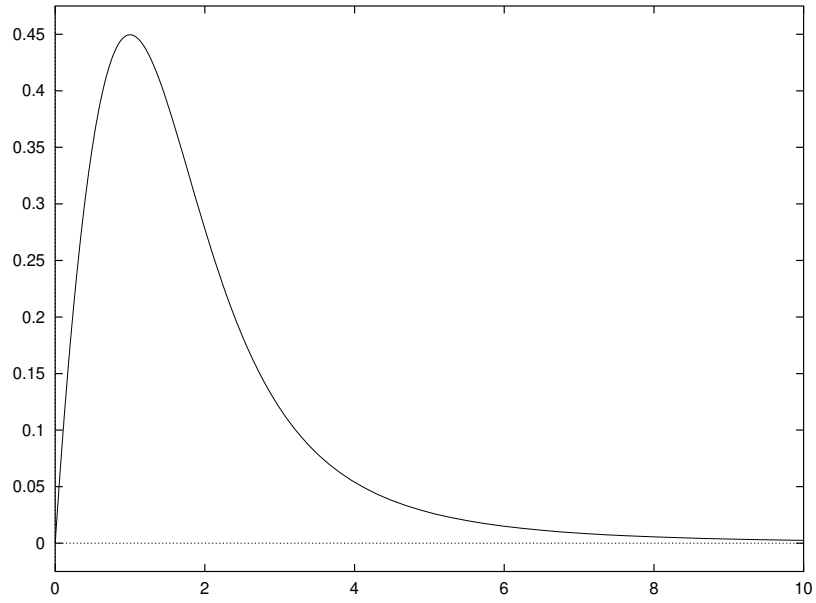

Figure 86. Limit scaled behaviour of the stable manifold of the origin under T^2 for $\mu \ll \omega \ll 1$, in the (r, s) variables.

phenomena we have looked at a behaviour of the amplitude like $A\omega^\beta \exp(-\pi/\omega)$. The value $B = -2$ has been obtained experimentally, but it is possible to obtain this result analytically (Gelfreich [23]).

Now we pass to the complete diffeomorphism, $\mu \neq 0$, assuming $\mu \ll \omega \ll 1$. In fact, we shall assume μ exponentially small in ω. The map T^2 is again close to the identity and can be written as the time-1 flow of a vector field plus a perturbation. In a vicinity of the origin it is enough to keep, in the vector field, the terms of first and second degree in u, v and the terms of first degree having μ as a factor. We obtain

$$\dot{u} = \omega(u + \omega v)^2 + \mu\omega v,$$
$$\dot{v} = -2\omega u v - \omega^2 v^2 - 2\mu v.$$

Introducing $\hat{v} = \omega v$, $\gamma = \mu/\omega$ and scaling time by ω we have

$$u' = (u + \hat{v})^2 + \gamma\hat{v},$$
$$\hat{v}' = -2u\hat{v} - \hat{v}^2 - 2\gamma\hat{v}.$$

Now we introduce new scaled variables, r, s, by $r = -(u + \hat{v}^2/2)/\gamma$, $s = (\hat{v}/4\gamma)^2$ and scale time by $-\gamma$, obtaining the vector field with components $(r^2 + 4s, 4s(1 - r))$, which is parameter independent. Going back one can check that the skipped terms modify the vector field by an $O(\gamma)$ perturbation when (v, s) move on any compact of $\mathbb{R}^2$, for γ small enough. We want to obtain an approximation of the unstable manifold of T^2 reaching the origin with slope $-2/\omega$. This is equivalent to looking at the unstable manifold of the last vector field, leaving $(0, 0)$ with slope 1. The equation can be written as $\frac{ds}{dr} = \frac{4s(1-r)}{r^2+4s}$. It is clear that when r goes from 0 to 1 the slope decreases monotonically from 1 to 0. From $r = 1$ on s decreases, but remaining positive for all $r > 0$. For r large one has $s = \sum_{r \geqslant 4} a_k/r^k$, $a_4 > 0$. Numerically one obtains $a_4 \simeq 37.853\,1794$. Figure 86 displays the behaviour of s versus r for that manifold.

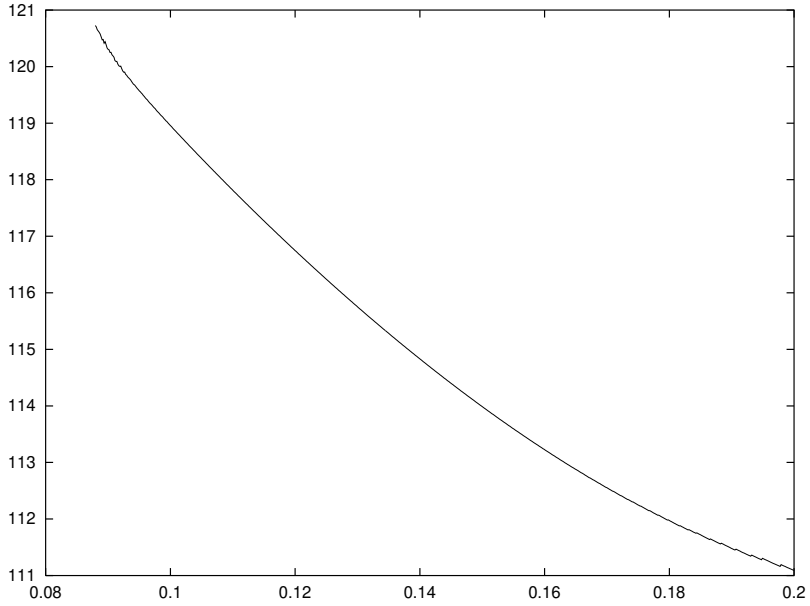

Figure 87. Numerical evidence of the asymptotic behaviour of μ as exponentially small with respect to ω. See the text for additional explanation.

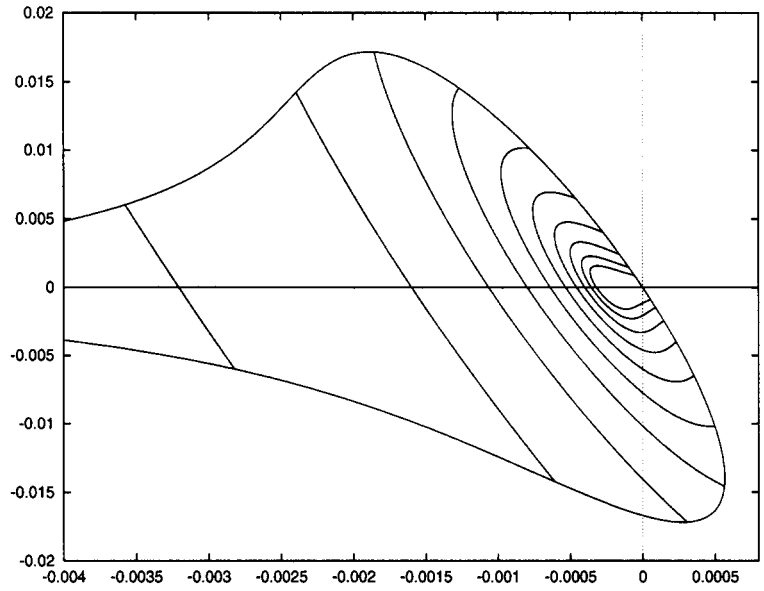

Figure 88. The stable manifold and some arcs of the stable one, at the homoclinic tangency.

Finally one has to derive the relation between μ and ω to have an homoclinic tangency. Going back to the u, v variables, the expression of the stable manifold for r large (compared with γ) is $v \simeq \frac{4\mu^3}{\omega^4}\frac{a_4^{1/2}}{u^2}$. This also gives how the amplitude of the waves of the unstable branch with respect to the (weak) stable branch, behave with respect to the value of u,

u^*, where they are mesured. At different points, u_1^*, u_2^* the respective amplitudes scale like $A_1/A_2 = u_2^{*2}/u_1^{*2}$. Figure 87 displays the experimental behaviour of the amplitude A, reduced to $u^* = 1$. If we measure A at u^*, to have an homoclinic tangency one should have $u^{*2}A\omega^B \mathrm{e}^{-\pi/3\omega} \simeq 4\mu^3 a_4^{1/2}\omega^{-4}$, and hence

$$\mu = \left(\frac{Au^{*2}}{4a_4^{1/2}}\right)^{1/3} \omega^{(4+B)/3}\mathrm{e}^{-\pi/3\omega}.$$

Using $B = -2$ one has $\mu = D\omega^{2/3}\mathrm{e}^{-\pi/3\omega}$. For $\omega = 0.02 \times 2\pi$, for instance, one has $\mu = 1.011\,46 \times 10^{-4}$. This allows us to obtain the approximate value $D = 1.7$. It fits with the values of $\mu(\omega)$ determined numerically in the range $\omega/2\pi \in [0.014, 0.03]$. Smaller values of ω produce numerical problems working with 16 decimal digits arithmetics.

Figure 88 displays the stable manifold of the origin for $\omega = 0.02 \times 2\pi$, $\mu = 1.01146 \times 10^{-4}$, and one every each 2500 waves of the unstable one in the window $[-0.004, 0.0008] \times [-0.02, 0.02]$. Again local representations as graphs to order 29 have been used for the manifolds, starting at order 2 for the unstable branch and 1 for the stable manifold. Summarizing, and letting aside numerical facts, the value of β for which a homoclinic tangency to the saddle node is produced, behaves like $\beta = -1 +$ exponentially small in ω.

References

[1] Arnold V I 1965 Small denominators I *Transl. Am. Math. Soc. 2nd Series* **46** 213–84

[2] Arnold V I 1983 *Geometrical Methods in the Theory of Ordinary Differential Equations* (New York: Springer)

[3] Aronson D G, Chory M A, Hall G R, McGehee R P 1982 Bifurcations from an invariant circle for two-parameter families of maps of the plane *Commun. Math. Phys.* **83** 303–54

[4] Bélair J and Glass L 1985 Universality and selfsimilarity in the bifurcations of circle maps *Physica* D **16** 143

[5] Benedicks M and Carleson L 1991 The dynamics of the Hénon map *Ann. Math.* **133** 73–169

[6] Bosch M and Tatjer J C 1991 On the codimension two bifurcations in families of one- and two-dimensional maps *Proc ECIT* vol 89 (Singapore: World Scientific) pp 9–18

[7] Bosch M 1992 Estudi de sistemes dinàmics mitjançant la reducció de la seva dimensió *PhD Thesis* Universitat de Barcelona

[8] Boyland P L 1986 Bifurcation of circle maps: Arnold tongues, bistability and rotation intervals *Commun. Math. Phys.* **106** 353–81

[9] Broer H W, Huitema G B and Takens F 1990 Unfoldings of quasi-periodic tori *Mem. Am. Math. Soc.* **421** 1–82

[10] Broer H W, Roussarie R and Simó C 1993 On the Bogdanov–Takens bifurcation for planar diffeomorphisms *Proc. Equadiff 91* (Singapore: World Scientific) pp 81–92

[11] Broer H W, Roussarie R and Simó C 1996 Invariant circles in the Bogdanov–Takens bifurcation for diffeomorphisms *Ergod. Theor. Dynam. Syst.* **16** 1147–72

[12] Broer H W and Takens F 1989 Formally symmetric normal forms and genericity *Dynam. Rep.* **2** 36–60

[13] Broer H W and Tangerman F M 1986 From a differentiable to a real analytic perturbation theory, applications to the Kupka Smale theorems *Ergod. Theor. Dynam. Syst.* **6** 345–62

[14] Cabré X and Fontich E 1995 Regularity and uniqueness of one dimensional invariant manifolds *Preprint* Universitat de Barcelona

[15] Carcassès J P 1993 Determination of different configurations of fold and flip bifurcation curves of one or two-dimensional maps *Int. J. Bifur. Chaos Appl. Sci. Eng.* **3** 869–902

[16] Carcassès J P, Mira C, Bosch M, Simó C and Tatjer J C 1991 'Crossroad area–spring area' transition (I). Parameter plane representation *Int J. Bifur. Chaos Appl. Sci. Eng.* **1** 183–96

[17] Carcassès J P, Mira C, Bosch, M, Simó C and Tatjer J C 1991 'Crossroad area–spring area' transition (II). Foliated parametric representation *Int. J. Bifur. Chaos Appl. Sci. Eng.* **1** 339–48

[18] Devaney R 1989 *An Introduction to Chaotic Dynamical Systems* 2nd edn (Reading, MA: Addison-Wesley)

[19] Díaz L, Rocha J and Viana M 1996 Strange attractors in saddle-node cycles: prevalence and globality *Inv. Math.* **125** 37–74

[20] Feigenbaum M J, Kadanoff L P and Shenker S J 1982 Quasiperiodicity in dissipative systems: renormalization group analysis *Physica* D **5** 370–86
[21] Fontich E and Simó C 1990 The splitting of separatrices for analytic diffeomorphisms *Ergod. Theor. Dynam. Syst.* **10** 295–318
[22] Fontich E and Simó C 1990 Invariant manifolds for near identity differentiable maps and splitting of separatrices *Ergod. Theor. Dynam. Syst.* **10** 319–46
[23] Gelfreich V G 1997 Reference systems for splitting of separatrices *Nonlinearity* **10** 175–93
[24] Giorgilli A, Lazutkin V F and Simó C 1997 Visualization of a hyperbolic structure in area preserving maps *Reg. Chaotic Dynam.* **2** 47–61
[25] Guckenheimer J and Holmes P 1983 *Nonlinear Oscilations, Dynamical Systems and Bifurcations of Vector Fields* (Berlin: Springer)
[26] Herman M R 1977 Mesure de Lebesgue et nombre de rotation *Lect. Notes Math.* **597** 271–93
[27] Herman M R Sur la conjugaison différentiable des diffeomorphismes du cercle à des rotations *Publ. Math. IHES* **49** 1979
[28] van der Heijden G H M 1994 Nonlinear drillstring dynamics, a quest for the origin of chaotic vibrations *PhD Thesis* Utrecht University
[29] Hirsch M W, Pugh C C and Shub M 1977 *Invariant Manifolds (Springer Lecture Notes in Mathematics 583)* (Berlin: Springer)
[30] Holmes P and Whitley D 1984 Bifurcations of one- and two-dimensional maps *Phil. Trans. R. Soc.* A **311** 43–102
[31] Lazutkin V F 1989 Splitting of separatrices for standard and semistandard mappings *Physica* D **40** 235–48
[32] López J M and Simó C An exploration of quadratic diffeomorphisms in $\mathbb{R}^3$, in preparation
[33] Mañé R 1978 Persistent manifolds are normally hyperbolic *Trans. Am. Math. Soc.* **246** 261–83
[34] Mira C 1987 *Chaotic Dynamics* (Singapore: World Scientific)
[35] Mira C, Kawakami H and Allam R 1993 The dovetail bifurcation structure and its qualitative changes *Int. J. Bifur. Chaos Appl. Sci. Eng.* **3** 903–14
[36] Mora L and Viana M 1993 Abundance of strange attractors *Acta Math.* **171** 1–71
[37] Neishtadt A I 1984 The separation of motions in systems with rapidly rotating phase *Prikl. Mat. Mekh.* **48** 133–9
[38] Newhouse S 1979 The abundance of wild hyperbolic sets and non-smooth stable sets for diffeomorphisms *Publ. Math. IHES* **50** 101–51
[39] Newhouse S, Palis J and Takens F Stable families of diffeomorphisms *Publ. Math. IHES* **57** 1983
[40] Nikitin A 1995 Separatrix splitting for the 'twist map'. A method of calculation of the coefficients of the splitting formula *Math. Preprint Series* **184** Universitat de Barcelona
[41] Nitecki Z 1971 *Differentiable Dynamics* (Cambridge, MA: MIT)
[42] Olvera A and Simó C 1987 An obstruction method for the destruction of invariant curves *Physica* D **28** 181–92
[43] Ostlund S, Rand D, Sethna J and Siggia E 1983 Universal properties of the transition from quasi-periodicity to chaos in dissipative systems *Physica* D **8** 303–42
[44] Palis J and de Melo W C 1982 *Geometric Theory of Dynamical Systems* (Berlin: Springer)
[45] Palis J and Takens F 1993 *Hyperbolicity and Sensitive Chaotic Dynamics at Homoclinic Bifurcations (Cambridge Studies in Advanced Mathematics 35)* (Cambridge: Cambridge University Press)
[46] Pumariño A and Rodríguez J A 1997 *Coexistence and Persistence of Strange Attractors (Lecture Notes in Mathematics 1658)* (Berlin: Springer)
[47] Rand D 1988 Universality and renormalization *New Directions in Dynamical Systems (London Math. Soc. L. N. Ser. 127)* ed T Bedford and J Swift
[48] Roussarie R and Simó C Universal models near homoclinic tangencies for planar maps, in preparation
[49] Shub M 1978 Stabilité globale des systèmes dynamiques *Astérisque* **56**
[50] Simó C 1979 On the Hénon–Pomeau attractor *J. Stat. Phys.* **21** (1979), 465-494
[51] Simó C 1990 Analytical and numerical computation of invariant manifolds *Modern Methods in Celestial Mechanics* ed D Benest and C Froeschlé (Paris: Editions Frontières) pp 285–330
[52] Simó C Direct numerical computation of coefficients in refined splitting formulas, in preparation
[53] Simó C 1997 Invariant curves of perturbations of non twist integrable area preserving maps *Preprint*
[54] Simó C, Broer H W and Roussarie R 1991 A numerical survey on the Takens–Bogdanov bifurcation for diffeomorphisms *ECIT 89* (Singapore: World Scientific) pp 320–34
[55] Simó C and Treschev D 1997 Evolution of the 'last' invariant curve in a family of area preserving maps: the case of the separatrix map *Preprint*
[56] Tatjer J C 1989 On the strongly dissipative Hénon map *ECIT 87* (Singapore: World Scientific) pp 331–7

[57] Tatjer J C 1990 Invariant manifolds and bifurcations for one and two dimensional maps *PhD Thesis* Universitat de Barcelona
[58] Tatjer J C 1992 Codimension two bifurcations near a cubic homoclinic tangency *ECIT 91* (Singapore: World Scientific) pp 308–18
[59] Tatjer J C and Simó C 1994 Basins of attraction near homoclinic tangencies *Ergod. Theor. Dynam. Syst.* **14** 351–90
[60] Viana M 1992 Saddle-node critical cycles and prevalence of strange attractors, course given at Groningen University
[61] Yoccoz J-C 1983 C^1-conjugaison des difféomorphismes du cercle *Lect. Notes Math.* **1007** 814–27
[62] Zaslavsky G, Zakharov M, Sagdeev R, Usikov D and Chernikov A 1986 Stochastic web and diffusion of particles in a magnetic field *Zh. Eksp. Teor. Fiz.* **91** 500–15